THE ASTROPHYSICAL JOURNAL SUPPLEMENT SERIES, 95:1–68, 1994 November

ATLAS OF QUASAR ENERGY DISTRIBUTIONS[1]

MARTIN ELVIS,[2] BELINDA J. WILKES,[2] JONATHAN C. MCDOWELL,[2] RICHARD F. GREEN,[3] JILL BECHTOLD,[4]
S. P. WILLNER,[2] M. S. OEY,[2,4] ELISHA POLOMSKI,[2,5] AND ROC CUTRI[4]
Received 1993 June 1; accepted 1994 April 21

ABSTRACT

We present an atlas of the spectral energy distributions (SEDs) of normal, nonblazar, quasars over the whole available range (radio to 10 keV X-rays) of the electromagnetic spectrum. The primary (UVSX) sample includes 47 quasars for which the spectral energy distributions include X-ray spectral indices and UV data. Of these, 29 are radio quiet, and 18 are radio loud. The SEDs are presented both in figures and in tabular form, with additional tabular material published on CD-ROM. Previously unpublished observational data for a second set of quasars excluded from the primary sample are also tabulated. The effects of host galaxy starlight contamination and foreground extinction on the UVSX sample are considered and the sample is used to investigate the range of SED properties. Of course, the properties we derive are influenced strongly by the selection effects induced by quasar discovery techniques. We derive the mean energy distribution (MED) for radio-loud and radio-quiet objects and present the bolometric corrections derived from it. We note, however, that the dispersion about this mean is large (~one decade for both the infrared and ultraviolet components when the MED is normalized at the near-infrared inflection). At least part of the dispersion in the ultraviolet may be due to time variability, but this is unlikely to be important in the infrared. The existence of such a large dispersion indicates that the MED reflects only some of the properties of quasars and so should be used only with caution.

Subject headings: atlases — galaxies: photometry — quasars: general

1. INTRODUCTION

One of the reasons that main-sequence stars are much better understood than quasars is that they radiate (almost) blackbody spectra with temperatures between ~4000 and ~30,000 K, so that their blackbody peak moves conveniently through the optical band. The resulting strong color changes allowed the early recognition of the main sequence in the Hertzprung-Russell diagram. By showing that most stars lie in a restricted band of color and luminosity, this diagram provided a crucial input to theories of stellar structure. The current lack of understanding of quasars may correspondingly be due to the distribution of their continuum light. Because the quasar phenomenon covers an extremely broad range of wavelengths, it is hard to see continuum features analogous to the blackbody peak in normal stars. Quasars emit almost constant power per decade of frequency from 100 μm to at least 100 keV (see, e.g., Fig. 1 of Carleton et al. 1987). While this equipartition is surprising and may be to some extent an observational artifact (Brissenden 1989; Elvis 1991), it contains too little information to constrain theoretical ideas. Overcoming this problem requires the assembly of spectral energy distributions (SEDs) for sizable samples of quasars over the whole accessible range of the electromagnetic spectrum from radio to hard X-rays (and in the future, gamma rays).

In this paper we present SEDs for a sample of 47 quasars. We concentrate on "normal" quasars with little or no polarization and no dramatic optical variability. Our primary selection criteria were (1) existing *Einstein* observations at good signal-to-noise ratio (to ensure good X-ray spectra), and (2) an optical magnitude bright enough to make an *IUE* spectrum obtainable. Making the primary selection at these wavelengths means that not all the sample are detected in the *IRAS* data.

Several previous studies of quasar SEDs have been published. Each emphasized a particular region, and none considered the X-rays in detail. Early work included SEDs for *IRAS*-bright AGNs by Edelson & Malkan (1986), and for hard X-ray–selected Seyfert galaxies by Ward et al. (1987). Infrared to optical SEDs for the PG quasars were presented by Sanders et al. (1989) with an emphasis on explaining the infrared. Near-infrared to ultraviolet SEDs for *IUE* observed quasars were presented by Sun & Malkan (1989). Our study is different in that it includes X-ray data, divided into three energy bands in many cases, for all the objects, and includes both *IUE* and *IRAS* data. The X-rays are important to define the total luminosity and are crucial in overall modeling as they seem to come most directly from the central source. The sample is fairly evenly divided between radio-quiet and radio-loud objects.

We present the data in § 4 and the necessary corrections for reddening, variability and, importantly, host galaxy contributions in § 5. Section 6 discusses the properties of the SEDs, including their mean and dispersion. First, however, we out-

[1] Based in part on data acquired with the *International Ultraviolet Explorer* satellite, operated at the Goddard Space Flight Center for the National Aeronautics and Space Administration, the Multiple Mirror Telescope (MMT), a joint facility of the Smithsonian Institution and the University of Arizona, and the Infrared Telescope Facility (IRTF), a joint facility of NASA and the University of Hawaii.

[2] Center for Astrophysics, 60 Garden Street, Cambridge, MA 02138.
[3] National Optical Astronomy Observatories, Kitt Peak National Observatory, Tucson, AZ 85726. KPNO is operated by the Association of Universities for Research in Astronomy, Inc., under contract with the NSF.
[4] Steward Observatory, University of Arizona, Tucson, AZ 85721.
[5] Center for EUV Astrophysics, Berkeley, CA.

line the features we are studying (§ 2) and the sample of quasars (§ 3).

2. CONTINUUM FEATURES

Figure 1 shows the radio–to–X-ray rest frame energy distributions of two typical quasars, 4C 34.47 and Mrk586. All energy distributions are plotted as log νf_ν versus log ν; since νf_ν is the flux per logarithmic frequency interval, such plots give the best indication of the frequency ranges where most energy is released. The X-ray data are indicated with a "bow-tie" symbol representing a power-law fit with both the best-fit slope and the 1 σ confidence limit slopes indicated. In general, no data are available in the extreme ultraviolet "gap" beyond the Lyman limit where our galaxy is opaque.

In the 1–100 μm infrared band, both quasars are almost flat (Ward et al. 1987; Neugebauer et al. 1987, hereafter N87). A single, nearly horizontal, power law fits the IR points reasonably well and intersects the X-ray point at about 1 keV. We will call deviations from this power law "continuum features." There are four prominent features of this kind:

1. The power output always drops in the submillimeter band (the millimeter break, labeled "mm-break" in Fig. 1), but the size of the drop varies dramatically from object to object. Quasars in which the drop is only 2 decades are called "radio loud" (e.g., 4C 34.47). The great majority of quasars have a much stronger millimeter break of 5 or even 6 decades (Condon et al. 1981; Kellermann et al. 1989) and are called "radio quiet" (e.g., Mrk 586). This distinction between radio-loud and radio-quiet quasars is the oldest in the quasar literature and goes back to the "blue interlopers" found in early radio source identification work (Sandage 1965). Radio-quiet objects are much the more common, by about a factor 10 (Kellerman et al. 1989). The millimeter-break is the strongest known feature in normal quasar continua, although it is less strong in objects selected at high radio frequencies.

2. The optical–ultraviolet continuum rises above the infrared and forms a "UV bump" (Shields 1978; Malkan & Sargent 1982; N87). Variability studies show that this is a separate component from the infrared (Cutri et al. 1985) since it varies much more strongly. This big bump is most often interpreted in terms of thermal emission from an accretion disk (e.g., Malkan 1983; Czerny & Elvis 1987). The strength of the feature in our study may be affected by selection effects since many quasars were discovered by ultraviolet excess techniques. The beginning of the bump is marked by an inflection between 1 and 1.5 μm in the rest frame; this "near-infrared inflection" is the only continuum feature whose wavelength is well defined (N87).

3. X-ray spectra of many radio-loud quasars and high-luminosity Seyfert 1 galaxies have rising slopes toward high frequencies in log νf_ν versus log ν energy distributions (Zamorani et al. 1981; Mushotzky 1984; Bezler et al. 1984; Turner & Pounds 1989; Williams et al. 1992). They cannot then be an extension of a flat, or slightly falling, infrared power law, as has been suggested for some objects by Carleton et al. (1987). A new emission component must be emerging in the X-rays above 1 keV in these objects.

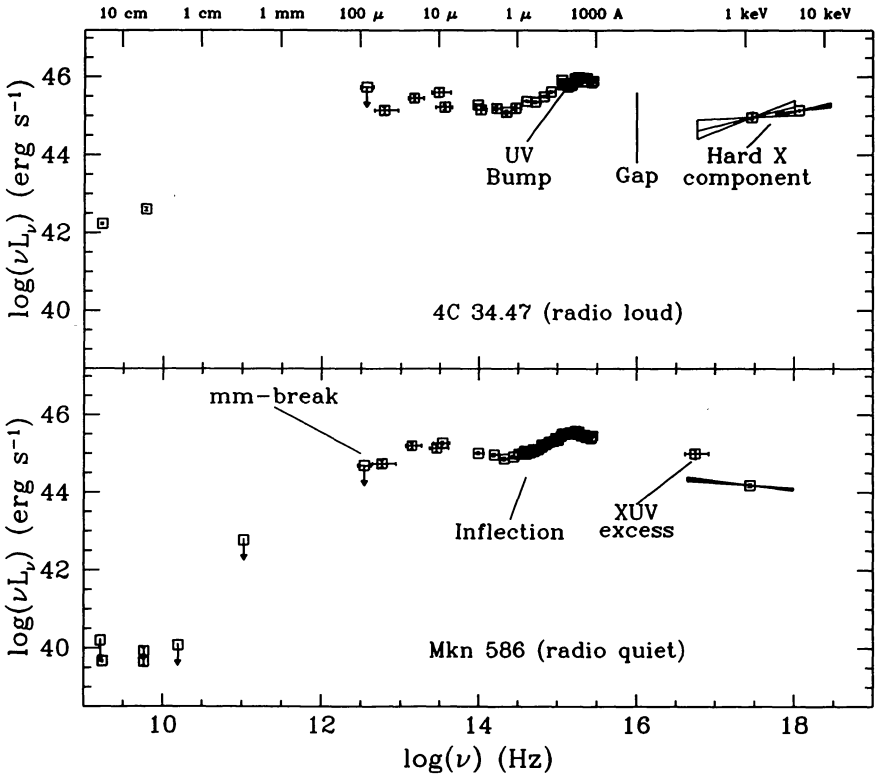

FIG. 1.—Examples of radio-loud (4C 34.47, *top*) and radio-quiet (Mrk 586, *bottom*) quasar energy distributions, illustrating the main continuum features. The energy distributions show the logarithm of the energy per unit logarithmic frequency interval, in the rest frame.

4. The most recently identified continuum feature is the "XUV excess" (e.g., Arnaud et al. 1985; Wilkes & Elvis 1987; hereafter WE87; Turner & Pounds 1989; Masnou et al. 1992). The 1 keV spectrum of quasars is often fitted with a power-law spectrum since the available spectral resolution is very low; studies using the *Einstein* IPC and *EXOSAT* showed that excess flux above this power law was often present in the ultrasoft (0.3 keV and below) region of the spectrum; the excess can be highly variable (e.g., Turner & Pounds 1988; Elvis et al. 1991). It is possible that the XUV excess is the same physical component as the ultraviolet bump since the energy distribution rises toward the EUV from both sides of the unobserved spectral region. WE87 found evidence for a soft excess in eight of their 33 quasars. Subsequent reanalysis of the 13 highest S/N quasars in this sample by Masnou et al. (1992) detected a soft excess in about half of the objects. A similar fraction was found by Turner & Pounds (1989) for Seyfert galaxies.

3. THE UVSX SAMPLE

We have carried out an extensive program of quasar continuum observations over the past 7 years, the results of which we present here. Since we believe it important to include X-ray observations, we restricted ourselves to objects that had been observed to high S/N with the Imaging Proportional Counter (IPC; Gorenstein, Harnden, & Fabricant 1979) instrument on the *Einstein Observatory* (*HEAO 2*; Giacconi et al. 1979) satellite. We note that this introduces a bias toward objects which are low redshift, moderate luminosity, and have strong X-ray–to–optical flux ratios (WE87); the sample is heterogenous and not flux limited. The objects were selected mainly from the PG (Schmidt & Green 1983), 3C, and Parkes catalogs. No single completeness criterion could be used, however, because of the quasi-random way in which the original *Einstein* observations were made.

We have selected a subsample of 47 quasars which have sufficient counts ($\gtrsim$300) in the IPC to give a reasonably constrained power-law spectral fit and which are optically bright enough ($V < 17$) to be observable with *IUE*: we designate this the "UVSX sample." Twenty-nine members of the sample are radio quiet, and 18 are radio loud. The X-ray and ultraviolet data have been combined with *IRAS* space-based infrared data and ground-based optical, infrared, and radio observations to construct the complete energy distributions. Thirty of the 47 objects are detected by IRAS at 60 μm; only 15 are detected at 100 μm.

The 47 quasars in the UVSX sample are listed in Table 1A. The sample has substantial overlap with the work of Elvis et al. (1986) and WE87. The table gives the common name of the quasar as well as its catalog number in the *Einstein Observatory* Source Catalog (Harris et al. 1991), and the name of the associated host galaxy where appropriate. Both B1950 and J2000 coordinates are provided, as well as the redshift and typical V magnitude. The estimate of the foreground Galactic hydrogen column density (in units of 10^{20} cm^{-2}) is listed together with a reference. Most of the column estimates are accurate values from Elvis, Lockman, & Wilkes (1989). Finally, each object is given a classification. The classifications are as follows: radio-quiet (RQ), broad absorption line (BAL, a subset of RQ), and radio-loud (RL). Radio-loud quasars are further subdivided where suitable data are available into superluminal (SL), flat spectrum compact (FSC), steep spectrum compact (SSC), and Fanaroff-Riley class 2 steep spectrum doubles (FR2). Further, following the convention of Véron-Cetty & Véron (1987) and Schmidt & Green (1983), radio-quiet objects with absolute visual magnitude fainter than -23.0 calculated according to their prescription (but using our cosmological parameters; see § 5.3) are designated as Seyfert 1 (Sy1); eight objects in the UVSX sample satisfy this criterion. Table 1B lists the corresponding properties of 23 other "IPC" quasars from our original program which were observed by *Einstein* or *EXOSAT* but are not included in the final UVSX sample either because of poor quality X-ray data, strong optical variability, or low optical flux. New ground-based data are presented in this paper for these quasars, but the data are not used in the main analysis.

Further properties of the quasars in the UVSX sample are listed in Table 2 and illustrated as histograms in Figure 2, with the shaded regions corresponding to the radio-loud objects. The numerical value of the radio-loudness, R_L, is defined to be the logarithm of the ratio of the observed core 5 GHz flux to the flux in the optical B band, and an object is considered to be radio loud if $R_L = \log (f_{5\,\mathrm{GHz}}/f_B) > 1$. Note that this definition is based on observed frame fluxes, but corrections to the rest frame do not make an important difference for the small redshifts encountered here. In each case an attempt has been made to estimate a core flux on arcsecond scales, since we are studying the properties of the compact central source at other wavelengths and wish to neglect the extended radio source, if any. We were unable to find maps of the two most southern sources, and the VLA fails to resolve the core of 3C 48 from the compact steep spectrum source in which it is embedded (Spencer et al. 1989). For sources where information on the fluxes of individual radio components was available, we have calculated the Browne parameter R_{CD} defined as the ratio of core to extended emission at 5 GHz and is believed to be correlated with source orientation (Orr & Browne 1982).

Monochromatic luminosities [log (νL_ν ergs s^{-1})] in the visual (L_V at 5400 Å in the rest frame) and X-ray (L_X at 2 keV) are tabulated, as are the bolometric luminosities derived later in this paper. The absolute visual magnitude is also given in Table 2, derived using the formulae of Véron-Cetty & Véron (1987) but using our chosen cosmological parameters (see § 5.3). α_x is the X-ray spectral index derived from the IPC results; the ultraviolet–to–X-ray two-point spectral slope α_{ox} is defined from 2500 Å to 2 keV in the rest frame. These spectral indices are conventional energy indices, $\alpha = -d \log f_\nu / d \log \nu$.

4. DATA

4.1. *Overview*

To assemble the SEDs for the 47 quasars required observations on 12 different telescopes, using 16 different instruments, in locations from ground-based to space. Because of this diversity of observing techniques it is necessary to describe each data set, and the corrections made to it, carefully.

4.2. *X-Ray*

The "X-ray band" covers two full decades of the spectrum, as much as the entire UV, optical, and infrared bands together.

1994ApJS...95....1E

TABLE 1A

UVSX SAMPLE QUASARS

Object	Name	2E Name	Host Galaxy	RA (B1950)	Dec (B1950)	RA (J2000)	Dec (J2000)	Redshift	V Mag	N_H[a]	Ref[b]	Class[c]
Q0003+158	PHL 658	2E 12		00 03 25.1	+15 53 07.4	00 05 59.2	+16 09 49.4	0.450	15.60	3.94	1	RL
Q0003+199	PG 0003+199		Mkn 335	00 03 45.0	+19 55 30.0	00 06 19.3	+20 12 11.9	0.025	13.75	3.98	4	Sy1
Q0007+106	PG0007+106	2E 29	III Zw 2A	00 07 56.7	+10 41 47.8	00 10 31.0	+10 58 29.2	0.089	15.16	6.09	1	FSC
Q0026+129	PG0026+129	2E 93	PGC 1790	00 26 38.1	+12 59 29.6	00 29 13.8	+13 16 04.4	0.142	15.32	4.93	1	RQ
Q0049+171	PG0049+171	2E 200	Mkn 1148	00 49 16.5	+17 09 41.0	00 51 54.8	+17 25 58.9	0.064	15.88	4.26	1	Sy1
Q0050+124	PG 0050+124	2E 209	I Zw 1	00 50 57.8	+12 25 20.0	00 53 34.9	+12 41 36.3	0.061	14.07	5.07	1	RQ
Q0052+251	PG0052+251	2E 217	PGC 3237	00 52 11.1	+25 09 24.0	00 54 52.2	+25 25 38.9	0.155	15.42	4.50	1	RQ
Q0054+144	PHL 909	2E 233		00 54 31.9	+14 29 58.6	00 57 09.9	+14 46 11.2	0.171	16.70	4.20	1	RQ
Q0121−590	2E 378	2E 378	Fairall 9	01 21 51.2	−59 03 58.9	01 23 45.7	−58 48 21.1	0.045	13.23	2.25	2	RQ
Q0134+329	3C 48	2E 444		01 34 49.8	+32 54 20.2	01 37 41.3	+33 09 35.2	0.367	16.00	4.35	1	SSC
Q0205+024	NAB0205+024	2E 526	Mkn 586	02 05 14.5	+02 28 42.7	02 07 49.8	+02 42 56.1	0.155	15.40	2.99	1	RQ
Q0312−770	PKS0312−770	2E 746		03 12 55.7	−77 03 01.0	03 11 54.7	−76 51 51.4	0.223	15.90	7.31	2	? (RL)
Q0414−060	3C 110	2E 962		04 14 49.2	−06 01 04.3	04 17 16.7	−05 53 45.1	0.781	16.20	5.12	4	RL
Q0637−752	PKS0637−752	2E 1720		06 37 23.4	−75 13 37.8	06 35 46.5	−75 16 17.1	0.651	15.75	8.16	2	? (RL)
Q0804+761	PG 0804+761	2E 1919		08 04 35.4	+76 11 32.0	08 10 58.5	+76 02 41.8	0.100	14.71	3.12	1	RQ
Q0837−120	3C 206	2E 2028		08 37 27.9	−12 03 54.2	08 39 50.6	−12 14 33.9	0.198	15.76	5.85	1	FR2
Q0844+349	PG0844+349	2E 2048	PGC 24702	08 44 33.9	+34 56 09.0	08 47 42.5	+34 45 04.6	0.064	14.00	3.39	1	RQ
Q0915+165	Mkn 704 AGN	2E 2116	Mkn 704	09 15 39.4	+16 30 59.0	09 18 26.0	+16 18 19.7	0.029	14.20	3.15	1	Sy1
Q0923+129	Mkn 705 AGN	2E 2139	Mkn 705	09 23 20.0	+12 57 04.0	09 26 03.3	+12 44 03.3	0.028	14.60	4.03	1	Sy1
Q1028+313	B2 1028+313	2E 2291		10 28 09.8	+31 18 20.6	10 30 59.1	+31 02 55.5	0.177	16.71	1.98	1	FSC
Q1100+772	3C 249.1	2E 2389		11 00 27.4	+77 15 09.0	11 04 13.8	+76 58 58.6	0.311	15.72	2.93	1	FR2
Q1116+215	PG1116+215	2E 2443		11 16 30.1	+21 35 43.0	11 19 08.9	+21 19 17.8	0.177	15.17	1.44	1	RQ
Q1137+660	3C 263	2E 2503		11 37 09.3	+66 04 27.0	11 39 57.0	+65 47 49.4	0.652	16.32	0.82	1	FR2/SL
Q1146−037	PKS1146−037	2E 2537		11 46 23.9	−03 47 30.0	11 48 57.4	−04 04 10.8	0.341	16.90	2.79	1	FR2
Q1202+281	GQ Comae	2E 2584	PGC 38224	12 02 08.9	+28 10 53.1	12 04 42.1	+27 54 11.4	0.165	15.51	1.72	1	RQ
Q1211+143	PG1211+143	2E 2620	PGC 39086	12 11 44.8	+14 19 53.0	12 14 17.6	+14 03 12.5	0.085	14.63	2.83	1	RQ
Q1219+755	Mkn 205 AGN	2E 2677	Mkn 205	12 19 33.8	+75 35 18.0	12 21 44.4	+75 18 40.1	0.070	15.24	2.74	1	RQ
Q1226+023	3C 273	2E 2729	PGC 41121	12 26 33.2	+02 19 43.2	12 29 06.7	+02 03 08.1	0.158	12.86	1.80	3	FSC/SL
Q1244+026	PG 1244+026	2E 2854		12 44 02.1	+02 38 31.0	12 46 35.3	+02 22 08.3	0.048	16.15	1.93	1	Sy1
Q1307+085	PG1307+085	2E 2978	PGC 45656	13 07 16.2	+08 35 47.0	13 09 47.0	+08 19 49.3	0.155	15.28	2.20	1	RQ
Q1351+695	Mkn 279 AGN	2E 3147	Mkn 279	13 51 53.6	+69 33 13.0	13 53 03.5	+69 18 29.4	0.031	14.46	1.64	1	Sy1
Q1352+183	PG 1352+183	2E 3148		13 52 11.5	+18 20 58.0	13 54 34.8	+18 06 16.0	0.152	15.50	1.84	1	RQ
Q1407+265	PG1407+265	2E 3196		14 07 07.7	+26 32 30.0	14 09 23.8	+26 18 20.8	0.94	15.73	1.38	1	RQ
Q1416−129	PG1416−129	2E 3238	PGC 51142	14 16 21.3	−12 56 58.0	14 19 03.8	−13 10 44.8	0.129	15.40	7.20	1	BAL
Q1426+015	PG1426+015	2E 3280	Mkn 1383	14 26 33.8	+01 30 27.0	14 29 06.6	+01 17 06.2	0.086	15.05	2.64	1	RQ
Q1501+106	Mkn 841 AGN	2E 3372	Mkn 841	15 01 36.4	+10 37 57.0	15 04 01.3	+10 26 17.1	0.036	15.09	2.23	1	Sy1
Q1545+210	3C 323.1	2E 3500		15 45 31.1	+21 01 28.0	15 47 43.5	+20 52 17.2	0.266	16.05	4.04	1	FR2
Q1613+658	PG1613+658	2E 3624	Mkn 876	16 13 36.3	+65 50 38.0	16 13 57.2	+65 43 10.1	0.129	15.37	2.66	1	RQ
Q1635+119	MC2 1635+119	2E 3737		16 35 25.9	+11 55 46.4	16 37 46.5	+11 49 49.8	0.146	16.50	4.29	1	RL
Q1704+608	3C 351	2E 3828		17 04 03.5	+60 48 31.1	17 04 41.4	+60 44 30.4	0.371	15.28	2.26	1	FR2
Q1721+343	4C 34.47	2E 3896		17 21 32.0	+34 20 41.8	17 23 20.8	+34 17 58.4	0.206	16.50	3.06	1	FSC/SL
Q1803+676	2E 4008	2E 4008	Kazaryan 102	18 03 37.4	+67 37 53.9	18 03 28.9	+67 38 09.5	0.136	16.00	5.00	1	RQ
Q2128−123	PKS 2128−123	2E 4484		21 28 52.7	−12 20 20.1	21 31 35.3	−12 07 04.3	0.501	15.46	4.83	1	RL
Q2130+099	PG2130+099	2E 4486	II Zw 136	21 30 01.3	+09 54 59.0	21 32 27.9	+10 08 17.4	0.061	14.62	4.20	1	RQ
Q2135−147	PHL 1657	2E 4497		21 35 01.2	−14 46 27.3	21 37 45.2	−14 32 55.4	0.200	15.53	4.45	1	FR2
Q2209+184	PG 2209+184	2E 4579		22 09 30.2	+18 27 01.0	22 11 53.7	+18 41 51.4	0.070	15.86	4.82	1	Sy1
Q2251−178	MR 2251−178	2E 4645		22 51 25.9	−17 50 54.2	22 54 05.8	−17 34 54.6	0.068	14.36	2.84	1	RQ

[a] Galactic column in units of 10^{20} cm^{-2}.

[b] REFERENCES for N_H value.—(1) Elvis, Lockman, & Wilkes 1989; (2) Heiles & Cleary 1989; (3) Dickey, Salpeter, & Terzian 1978; (4) Stark et al. 1984, 1992.

[c] The classes of object based on optical luminosity and radio spectrum and morphology are RQ (radio-quiet); Sy1 (low luminosity radio-quiet, or Seyfert 1); BAL (radio-quiet with broad absorption lines); RL (radio-loud); SL (radio-loud superluminal); FSC (flat spectrum compact radio-loud); SSC (steep spectrum compact radio-loud); and FR2 (radio-loud Fanaroffs Riley class 2 steep spectrum doubles).

1994ApJS...95....1E

TABLE 1B

OTHER "IPC" QUASARS[a]

Object	Name	2E Name	Host Galaxy	RA (B1950)	Dec (B1950)	RA (J2000)	Dec (J2000)	Redshift	V Mag	N_H[a]	Ref[b]	Class[c]
Q0112−017	PKS 0112−017	2E 335		01 12 43.9	−01 42 54.8	01 15 17.1	−01 27 04.3	1.365	17.41	5.37	1	RL
Q0133+207	3C 47	2E 437		01 33 20.4	+20 42 10.6	01 36 24.4	+20 57 27.8	0.425	17.30	5.41	4	RL
Q0219+428	3C 66A	2E 558		02 19 30.0	+42 48 30.4	02 22 39.6	+43 02 08.5	0.444	15.50	7.48	4	BL
Q0323+022	H			03 23 38.0	+02 14 47.2	03 26 13.9	+02 25 14.8	0.147	16.50	8.68	1	BL
Q0424−131	PKS 0424−131	2E 1048		04 24 47.8	−13 09 33.4	04 27 07.3	−13 02 53.5	2.165	17.50	3.95	4	RL
Q0923+392	4C 39.25	2E 2141		09 23 55.3	+39 15 23.5	09 27 03.0	+39 02 20.7	0.699	17.86	1.69	1	FSC/SL
Q1012+008	PG 1012+008			10 12 20.8	+00 48 33.0	10 14 54.9	+00 33 36.8	0.185	16.00	3.22	1	RQ
Q1121+422	PG 1121+422			11 21 52.1	+42 16 54.0	11 24 35.5	+42 00 24.9	0.234	16.02	2.33	1	RQ
Q1217+023	PKS 1217+023	2E 2661		12 17 38.4	+02 20 20.9	12 20 11.9	+02 03 42.1	0.240	16.53	1.97	1	RL
Q1253−055	3C 279	2E 2900		12 53 35.9	−05 31 08.4	12 56 11.2	−05 47 22.1	0.538	17.75	2.22	1	FSC/SL
Q1346−036	Q1346−036			13 46 08.3	−03 38 30.5	13 48 44.0	−03 53 24.6	2.344	17.27	2.49	4	RQ
Q1351+640	PG 1351+640			13 51 46.3	+64 00 28.4	13 53 15.8	+63 45 44.8	0.088	14.84	2.29	4	RQ
Q1435−067	PG 1435−067	2E 3305		14 35 37.5	−06 45 22.0	14 38 16.4	−06 58 18.3	0.129	15.54	5.08	4	RQ
Q1517+239	LB 9612			15 17 08.2	+23 56 52.6	15 19 19.5	+23 46 02.6	1.898	16.40	3.91	4	RQ
Q2112+059	PG 2112+059			21 12 23.6	+05 55 12.0	21 14 52.7	+06 07 41.6	0.466	15.52	6.49	4	RQ
Q2120+168	3C 432	1E 2120+168		21 20 25.5	+16 51 46.4	21 22 46.3	+17 04 38.6	1.805	17.96	7.39	4	RL
Q2126−158	PKS 2126−158	2E 4479		21 26 26.7	−15 51 51.5	21 29 12.1	−15 38 42.1	3.260	17.30	4.85	1	RL
Q2214+139	Mkn 304 AGN	2E 4585	Mkn 304	22 14 45.8	+13 59 20.0	22 17 12.2	+14 14 20.8	0.067	14.66	5.23	1	RQ
Q2233+134	PG 2233+134	2E 4626		22 33 39.8	+13 28 21.0	22 36 07.7	+13 43 54.9	0.325	16.04	4.89	4	BAL
Q2251+113	4C 11.72			22 51 40.6	+11 20 39.6	22 54 10.4	+11 36 39.2	0.323	15.77	5.53	1	RL
Q2254+024	PKS 2254+024	2E 4661		22 54 44.6	+02 27 13.8	22 57 17.6	+02 43 17.3	2.090	18.00	5.88	1	RL
Q2304+042	PG 2304+042			23 04 30.1	+04 16 41.0	23 07 02.7	+04 32 55.3	0.042	15.44	5.52	1	Sy1

[a] Other quasars for which new observational data are tabulated. These were in our original program but were later excluded from our study for excessive variability or inadequate X-ray data. See notes to Table 1A.

TABLE 2

UVSX SAMPLE PROPERTIES

Object	$\log L_V$[a]	$\log L_X$[b]	$\log L_{Bol}$[c]	M_V[d]	R_L[e]	R_{CD}[f]	α_x[g]	α_{ox}[h]
Q0003+158	45.94	45.38	46.14	−26.44	1.83		2.2	1.37
Q0003+199	44.29	43.39	45.48	−22.45	−0.55		2.0	1.47
Q0007+106	44.84	44.39	45.91	−23.89	1.79	0.89	0.4	1.33
Q0026+129	45.14	44.53	46.12	−24.50	−1.06	0.04	0.9	1.35
Q0049+171	43.99	44.00	45.20	−21.79	−0.11	> 3.25	0.6	1.20
Q0050+124	44.90	43.91	46.10	−23.94	−0.50		1.7	1.44
Q0052+251	45.04	44.59	46.34	−24.46	−0.75	1.31	1.1	1.39
Q0054+144	45.16	44.37	46.21	−24.61	−0.23		0.4	1.34
Q0121-590	44.66	44.23	45.85	−23.60	< 0.04		0.9	1.37
Q0134+329	45.55	44.96	46.92	−25.94	2.33	0.04	0.7	1.28
Q0205+024	45.03	44.14	46.17	−24.33	−0.39	> 2.67	1.2	1.53
Q0312-770	45.31	44.64	46.24	−24.97	2.64	10.98	0.1	1.16
Q0414-060	46.22	45.45	46.26	−27.12	2.71		0.5	1.42
Q0637-752	46.48	45.78	46.55	−27.78	3.56	> 10.00	0.5	1.33
Q0804+761	45.01	44.33	46.16	−24.31	−0.72		1.0	1.44
Q0837-120	44.93	44.97	46.21	−24.21	2.42	0.27	0.7	1.15
Q0844+349	44.63	43.46	45.48	−23.54	< −1.22		0.6	1.60
Q0915+165	43.65	43.24	45.04	−22.56	0.02		0.3	1.23
Q0923+129	43.61	43.19	45.26	−21.81	< 0.48		0.7	1.31
Q1028+313	44.84	44.51	46.04	−23.96	2.03	1.69	0.8	1.30
Q1100+772	45.56	44.90	46.63	−25.52	1.59	0.13	1.0	1.40
Q1116+215	45.48	44.38	46.58	−25.38	−0.47	2.21	1.0	1.62
Q1137+660	46.14	45.60	46.11	−26.93	2.05	0.20	0.7	1.31
Q1146-037	44.77	45.01	45.95	−23.92	2.63		0.3	1.22
Q1202+281	44.64	44.54	46.11	−23.72	−0.19	3.61	1.1	1.26
Q1211+143	45.14	44.37	46.26	−24.42	−0.74	0.01	2.0	1.39
Q1219+755	44.51	44.13	45.45	−23.34	−0.30		0.8	1.21
Q1226+023	46.18	45.56	46.27	−27.03	3.00	2.49	0.5	1.37
Q1244+026	43.42	43.17	44.86	−21.57	−0.45		1.4	1.33
Q1307+085	45.14	44.36	46.16	−24.58	< −0.92		0.9	1.42
Q1351+695	43.20	43.54	45.18	−22.07	0.22		1.1	1.37
Q1352+183	44.95	44.07	45.93	−24.06	< −0.88		1.5	1.46
Q1407+265	46.45	45.74	46.58	−27.68	0.28	0.58	1.2	1.40
Q1416-129	44.59	44.62	45.81	−23.54	−0.18	0.29	0.9	1.26
Q1426+015	44.82	44.34	46.09	−23.88	−0.59	3.32	1.1	1.41
Q1501+106	43.95	43.75	45.34	−21.95	−0.87	0.50	0.9	1.28
Q1545+210	45.43	45.00	46.50	−25.31	1.28	0.05	0.8	1.37
Q1613+658	44.89	44.36	46.17	−24.21	−0.47	0.35	1.1	1.36
Q1635+119	44.66	43.99	45.56	−23.31	2.02	0.30	0.7	1.31
Q1704+608	45.82	44.50	46.82	−26.14	0.70	0.01	0.1	1.61
Q1721+343	45.30	45.08	46.51	−24.96	2.19	0.86	0.5	1.28
Q1803+676	44.89	44.12	45.73	−23.84	< −0.58		−0.2	1.45
Q2128-123	45.97	45.25	46.00	−26.51	3.38	> 20.00	0.5	1.38
Q2130+099	44.50	43.61	45.72	−23.26	−0.47	1.73	0.8	1.52
Q2135-147	45.26	44.76	46.31	−24.96	1.76	0.12	0.7	1.25
Q2209+184	44.14	43.89	45.30	−22.99	2.21		0.8	1.32
Q2251-178	44.82	44.38	45.75	−23.85	−1.02		0.4	1.28

[a] Monochromatic luminosity (ergs cm^{-2} s^{-1}) at 5400 Å.
[b] Monochromatic luminosity (ergs cm^{-2} s^{-1}) at 1 keV.
[c] Bolometric luminosity (ergs s^{-1}).
[d] Absolute visual magnitude, assuming $H_0 = 50$, $\Omega_0 = 1$.
[e] Radio loudness.
[f] Browne R parameter (radio core dominance).
[g] Energy index at 1 keV.

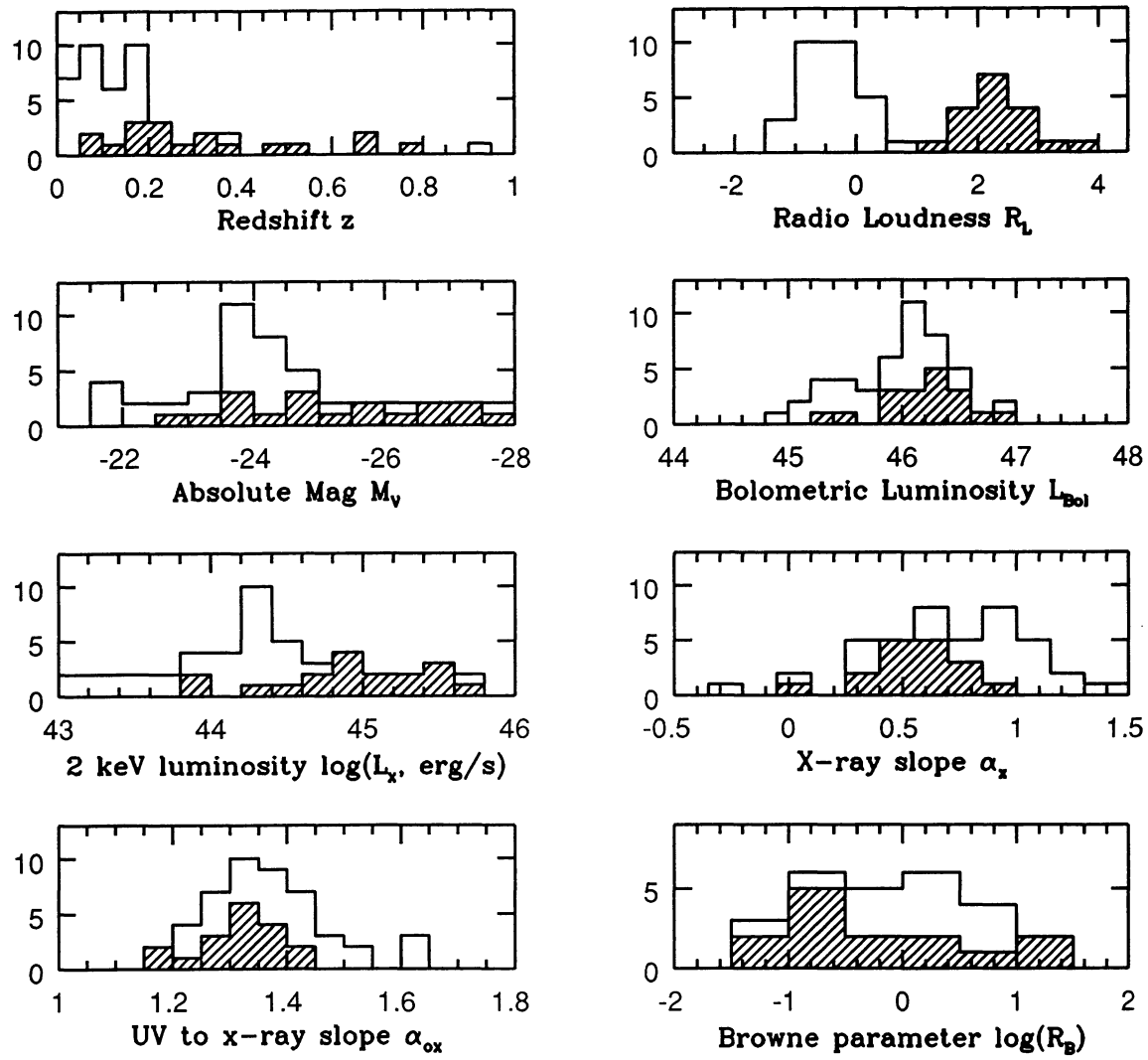

FIG. 2.—Histograms of sample properties. Shaded bins correspond to radio-loud objects, $R_L > 1$. The absolute magnitude is calculated using the corrections of Véron-Cetty & Véron (1987), but with our value of Ω_0. The bolometric luminosity is derived from the observed energy distributions as described in the text. The monochromatic X-ray luminosity is $\nu L(\nu)$ at 2 keV in the rest frame, estimated from the IPC spectral fits. R_{CD}, the ratio of radio core to extended luminosity (Orr & Browne 1982), is an indicator of the source orientation; it was possible to estimate this for only a subset of the sources.

Even though most X-ray spectra have low resolution, it is still useful to divide the band into three parts: "hard X-ray," covering 2–10 keV; "soft X-ray," covering 0.3–2 keV; and "ultrasoft X-ray," covering 0.1–0.3 keV. All the 47 objects in our sample were observed in 1979 or 1980 with the IPC instrument on *Einstein*. The limited spectral resolution of this instrument allows us to characterize the 0.1–3.5 keV ultrasoft and soft X-ray spectrum as a single power law modified by foreground absorption, although the true spectrum may be much more complex. For most of the objects in the sample, the data and spectral fits are presented in WE87. Although the foreground Galactic absorption is now well determined for our objects, we choose to retain the earlier fits in which the Galactic absorption is allowed to vary freely, since in the absence of hard X-ray data to constrain the 1 keV slope, the presence of an ultrasoft excess in the incident spectrum is almost equivalent to a reduction in the absorption, and thus a better estimate of the slope in the soft band (at greater energies than the excess) is obtained than if the absorption is fixed at its true value (see Masnou et al. 1992).

Masnou et al. (1992) searched for ultrasoft excesses in thirteen of the highest signal-to-noise observations. Those authors re-analysed the *Einstein* data using a two power law model and including data out to 10 keV from the MPC instrument on *Einstein,* revealing the presence of an ultra-soft X-ray excess component in eight of the objects. This is indicated as a separate data point at 0.2 keV on our energy distribution plots (Fig. 8). In these two power-law fits, the presence of the hard X-ray data means that the best estimate of the 1 keV slope is obtained by fixing the foreground absorption at the known Galactic (Elvis et al. 1989) value. The object PG 1211+143 was studied in a separate paper by Elvis et al. (1991). These results are summarized in Table 3A together with 18 previously unpublished spectral fits. The analysis for the new fits was identical to

1994ApJS...95....1E

TABLE 3A

ADOPTED X-RAY POWER-LAW FITS

Object	0.2 keV flux (μJy)	1 keV Energy index	1 keV flux (μJy)	Ref	4 keV Energy index	4 keV flux (μJy)	Ref
Q0003+158		$2.2\pm^{2.8}_{1.3}$	$1.40\pm^{6.0}_{0.6}$	1		<1.5	9
Q0003+199		2.0	6.5–8.5	10	1.0	0.8–1.1	10
Q0007+106		$0.4\pm^{0.9}_{0.3}$	$1.97\pm^{2.49}_{0.52}$	2	$0.66\pm^{0.09}_{0.14}$	2.08	6
Q0026+129	$5.9\pm^{1.4}_{1.1}$	$0.88\pm^{0.05}_{0.05}$	$1.41\pm^{0.03}_{0.03}$	3	$0.86\pm^{0.39}_{0.38}$	0.43	5
Q0049+171		$1.2\pm^{2.8}_{0.6}$	$2.58\pm^{5.95}_{0.67}$	1	$1.03\pm^{0.29}_{0.29}$	0.57	5
Q0050+124		$1.9\pm^{1.7}_{0.8}$	$3.60\pm^{6.7}_{1.3}$	1		<1.1	9
Q0052+251		$1.2\pm^{1.7}_{0.6}$	$1.63\pm^{3.5}_{0.5}$	1	$0.84\pm^{0.53}_{0.53}$	0.28	5
Q0054+144	$5.18\pm^{1.6}_{1.6}$	$0.41\pm^{0.07}_{0.07}$	$0.52\pm^{0.04}_{0.04}$	3	$0.07\pm^{0.67}_{0.64}$	0.23	12
Q0121−590		$0.9\pm^{0.2}_{0.1}$	$9.04\pm^{0.72}_{0.60}$	1	$1.07\pm^{0.07}_{0.07}$	0.91	6
Q0134+329		$0.7\pm^{0.4}_{0.4}$	$0.50\pm^{0.14}_{0.10}$	2			
Q0205+024	$18.8\pm^{4.5}_{5.0}$	$1.2\pm^{0.07}_{0.07}$	$0.58\pm^{0.06}_{0.06}$	3			
Q0312−770		$0.1\pm^{0.6}_{0.2}$	$0.49\pm^{0.59}_{0.09}$	2			
Q0414-060		$0.5\pm^{1.7}_{0.3}$	$0.32\pm^{0.8}_{0.1}$	1			
Q0637−752	<34.8	$0.46\pm^{0.10}_{0.10}$	$0.98\pm^{0.05}_{0.05}$	3	$0.93\pm^{0.64}_{0.60}$	0.31	5
					$0.83\pm^{0.15}_{0.08}$	0.59	7
Q0804+761		$1.01\pm^{0.51}_{0.45}$	$2.00\pm^{0.46}_{0.41}$	1	$1.08\pm^{0.16}_{0.11}$	0.38	7
Q0837−120		$0.65\pm^{0.27}_{0.23}$	$1.74\pm^{0.31}_{0.19}$	1	$0.89\pm^{0.28}_{0.17}$	0.36	7
Q0844+349		$0.53\pm^{0.62}_{0.34}$	$0.49\pm^{0.13}_{0.03}$	1		<1.8	9
Q0915+165		$0.3\pm^{0.3}_{0.2}$	$1.28\pm^{0.16}_{0.09}$	1		0.5	9
Q0923+129		$0.7\pm^{0.4}_{0.4}$	$1.45\pm^{0.27}_{0.24}$	1			
Q1028+313	$7.5\pm^{2.0}_{2.1}$	$0.62\pm^{0.06}_{0.06}$	$0.76\pm^{0.07}_{0.07}$	3			
Q1100+772		$1.0\pm^{0.3}_{0.5}$	$0.69\pm^{0.19}_{0.13}$	2		<5.7	9
Q1116+215		$1.0\pm^{0.3}_{0.2}$	$0.68\pm^{0.12}_{0.06}$	2		<1.7	9
Q1137+660		$0.7\pm^{0.4}_{0.1}$	$0.39\pm^{0.08}_{0.02}$	2			
Q1146−037		$0.3\pm^{0.5}_{0.2}$	$0.56\pm^{0.26}_{0.07}$	2			
Q1202+281		$1.1\pm^{0.2}_{0.4}$	$1.19\pm^{0.27}_{0.25}$	2		<1.6	9
Q1211+143		$2.0\pm^{0.3}_{0.2}$	$5.5\pm^{0.8}_{0.7}$	4	$1.02\pm^{0.23}_{0.22}$	0.64	5
					$1.11\pm^{0.17}_{0.13}$	0.50	7
Q1219+755	$16.7\pm^{2.4}_{2.5}$	$0.78\pm^{0.03}_{0.03}$	$2.24\pm^{0.08}_{0.08}$	3	$1.17\pm^{0.67}_{0.60}$	0.45	5
					$0.91\pm^{0.09}_{0.09}$	0.57	7
Q1226+023	$48.9\pm^{3.3}_{3.3}$	$0.47\pm^{0.03}_{0.03}$	$9.8\pm^{0.2}_{0.2}$	3	$0.53\pm^{0.03}_{0.03}$	5.05	5
					$0.44\pm^{0.02}_{0.02}$	5.84	7
Q1244+026		$1.4\pm^{1.1}_{0.4}$	$0.78\pm^{0.11}_{0.12}$	1		<1.2	9
Q1307+085		$0.9\pm^{0.5}_{0.2}$	$0.81\pm^{0.12}_{0.06}$	2	$0.86\pm^{0.15}_{0.08}$	0.40	7
Q1351+695		$1.1\pm^{0.2}_{0.3}$	$3.7\pm^{0.3}_{0.3}$	1			
Q1352+183		$1.5\pm^{0.7}_{0.6}$	$0.56\pm^{0.04}_{0.09}$	1		0.10	7
Q1407+265		$1.2\pm^{0.9}_{0.2}$	$0.44\pm^{0.17}_{0.05}$	2		0.10	7

TABLE 3A—*Continued*

Object	0.2 keV flux (μJy)	1 keV Energy index	1 keV flux (μJy)	Ref	4 keV Energy index	4 keV flux (μJy)	Ref
Q1416−129		$0.9\pm^{0.5}_{0.5}$	$2.15\pm^{3.50}_{0.70}$	2	$0.10\pm^{0.10}_{0.10}$	0.35	7
Q1426+015	<50.4	$1.12\pm^{0.1}_{0.1}$	$3.05\pm^{0.09}_{0.09}$	3	$0.46\pm^{0.25}_{0.25}$	0.62	5
Q1501+106	$49.3\pm^{8.3}_{9.3}$	$0.93\pm^{0.04}_{0.04}$	$4.2\pm^{0.3}_{0.3}$	3	$0.42\pm^{0.16}_{0.16}$	1.04	5
Q1545+210		$0.8\pm^{0.3}_{0.5}$	$1.10\pm^{0.43}_{0.29}$	2		<1.4	9
Q1613+658	<20.3	$1.10\pm^{0.2}_{0.3}$	$1.40\pm^{0.04}_{0.04}$	3		$0.8\pm^{0.3}_{0.3}$	9
Q1635+119		$0.7\pm^{1.7}_{0.6}$	$0.35\pm^{0.83}_{0.09}$	1			
Q1704+608		$0.4\pm^{0.6}_{0.4}$	$0.15\pm^{0.06}_{0.03}$	1		<1.4	9
Q1721+343		$0.5\pm^{0.4}_{0.3}$	$1.93\pm^{0.73}_{0.20}$	2	$0.64\pm^{0.17}_{0.14}$	0.67	8
Q1803+676		$-0.2\pm^{0.4}_{0.3}$	$0.33\pm^{0.20}_{0.06}$	2			
Q2128-123		$0.5\pm^{0.7}_{0.4}$	$0.49\pm^{0.27}_{0.11}$	1			
Q2130+099	$22.8\pm^{5.4}_{5.3}$	$0.81\pm^{0.07}_{0.07}$	$0.91\pm^{0.08}_{0.08}$	3	$1.27\pm^{0.36}_{0.36}$	0.36	5
					$1.29\pm^{0.19}_{0.16}$	0.31	7
Q2135−147	<9.7	$0.73\pm^{0.05}_{0.05}$	$1.10\pm^{0.02}_{0.02}$	3	$0.83\pm^{0.33}_{0.31}$	0.57	5
					$0.86\pm^{0.08}_{0.08}$	0.78	7
Q2209+184		$0.8\pm^{0.5}_{0.5}$	$1.31\pm^{0.39}_{0.27}$	1			
Q2251-178		$0.4\pm^{0.6}_{0.6}$	$3.30\pm^{2.3}_{1.3}$	1			

REFERENCES.—(1) This paper; (2) Wilkes & Elvis 1987; (3) Masnou et al 1992; (4) Elvis et al. 1991; (5) Comastri et al. 1992; (6) Turner & Pounds 1989; (7) Williams et al. 1992; (8) Ohashi et al. 1992; (9) Della Ceca et al. 1990; (10) Turner & Pounds 1988; (11) Tananbaum et al. 1986; (12) Saxton et al. 1993.

1994ApJS...95....1E

TABLE 3B

OBSERVATIONAL DETAILS FOR NEW X-RAY POWER-LAW FITS[a]

Object	Sequence	Date	Exposure (s)	Gain	PHA Channels	Fit Counts	Count Rate	α	N_H	χ^2
Q0003+158	5360	1980 Jan 3	2211	11.7	2:9	560	0.11	2.20	21.38	9.9
		1980 Jun 15	2955	16.0						
Q0049+171	8431	1980 Jul 22	1373	15.5	2:10	488	0.36	1.16	20.94	9.6
Q0050+124	2632	1979 Jul 20	1552	14.6	2:10	555	0.36	1.85	21.18	6.7
Q0052+251	5334	1980 Jan 10	1472	16.4	2:11	351	0.24	1.16	20.90	8.7
Q0121-590	0523	1979 Nov 25	2566	12.6	1:9	5230	2.04	0.92	20.23	7.5
Q0414-060	0521	1979 Feb 25	4083	14.8	2:10	241	0.06	0.48	20.65	1.8
Q0804+761	5336	1980 Sep 27	1303	14.1	2:10	465	0.36	1.01	20.49	10.2
Q0837-120	8933	1981 Apr 21	5367	16.2	2:11	1717	0.32	0.66	20.61	12.6
Q0844+349	5337	1979 Oct 29	1659	18.7	2:12	1748	1.05	0.80	20.70	17.9
Q0915+165	3467	1979 Nov 6	1128	16.5	2:12	904	0.33	0.34	19.71	8.3
		1979 Nov 13	1622	19.5						
Q0923+129	6708	1980 May 7	2039	16.6	2:11	610	0.30	0.70	20.35	6.5
Q1244+026	8433	1980 Jul 13	1232	15.7	2:10	394	0.32	1.40	19.75	8.0
Q1351+695	10596	1981 Feb 9	1547	18.3	2:12	1486	0.96	1.06	20.20	12.6
Q1352+183	5377	1981 Jan 11	2669	12.8	1:9	418	0.16	1.54	20.30	3.0
Q1704+608	5688	1980 Jan 1-May 2	38084	16.6	2:11	1129	0.03	0.43	20.47	6.6
Q2128-123	8413	1980 May 9	5850	16.7	2:11	531	0.09	0.52	20.60	3.3
Q2209+184	8438	1980 Jun 15	1766	16.1	2:11	433	0.25	0.77	20.56	7.5
Q2251-178	2074	1979 May 22	1958	11.8	1:9	994	0.51	0.37	21.20	12.6

[a] For details of analysis, see Wilkes & Elvis 1987. For normalizations and errors on fit parameters, see Table 3A.

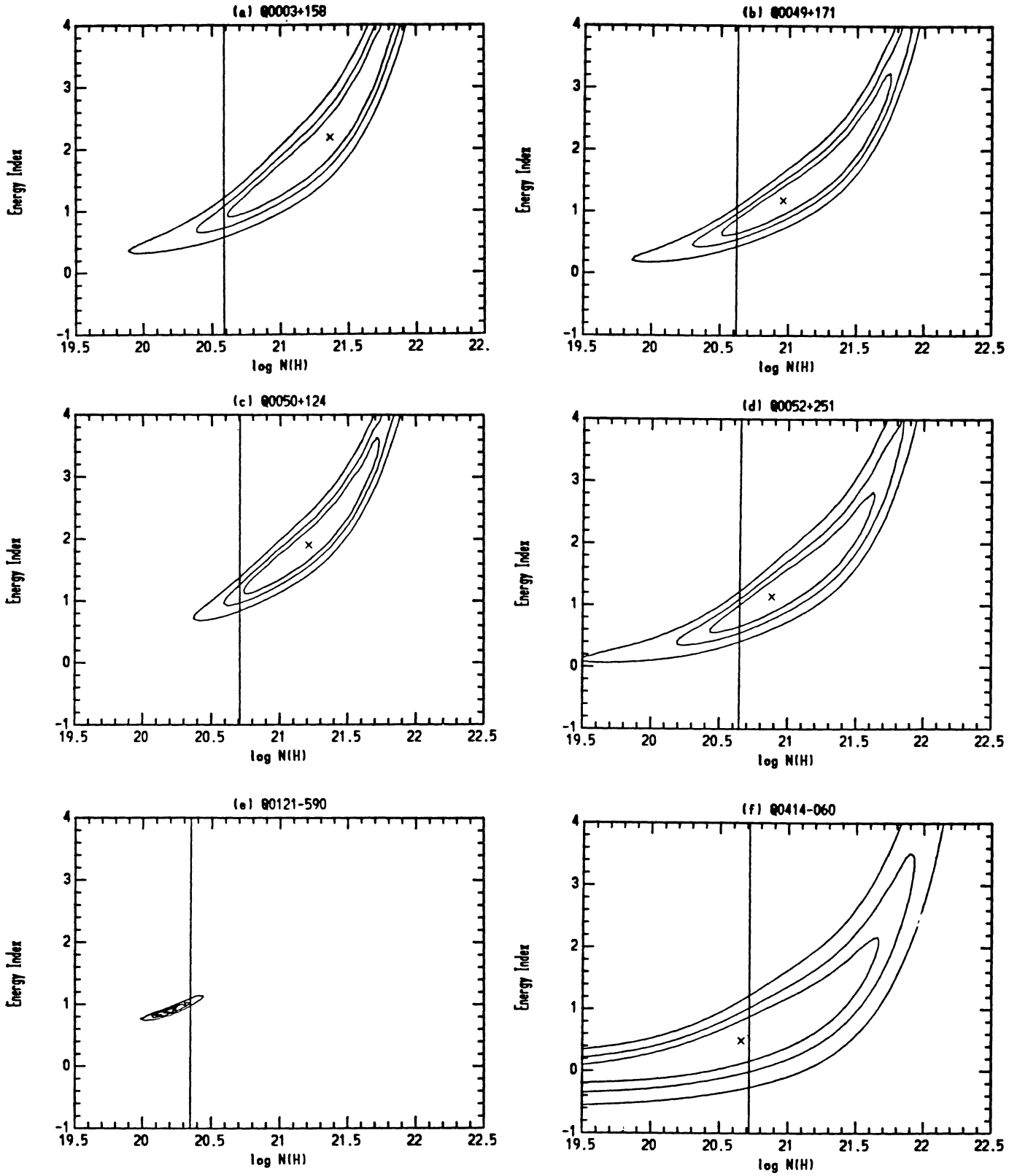

FIG. 3.—Contour plots of χ^2 goodness of fit as a function of fitted spectral index and foreground hydrogen column density. For details, refer to Wilkes and Elvis (1987). The vertical line indicates the actual galactic hydrogen column. The contours correspond to an increase of χ^2 above the minimum of 2.30, 4.61 and 9.21.

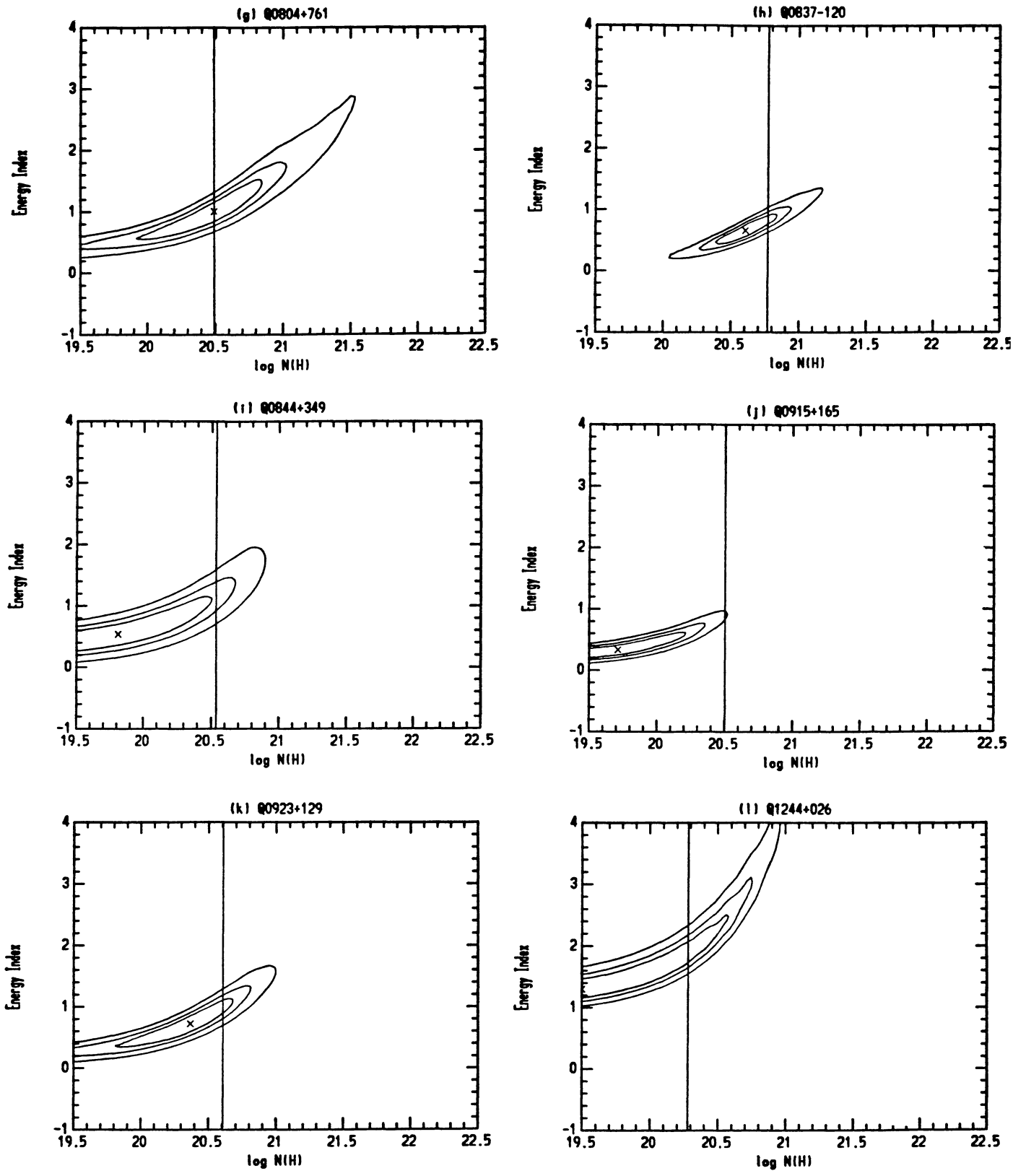

FIG. 3—*Continued*

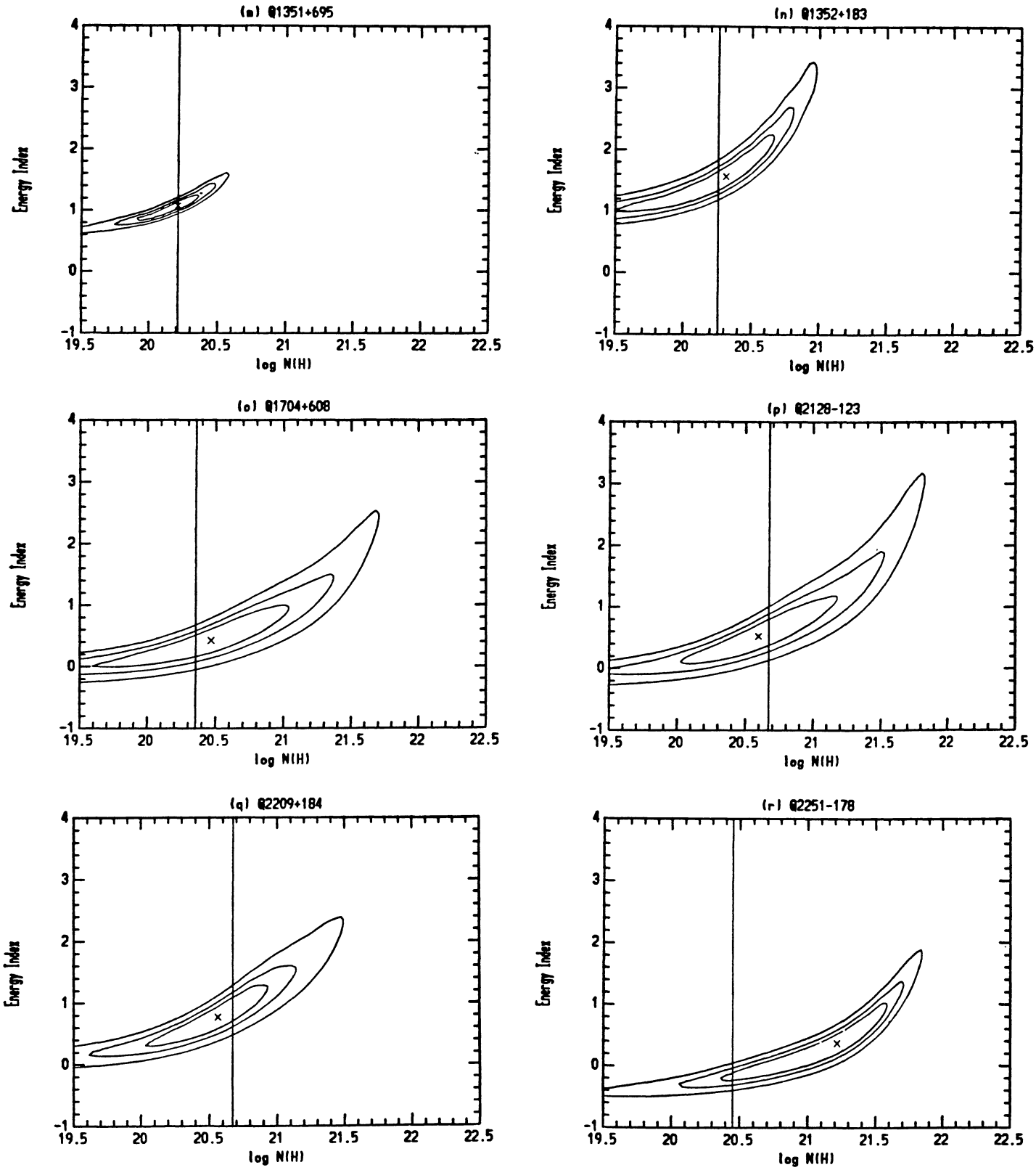

FIG. 3—*Continued*

TABLE A1

ADOPTED CONTINUUM BANDS

Central Wavelength	Wavelength Range (Å)	Central Wavelength	Wavelength Range (Å)
725	700-750	2600	2550-2650
775	750-800	2675	2650-2700
825	800-850	2950	2900-3000
875	850-900	3050	3000-3100
925	900-950	3150	3100-3200
975	950-1000	3250	3200-3300
1075	1050-1100	3800	3750-3850
1125	1100-1150	4500	4450-4550
1300	1275-1325	4600	4550-4650
1350	1325-1375	5200	5100-5300
1475	1450-1500	5400	5300-5500
1625	1600-1650	5600	5500-5700
1675	1650-1700	5800	5700-5900
1725	1700-1750	6000	5900-6100
1775	1750-1800	6175	6100-6250
1825	1800-1850	6875	6850-6900
2000	1950-2050	7000	6900-7100
2100	2050-2150	7200	7100-7300
2200	2150-2250	7400	7300-7500
2300	2250-2350	7600	7500-7700
2400	2350-2450	7800	7700-7900
2500	2450-2550	8000	7900-8100

NOTE.—Continuum spectrophotometry has been binned into the rest frame bandpasses defined by this table, chosen to avoid strong emission lines as described in the text.

that of WE87. Contour plots for the new fits are presented in Figure 3, and observational details are presented in Table 3(b); refer to WE87 for details.

Hard X-ray data are available for over half the sample, from *EXOSAT* ME (Turner & Pounds 1989; Comastri et al. 1992) and *Ginga* observations (Williams et al. 1992; Ohashi et al. 1992) and the corresponding power-law fits are also listed in Table 3. It should be borne in mind that these power-law fits are only a parameterization; in higher spectral resolution observations, bright AGNs often show a complex "Compton reflection" spectrum.

4.3. *Ultraviolet*

All of the 47 UVSX sample objects have been observed with both the long- and short-wavelength cameras on the *International Ultraviolet Explorer* between 1978 and 1989. A total of 19 exposures were made explicitly for this program, many of which were long-wavelength observations needed to fill in preexisting short-wavelength data. In addition, 108 further spectra were extracted from the Regional Data Analysis Facility archive. Both sets of data were analysed uniformly using the GEX Gaussian extraction algorithm (Urry & Reichert 1988) which is the most effective for our faint targets. Bad data points (reseau marks, cosmic-ray hits, and microphonic noise in the LWR) were removed interactively. We then averaged the ultraviolet flux within each of a set of wavelength bands chosen to avoid strong emission lines, converting the somewhat noisy spectra to a small set of relatively well determined continuum flux estimates.

For both ultraviolet and optical data (see next section), we defined continuum wavelength bands fixed in the rest frame of the object, with widths 50 Å wide shortward of 1900 Å, 100 Å wide shortward of 5000 Å, and 200 Å wide beyond that wavelength. Bands which overlapped a region of avoidance 8000 km s^{-1} to either side of strong broad lines or 2000 km s^{-1} to either side of strong narrow lines were omitted. We avoid the lines Lyα λ1215, O IV λ1402, C IV λ 1549, C III] λ1909, Mg II λ2798, Ne V λ3426, [O II] λ3727, [OIII] λ4959, 5007, Ne II λ3869/3968, O I λ6300, and the Balmer lines Hα–Hδ. Weak lines, the Balmer continuum, and the blended [Fe II] lines are not avoided and so these are included in our "continuum" fluxes. The continuum bands used may be found in Table A1; in the published version of this paper, Tables A1–A5 and B1–B47 are available only on the AAS CD-ROM disk, Vol. 3. Formatted, printed versions of the tables are available from the authors on request.

Table A2 lists the *IUE* exposures and the observed frequencies and fluxes corresponding to each continuum band. The fluxes are given as log (νf_ν/Jy Hz) in the observed frame, and that they are not corrected for foreground extinction. (1 Jy Hz = 10^{-23} ergs cm^{-2} s^{-1}). The first column on each page gives the rest frame wavelengths of each band. Then there is a header column for each object which gives the name of the object and the logarithm of the corresponding observed frequencies in Hz. This is followed by two columns for each observation giving the date of the observation (in the first row) followed by the logarithmic fluxes (log [$\nu F(\nu)$/1 Jy Hz]) in the first column and the uncertainties in the logarithmic fluxes in the second column. The uncertainties are 1 σ internal statistical errors derived from the scatter in the individual data points prior to binning.

TABLE B1

OBSERVED ENERGY DISTRIBUTION: Q0003+158

$\log(\nu_0)$ (Hz)	$\log(\nu_1)$ (Hz)	$\log(\nu_2)$ (Hz)	$\log(\nu F(\nu))$ (Jy Hz)	Date	Aperture (arcsec)	Filter or Detector	Instrument (or Telescope)	Reference (see notes)
9.70	9.70	9.70	$8.81^{+0.00}_{-0.00}$	1983 Nov	18.0	-	VLA	AJ098,1195
12.48	12.40	12.56	< 11.84	1983	300.0	IRAS4	IRAS(AO)	Table11
12.70	12.57	12.87	< 11.54	1983	300.0	IRAS3	IRAS(AO)	Table11
13.08	13.00	13.20	< 11.98	1983	300.0	IRAS2	IRAS(AO)	Table11
13.40	13.30	13.55	< 12.00	1983	300.0	IRAS1	IRAS(AO)	Table11
13.93	13.88	14.00	$11.47^{+0.08}_{-0.08}$	1988 Jan 31	5.0	L	MMT	Table9
14.13	14.11	14.19	$11.47^{+0.02}_{-0.02}$	1984 Sep 14	5.0	K	MMT	Table9
14.13	14.11	14.19	$11.51^{+0.02}_{-0.02}$	1988 Jan 31	5.0	K	MMT	Table9
14.13	14.11	14.19	$11.58^{+0.02}_{-0.02}$	1980 Oct 19	5.0	K	Hale	ApJS63,615
14.26	14.23	14.31	$11.56^{+0.02}_{-0.02}$	1984 Sep 14	5.0	H	MMT	Table9
14.26	14.23	14.31	$11.60^{+0.02}_{-0.02}$	1988 Jan 31	5.0	H	MMT	Table9
14.26	14.23	14.31	$11.68^{+0.02}_{-0.02}$	1980 Oct 19	5.0	H	Hale	ApJS63,615
14.38	14.35	14.45	$11.64^{+0.02}_{-0.02}$	1984 Sep 14	5.0	J	MMT	Table9
14.38	14.35	14.45	$11.70^{+0.02}_{-0.02}$	1988 Jan 31	5.0	J	MMT	Table9
14.38	14.35	14.45	$11.77^{+0.03}_{-0.03}$	1980 Oct 19	5.0	J	Hale	ApJS63,615
14.57	14.56	14.58	$11.87^{+0.01}_{-0.01}$	1980 Nov 14	15.0	AB	Hale	ApJS63,615
14.58	14.58	14.59	$11.86^{+0.01}_{-0.01}$	1980 Nov 14	15.0	AB	Hale	ApJS63,615
14.60	14.59	14.61	$11.89^{+0.01}_{-0.01}$	1980 Nov 14	15.0	AB	Hale	ApJS63,615
14.66	14.66	14.67	$11.94^{+0.00}_{-0.00}$	1980 Nov 14	15.0	AB	Hale	ApJS63,615
14.74	14.73	14.74	$12.05^{+0.01}_{-0.01}$	1980 Nov 14	15.0	AB	Hale	ApJS63,615
14.76	14.75	14.77	$12.11^{+0.00}_{-0.00}$	1980 Nov 14	15.0	AB	Hale	ApJS63,615
14.80	14.80	14.81	$12.13^{+0.00}_{-0.00}$	1980 Nov 14	15.0	AB	Hale	ApJS63,615
14.82	14.81	14.82	$12.13^{+0.00}_{-0.00}$	1980 Nov 14	15.0	AB	Hale	ApJS63,615
14.83	14.82	14.84	$12.12^{+0.00}_{-0.00}$	1980 Nov 14	15.0	AB	Hale	ApJS63,615
14.85	14.84	14.85	$12.13^{+0.02}_{-0.02}$	1980 Nov 14	15.0	AB	Hale	ApJS63,615
14.89	14.88	14.89	$12.13^{+0.00}_{-0.00}$	1980 Nov 14	15.0	AB	Hale	ApJS63,615
14.97	14.96	14.98	$12.29^{+0.06}_{-0.07}$	1982 Oct 21	15.0	-	LWR14452	RDAF
14.99	14.98	15.00	$12.12^{+0.03}_{-0.03}$	1982 Oct 21	15.0	-	LWR14452	RDAF
15.01	15.00	15.03	$12.09^{+0.03}_{-0.03}$	1982 Oct 21	15.0	-	LWR14452	RDAF
15.05	15.05	15.06	$12.04^{+0.03}_{-0.03}$	1982 Oct 21	15.0	-	LWR14452	RDAF
15.07	15.06	15.07	$12.07^{+0.03}_{-0.04}$	1982 Oct 21	15.0	-	LWR14452	RDAF
15.08	15.07	15.09	$12.05^{+0.03}_{-0.04}$	1982 Oct 21	15.0	-	LWR14452	RDAF
15.09	15.09	15.10	$12.16^{+0.03}_{-0.04}$	1982 Oct 21	15.0	-	LWR14452	RDAF
15.10	15.10	15.11	$12.04^{+0.05}_{-0.05}$	1982 Oct 21	15.0	-	LWR14452	RDAF
15.15	15.14	15.15	$12.22^{+0.04}_{-0.04}$	1982 Oct 21	15.0	-	LWR14452	RDAF
15.19	15.18	15.19	$12.08^{+0.03}_{-0.03}$	1982 Oct 20	15.0	-	SWP18342	RDAF
15.20	15.19	15.21	$12.12^{+0.02}_{-0.02}$	1982 Oct 20	15.0	-	SWP18342	RDAF
15.26	15.25	15.27	$12.06^{+0.03}_{-0.03}$	1982 Oct 20	15.0	-	SWP18342	RDAF
15.28	15.27	15.29	$12.14^{+0.02}_{-0.03}$	1982 Oct 20	15.0	-	SWP18342	RDAF
15.33	15.32	15.34	$12.03^{+0.02}_{-0.03}$	1982 Oct 20	15.0	-	SWP18342	RDAF
15.35	15.34	15.36	$12.03^{+0.02}_{-0.02}$	1982 Oct 20	15.0	-	SWP18342	RDAF
15.37	15.36	15.39	$12.06^{+0.02}_{-0.03}$	1982 Oct 20	15.0	-	SWP18342	RDAF
17.38	16.68	17.93	$11.53^{+0.72}_{-0.24}$	1980	360.0	IPC	IPC	Table3
17.99	17.68	18.38	< 12.16	1977 Dec 29		HEAO	HEAO/A2	ApJS72,471

The optical spectrophotometry for the probable high-redshift object PG 1407+265 (see discussion below) is also included in Table A2 for convenience, since the rest wavelengths for the observed optical spectrum lie in the ultraviolet.

4.4. *Optical*

Spectrophotometric observations for 14 objects were obtained with the Blue (~3200–6400 Å) Spectrograph or the FOGS (Faint Object Grism Spectrograph, ~4500–7500 Å) on the MMT. Blue spectrograph observations were made through a 5″ circular aperture at air mass below 1.4 to minimize light lost due to atmospheric dispersion. Objects were then reobserved at higher resolution through a 1″ × 3″ aperture. A nearby standard star was observed immediately before or after the quasar observation. For FOGS the large aperture used was 10″ × 20″, and the small one was a long slit 1″ wide. In all cases

the large-aperture observations were used to flux calibrate the accompanying, higher S/N, small-aperture observations yielding spectrophotometric data with ~5–10 Å spectral resolution. This secondary flux calbration was made by normalizing the line-free continuum of the small-aperture spectrum to that of the large-aperture spectrum. Since the amount of galaxy contamination in the lower luminosity objects depends on aperture size, subsequent galaxy subtraction was made with reference to the size of the large aperture. The equivalent widths of the emission lines are those of the central point source. They are not used in our energy distribution study, and we will discuss them no further here. The data were reduced in the standard manner, using IRAF. To ensure the photometric accuracy of these spectra, *BVRI* CCD photometric data were obtained on the FLWO (F. L. Whipple Observatory) 24 inch (0.6 m) telescope within 1 week of the MMT observations. Table 4A gives the *BVRI* photometry values, estimated within a 14″ aperture; the values have been corrected to the Johnson system in which Vega has magnitude +0.03. In Table 4B we also present photometry obtained at Mount Lemmon by one of us (R. C.). This photometry is in a 12″ aperture except for those dates marked with an asterisk which are in a 17″ aperture; see Cutri et al. (1985) for observational details. Table A3 lists the continuum fluxes observed with FOGS and MMT spectrograph, in the same format as Table A2. As with the *IUE* data, emission lines have been avoided by averaging the logarithmic fluxes in the line-free, rest frame continuum bands listed in Table A1.

Optical spectrophotometry for the 27 PG objects in our program were presented by N87. These data were already corrected for Galactic reddening; this correction is removed here using the same law used by those authors for consistency with our database (G. Neugebauer, private communication). This allows us, and others, to apply a uniform Galactic dereddening to all of our optical, ultraviolet, and soft X-ray data. Since the values of $E(B-V)$ used in N87 were not given in that paper, we tabulate them here (Table 5) for all the objects in that paper together with the values obtained using the prescription described below (§ 6.2).

Our figures and subsequent analysis also include optical data from Neugebauer et al. (1979), Sun & Malkan (1989), Treves et al. (1988), Sitko et al. (1982), Condon et al. (1981), Adam (1978, 1985), and McAlary et al. (1983). These data and other data from the literature discussed below are included in the full energy distribution tables (Tables B1–B47, on CD-ROM).

4.5. *Near-Infrared* (1–3.5 μm)

Table 6 records measurements of *JHKL* (1.2–3.5 μm) photometry obtained explicitly for this program at the MMT and the IRTF. The table gives the magnitudes and uncertainties, the date of observation, and the telescope and beam size used. All magnitudes were derived from comparisons with standard stars (Tokunaga 1984; Elias et al. 1982). Magnitudes are listed on the instrumental system, i.e., without color corrections, and correspond to a system in which Vega has magnitude zero in all bands. The MMT observations used a filter ("N34") centered at 3.4 μm with spectral bandwidth 0.2 μm instead of the standard "*L*" filter. The *J* filters used at the MMT and the IRTF have an effective wavelength of 1.25 μm (Willner et al. 1985). Chopper throws were 15″ or greater for all observations.

We have also included infrared photometry in the figures and analysis from Glass (1986), Rieke (1978), Condon et al. (1981), Hyland & Allen (1982), Sitko et al. (1982), Rudy, LeVan, & Rodriguez (1982), Ward et al. (1987), and N87.

4.6. *Far-Infrared* (≥10 μm)

Table 7 gives measurements at *N* and *Q* (10 and 20 μm) made at IRTF and the United Kingdom Infrared Telescope (UKIRT) explicitly for this program. At the IRTF, the CT1 bolometer was used with a 6″ beam and an east-west chopper throw of 30″. At UKIRT the UKT8 system was used with an 8″ beam and a 20″ east-west chopper throw. Magnitudes were derived as described above.

The *Infrared Astronomical Satellite* (*IRAS*; Neugebauer et al. 1984) surveyed the sky in 1983 at far infrared wavelengths (12–100 μm). We have determined fluxes or upper limits at the positions of each of our sources. Where pointed Additional Observations (AO) were made, these were used; otherwise "lineadd" (LA) estimates were made from the survey scans. This procedure allows a better estimate of the local background and uncertainties in a particular measurement than the "coadd" maps. The coadded survey maps were used to check for the presence of contaminating cirrus. The results are listed in Table 8; they are consistent with the results of Neugebauer et al. (1986) and Sanders et al. (1989) where we have objects in common (for the UVSX sample, six objects are previously unpublished). In some cases, the 100 μm upper limits are rather poor because of the presence of cirrus in the region of the source. Upper limits (3 σ) are listed for each source when no detection was made in the *IRAS* bands.

4.7. *Radio and Millimeter*

We have gathered core radio fluxes at 5 GHz for the UVSX sample from the literature (Table 9). The PG sample study with the VLA by Kellerman et al. (1989) was given preference over other references in the calculation of radio-loudness. By "core" we mean the flat spectrum compact component which appears to be physically distinct from the steep spectrum diffuse emission. Since this steep spectrum emission can itself be relatively compact in angular size (e.g., 3C 48), we do not use a fixed angular size to define the core, although in practice because detailed spectral information is not usually available we often use flux unresolved within a 1″ beam as our criterion. In the absence of spectral data this is an upper limit on the flat spectrum 5 GHz core flux. Beam sizes are given in the table. In Table 9 we also list measurements at other frequencies and estimates of the flux of any extended radio source associated with the object.

Millimeter-wave data or upper limits are available for about half the sample (Table 10). Only III Zw 2 and 3C 273 are strong millimeter emitters, but six other sources have weak detections.

5. CORRECTIONS

5.1. *Magnitude Scales*

To include the optical and near-infrared photometric data in the energy distributions, we have adopted for each band an

TABLE 4A

OPTICAL CCD PHOTOMETRY

Object	V	B-V	V-R	R-I	Date
		UVSX SAMPLE QUASARS			
Q0003+199	13.838 ±0.040	0.290 ±0.027	0.532 ±0.017	0.178 ±0.064	1985 Sep 16
Q0007+106	15.155 ±0.071	0.507 ±0.041	0.582 ±0.035	0.489 ±0.039	1986 Sep 28
Q0026+129	15.314 ±0.040	0.363 ±0.027	0.243 ±0.017	0.624 ±0.064	1985 Sep 16
	15.325 ±0.053	0.395 ±0.061	0.253 ±0.035	0.603 ±0.018	1986 Sep 26
Q0050+124	14.083 ±0.071	0.509 ±0.041	0.470 ±0.035	0.336 ±0.039	1986 Sep 28
Q0054+144	11.726 ±0.040	0.280 ±0.027	0.209 ±0.017	0.209 ±0.064	1985 Sep 16
	11.811 ±0.053	0.291 ±0.061	0.252 ±0.035	0.201 ±0.018	1986 Sep 26
Q0134+329	16.007 ±0.040	0.403 ±0.027	0.452 ±0.017	0.223 ±0.064	1985 Sep 16
Q0205+024	15.549 ±0.053	0.276 ±0.061	0.163 ±0.011	0.582 ±0.047	1986 Sep 25
Q0414–060	16.095 ±0.032	0.287 ±0.009	0.132 ±0.017	0.138 ±0.013	1986 Feb 03
Q0804+762	14.708 ±0.032	0.321 ±0.009	0.318 ±0.017	0.481 ±0.013	1986 Feb 03
Q0844+349	14.500 ±0.053	0.334 ±0.061	0.479 ±0.035	0.247 ±0.018	1986 Sep 26
Q0923+129	14.615 ±0.069	0.569 ±0.028	0.581 ±0.027	0.435 ±0.023	1986 May 13
Q0923+392	17.015 ±0.052	0.057 ±0.045	0.226 ±0.020	0.417 ±0.012	1985 May 14
Q1028+313	15.920 ±0.055	0.316 ±0.027	0.240 ±0.020	0.679 ±0.016	1985 May 13
Q1116+215	14.725 ±0.069	0.129 ±0.028	0.135 ±0.027	0.606 ±0.023	1986 May 13
Q1137+660	15.951 ±0.030	0.121 ±0.037	0.187 ±0.026	0.215 ±0.029	1986 May 14
Q1146–037	18.115 ±0.030	-0.181 ±0.037	0.687 ±0.026		1986 May 14
Q1202+281	15.918 ±0.055	0.254 ±0.027	0.126 ±0.020	0.631 ±0.016	1985 May 13
Q1211+143	14.252 ±0.052	0.267 ±0.045	0.386 ±0.020	0.274 ±0.012	1985 May 14
Q1219+755	14.828 ±0.041	0.410 ±0.032	0.518 ±0.028	0.359 ±0.058	1985 May 11
	15.032 ±0.069	0.464 ±0.028	0.550 ±0.027	0.365 ±0.023	1986 May 13
Q1226+023	12.810 ±0.069	0.176 ±0.028	0.096 ±0.027	0.584 ±0.023	1986 May 13
Q1307+085	15.115 ±0.069	0.208 ±0.028	0.139 ±0.027	0.555 ±0.023	1986 May 13
Q1407+265	15.740 ±0.030	0.334 ±0.037	0.197 ±0.026	0.196 ±0.029	1986 May 14
Q1416–129	16.101 ±0.052	0.319 ±0.045	0.235 ±0.020	0.902 ±0.012	1985 May 14
Q1426+015	14.547 ±0.055	0.313 ±0.027	0.426 ±0.020	0.432 ±0.016	1985 May 13
	14.670 ±0.069	0.349 ±0.028	0.473 ±0.027	0.432 ±0.023	1986 May 13
Q1501+106	14.265 ±0.069	0.345 ±0.028	0.559 ±0.027	0.193 ±0.023	1986 May 13
Q1545+210	16.023 ±0.041	0.257 ±0.032	0.350 ±0.028	0.519 ±0.058	1985 May 11
	16.015 ±0.069	-0.023 ±0.028	0.390 ±0.027	0.551 ±0.023	1986 May 13
Q1613+658	14.915 ±0.055	0.436 ±0.027	0.292 ±0.020	0.759 ±0.016	1985 May 13
Q1635+119	16.796 ±0.052	0.478 ±0.045	0.418 ±0.020	0.735 ±0.012	1985 May 14
Q1721+343	15.465 ±0.055	0.120 ±0.027	0.212 ±0.020	0.597 ±0.016	1985 May 13
Q1803+676	15.892 ±0.041	0.345 ±0.032	0.248 ±0.028	0.783 ±0.058	1985 May 11
Q2128–123	15.965 ±0.071	0.180 ±0.041	0.172 ±0.035	0.282 ±0.039	1986 Sep 28
Q2130+099	14.743 ±0.041	0.366 ±0.032	0.540 ±0.028		1985 May 11
	14.674 ±0.053	0.296 ±0.061	0.477 ±0.035	0.219 ±0.018	1986 Sep 26
Q2135–147	15.648 ±0.040	0.376 ±0.027	0.266 ±0.017	0.679 ±0.064	1985 Sep 16
	15.775 ±0.053	0.031 ±0.061	0.460 ±0.035	0.705 ±0.018	1986 Sep 26
Q2209+184	15.444 ±0.052	0.652 ±0.045	0.545 ±0.020		1985 May 14
	15.457 ±0.040	0.650 ±0.027	0.616 ±0.017	0.295 ±0.064	1985 Sep 16
	15.405 ±0.053	0.603 ±0.061	0.592 ±0.035	0.404 ±0.018	1986 Sep 26
		OTHER "IPC" QUASARS			
Q0133+207	17.438 ±0.071	0.267 ±0.041	0.314 ±0.035	0.502 ±0.039	1986 Sep 28
Q1012+008	15.586 ±0.069	0.425 ±0.028	0.261 ±0.027	0.648 ±0.023	1986 May 13
Q1121+422	16.252 ±0.030	0.331 ±0.037	0.221 ±0.026	0.416 ±0.029	1986 May 14
Q1217+023	16.754 ±0.052	0.163 ±0.045	0.414 ±0.020	0.854 ±0.012	1985 May 14
Q1435–067	16.009 ±0.069	0.123 ±0.028	0.236 ±0.027	0.758 ±0.023	1986 May 13
Q2112+059	15.774 ±0.056	0.288 ±0.021	0.414 ±0.011	0.260 ±0.047	1986 Sep 25
	15.854 ±0.027	0.167 ±0.037	0.396 ±0.004	0.375 ±0.059	1986 Sep 29
Q2120+168	18.283 ±0.027	0.296 ±0.037	-1.303 ±0.035	0.333 ±0.039	1986 Sep 28
Q2214+139	14.982 ±0.056	0.613 ±0.021	0.610 ±0.011	0.310 ±0.047	1986 Sep 25
	15.066 ±0.027	0.584 ±0.037	0.635 ±0.004	0.380 ±0.059	1986 Sep 29
Q2233+134	16.707 ±0.071	-0.011 ±0.041	0.284 ±0.035	0.408 ±0.039	1986 Sep 28
	16.747 ±0.027	0.025 ±0.037	0.272 ±0.011	0.106 ±0.047	1986 Sep 25
Q2251+113	15.739 ±0.056	0.209 ±0.021	0.423 ±0.011	0.517 ±0.047	1986 Sep 25
Q2254+024	17.959 ±0.027	0.083 ±0.037	0.456 ±0.035	0.463 ±0.039	1986 Sep 28
Q2304+042	15.496 ±0.053	0.825 ±0.061	0.743 ±0.035	0.441 ±0.018	1986 Sep 26

TABLE 4B

OPTICAL PHOTOMETRY: *UBVRI* DATA FROM MOUNT LEMMON

Object	U	B	V	R	I	Date
Q0049+171	16.20	17.02	16.57	15.74	15.51	1987 Jan 25
Q0414−060	15.91	16.47	16.16	15.82	15.46	1981 Oct 24*
	15.92	16.43	16.15	15.77	15.50	1982 Oct 25*
	15.79	16.45	16.13	15.90	15.65	1981 Nov 23
	16.15	16.75	16.57	16.05	15.74	1982 Dec 19
	16.18	16.68	16.28	16.14	16.81	1982 Dec 20
	16.17	16.78	16.40	16.09	16.84	1982 Dec 21
	16.01	16.59	16.37	16.03	15.80	1983 Feb 15
	15.81	16.31	16.08	15.81	15.51	1984 Oct 28
	15.99	16.62	16.24	16.06	15.84	1987 Jan 24
	16.00	16.51	16.20	15.95	15.65	1987 Jan 25
Q0837−120	15.47	16.34	16.26	15.82	15.26	1985 Apr 12
	16.24	16.95	16.70	16.48	15.61	1987 Jan 24
	16.21	16.92	16.62	16.54		1987 Jan 25
Q1211+143	13.54	14.40	14.07	13.60	13.43	1985 Apr 12
	13.71	14.46	14.19	13.66	13.51	1987 Jan 25
Q1226+023	11.74	12.70	12.54	12.24	11.86	1982 May 29
	11.72	12.73	12.53	12.27	11.86	1982 Jun 13
	11.81	12.72	12.51	12.25	11.84	1982 Jun 15
	11.83	12.68	12.50	12.19	11.78	1982 Jul 1
	11.73	12.63	12.46	12.17	11.70	1982 Jul 2
	11.84	12.72	12.50	12.16	11.70	1983 Feb 21
	12.14	13.08	12.83	12.57	12.12	1985 Apr 12
	12.09	12.90	12.73	12.47	12.00	1987 Jan 25
Q1416−129	15.46	16.46	16.10	15.57	15.12	1985 Apr 12
Q1426+015	13.77	14.75	14.49	13.98	13.69	1985 Apr 12
Q2128-123	15.93	16.43	16.22	16.17	15.33	1981 Oct 26*
	15.78	16.31	16.23	16.02	15.25	1981 Nov 21*
	15.69	16.29	16.17	15.95	15.27	1982 Jun 14
			15.71			1983 Oct 12
	15.11	15.73	15.59	15.82	14.79	1984 Oct 29
Q2130+099	14.09	14.94	14.67	14.09	13.70	1986 Sep 26
Q2135-147	15.05	15.83	15.65	15.20	14.61	1981 Oct 26*
	15.17	15.82	15.66	15.24	14.50	1981 Nov 21*
	15.27	16.05	15.82	15.29	14.73	1982 Jun 16
	15.24	15.98	15.82	15.36	14.78	1982 Jul 2
	15.17	15.97	15.79	15.27	14.57	1984 Oct 29

* Photometry in 17″ aperture. All other observations were made in a 12″ aperture.

absolute zero point appropriate for a locally flat energy distribution. The wavelengths for which these zero points remain the best estimate of the energy distribution even when the local spectrum is not flat are slightly different from the usual nominal wavelengths of the filters, but the uncertainties are such that we have retained the nominal wavelengths. In Table 11 we tabulate for each band both the flux of Vega at the nominal wavelength and the flux at the nominal wavelength of an object with a flat energy distribution and the same magnitude as Vega. We used the Hayes (1985) calibration of Vega, extended to other wavelengths by matching to a Kurucz (1979) theoretical model (9400 K, log g = 3.95). We convolved the Vega energy distribution with atmospheric transmission curves from Mountain et al. (1985) and Manduca & Bell (1979), filter shapes from Tokunaga (1986) for the infrared IRTF filters, and Johnson (1965) and Azusienis & Straizys (1969) for the optical bands to obtain absolute calibrations corresponding to $\nu F(\nu)$ = constant. The color corrections corresponding to the difference of the Vega spectrum from a flat energy distribution are of order 10% for the optical bands. The results are not very sensitive to the details of the transmission curves; calculations using simple rectangular bandpasses gave results which agreed to within 1% or less except for the U filter. In the infrared the color corrections are smaller (of order 5%), and the uncertainties due to atmospheric transmission and the sensitivity to the shape of the bandpass are both larger and comparable to the correction. Nevertheless, we adopt our best estimates as described above. The zero point of the Hayes calibration is somewhat high relative to earlier work, and in particular AB79 fluxes (Oke & Gunn 1983) need to be corrected upward by 1.5% to agree with it, although this change is insignificant compared to other uncertainties in the energy distributions. It should also be noted that since the optical photometry of Table 12 is on the Johnson system, it should be corrected for the nonzero magnitude of Vega (+0.03 mag) before these zero points are applied.

5.2. *Extinction Corrections*

Corrections for foreground (Galactic) extinction are important in the optical, UV, and soft X-ray. The X-ray spectral fits of Table 3 already include correction for the line-of-sight absorption column as discussed above. Separately, a single ex-

TABLE 5

ADOPTED $E(B-V)$ VALUES FOR PG QUASARS

Object PG	E(B-V) (N87)	E(B-V) (This paper)	Object PG	E(B-V) (N87)	E(B-V) (This paper)	Object PG	E(B-V) (N87)	E(B-V) (This paper)
0002+05	0.18	0.08	1115+40	0.04	0.04	1407+26	0.02	0.03
0003+15	0.10	0.06	1116+21	0.02	0.03	1411+44	0.07	0.02
0007+10	0.17	0.12	1119+12	0.03	0.05	1415+45	0.07	0.02
0014+16	0.21	0.08	1121+42	0.01	0.05	1416−12	0.35	0.14
0026+12	0.16	0.10	1126−04	0.07	0.09	1426+01	0.16	0.05
0043+03	0.03	0.06	1138+04	0.05	0.04	1427+48	0.00	0.04
0044+03	0.03	0.06	1148+54	0.01	0.02	1435−06	0.18	0.10
0049+17	0.11	0.09	1151+11	0.04	0.05	1440+35	0.00	0.02
0052+25	0.11	0.09	1202+28	0.00	0.03	1444+40	0.00	0.03
0117+21	0.11	0.10	1206+45	0.05	0.03	1448+27	0.00	0.05
0157+00	0.08	0.05	1211+14	0.03	0.06	1501+10	0.13	0.04
0804+76	0.12	0.06	1216+06	0.05	0.03	1512+37	0.03	0.03
0832+25	0.11	0.07	1222+22	0.04	0.04	1519+22	0.04	0.08
0838+77	0.04	0.05	1226+02	0.03	0.04	1522+10	0.10	0.06
0844+34	0.07	0.07	1229+20	0.02	0.05	1534+58	0.01	0.05
0906+48	0.03	0.04	1241+17	0.03	0.04	1535+54	0.01	0.03
0923+19	0.07	0.08	1244+02	0.05	0.04	1543+48	0.03	0.03
0931+43	0.04	0.03	1247+26	0.05	0.02	1545+21	0.11	0.08
0935+41	0.04	0.03	1248+40	0.12	0.03	1552+08	0.07	0.07
0946+30	0.04	0.04	1254+04	0.02	0.04	1612+26	0.07	0.08
0947+39	0.04	0.03	1259+59	0.03	0.03	1613+65	0.00	0.05
0953+41	0.04	0.03	1302−10	0.11	0.07	1617+17	0.18	0.09
1001+05	0.07	0.04	1307+08	0.05	0.04	1626+55	0.02	0.04
1004+13	0.04	0.07	1309+35	0.00	0.02	1630+37	0.05	0.02
1008+13	0.12	0.08	1310−10	0.06	0.06	1634+70	0.14	0.11
1011−04	0.03	0.07	1329+41	0.05	0.02	1700+51	0.02	0.05
1012+00	0.04	0.06	1333+17	0.00	0.04	1704+60	0.04	0.05
1048−09	0.11	0.06	1338+41	0.05	0.02	1718+48	0.07	0.05
1048+34	0.01	0.04	1351+23	0.00	0.03	2112+05	0.26	0.13
1049−00	0.07	0.08	1351+64	0.03	0.05	2130+09	0.13	0.08
1100+77	0.09	0.06	1352+18	0.00	0.04	2209+18	0.16	0.10
1103−00	0.06	0.08	1352+01	0.14	0.04	2233+13	0.11	0.10
1112+43	0.01	0.03	1354+21	0.04	0.04	2251+11	0.15	0.11
1114+44	0.04	0.04	1402+26	0.02	0.03	2302+02	0.25	0.10
1115+08	0.04	0.07	1404+22	0.02	0.04	2344+09	0.26	0.10
						2349−01	0.11	0.07

NOTE.—Dereddening values used in Neugebauer et al. 1987. These values were used to rederive the as-observed fluxes for the PG objects so that we could apply our own dereddening correction.

tinction correction (which may correspond to a different hydrogen column) is applied to the remainder of the data, using an extinction law based on that of Savage & Mathis (1979) in the visible and ultraviolet, and Rieke & Lebofsky (1985) in the infrared beyond 3 μm (see Table A4). The magnitude of the correction has been estimated from the Galactic neutral hydrogen column by assuming a fixed conversion of $N(\mathrm{HI})/E(B-V) = 5.0 \times 10^{21}$ cm^2 mag^{-1} (Burstein & Heiles 1978). The Galactic H I column (Table 1) has been accurately measured with a narrow beam and good stray radiation corrections in all but a few cases using the 140 foot (43 m) Green Bank radio telescope (Elvis et al. 1989). The value for 3C 273 was taken from Dickey, Salpeter, & Terzian (1978). In the three remaining cases it has been estimated from Heiles & Cleary (1979) or Stark et al. (1984, 1992).

5.3. *Cosmological Model*

We have adopted a standard Friedmann-Robertson-Walker cosmological model with Ω_0 ($=2q_0$) = 1 and H_0 = 50km s^{-1} Mpc^{-1}. After Galactic reddening corrections were applied, the data were blueshifted to the rest frame. Since in the rest frame we are working with the complete energy distributions, no k-corrections and no assumptions about the intrinsic spectrum are required.

5.4. *Host Galaxies*

Although the overall energy output of our sample objects is dominated by the active nucleus, in the near infrared the host galaxy often makes the dominant contribution.

We have constructed a host galaxy spectral template SED based on the Sbc galaxy model of Coleman, Wu, & Weedman (1980). We have extended this to the near-infrared using *JHKL* colors characteristic of both spirals and ellipticals (Frogel 1985; de Vaucouleurs & Longo 1988). The adopted starlight template is listed in Table A5 and shown in Figure 4. Figure 4 clearly shows that the inflection in the quasar energy distribution occurs in the same spectral region where the galaxy starlight dominates, emphasizing the importance of making a correction for this starlight. The quasar rapidly dominates as one moves toward the optical/UV, so the difference between spiral and elliptical templates is unimportant except in determining the normalization. For this reason we have

TABLE 6

NEAR-INFRARED PHOTOMETRY[b]

Object	J 1.2μm	H 1.65μm	K 2.2μm	3.4μm $\Delta\lambda = 0.2\mu$m	L′ 3.8μm	Date UT	Telescope	Beam arcsec
				UVSX SAMPLE QUASARS				
Q0003+158	14.89±0.06	14.30±0.06	13.78±0.06			1984 Sep 14	MMT	5″
	14.76±0.05	14.20±0.05	13.68±0.05	12.42±0.19		1988 Jan 31	MMT	5″
Q0003+199	12.36±0.06	11.41±0.06	10.30±0.06	8.77±0.07		1984 Sep 14	MMT	5″
Q0007+106	13.41±0.05	12.51±0.05	11.34±0.05	9.89±0.05		1985 Sep 27	MMT	5″
Q0026+129	13.86±0.06	13.30±0.06	12.47±0.06	10.87±0.20		1984 Sep 14	MMT	5″
	14.00±0.05	13.52±0.06	12.49±0.05	11.01±0.11		1985 Sep 26	MMT	5″
Q0049+171	14.73±0.06	13.98±0.06	13.07±0.06			1984 Sep 14	MMT	5″
	15.52±0.05	14.79±0.05	13.94±0.05	$12.45^{+0.46}_{-0.32}$		1988 Jan 31	MMT	5″
	15.11±0.09	14.45±0.04	13.96±0.05			1986 Sep 15	Mt. Lemmon	12″
	14.94±0.09	14.34±0.04	13.33±0.04			1986 Sep 27	Mt. Lemmon	12″
Q0050+124	12.17±0.06	11.13±0.06	9.90±0.06	8.35±0.06		1984 Sep 14	MMT	5″
Q0054+144	14.08±0.06	13.21±0.06	12.11±0.06	10.65±0.12		1984 Sep 14	MMT	5″
	14.08±0.05	13.24±0.05	12.01±0.05	10.43±0.08		1985 Sep 26	MMT	5″
Q0134+329	14.67±0.06	13.90±0.06	12.81±0.06			1984 Sep 14	MMT	5″
	14.67±0.05	13.97±0.05	12.80±0.05	$12.01^{+0.86}_{-0.47}$		1985 Sep 26	MMT	5″
	14.62±0.05	13.85±0.05	12.74±0.05	11.24±0.09		1985 Sep 27	MMT	5″
Q0205+024	14.32±0.06	13.62±0.06	12.62±0.06			1984 Sep 14	MMT	5″
	14.40±0.05	13.70±0.05	12.61±0.05	11.20±0.09		1985 Sep 27	MMT	5″
Q0414-060	15.04±0.10	14.67±0.06	14.83±0.56			1981 Oct 24	Mt. Lemmon	12″
	14.66±0.06	14.64±0.07	13.92±0.11			1981 Oct 25	Mt. Lemmon	12″
	15.22±0.06	14.80±0.06	14.06±0.05			1982 Dec 19	Mt. Lemmon	12″
	15.16±0.06	14.78±0.05	14.08±0.07			1982 Dec 20	Mt. Lemmon	12″
	14.86±0.07	14.80±0.05	14.08±0.04			1982 Dec 21	Mt. Lemmon	12″
	14.71±0.07	14.85±0.06	13.96±0.05			1983 Feb 15	Mt. Lemmon	12″
	14.79	14.72	13.99			1984 Oct 28	Mt. Lemmon	8″
	14.88±0.07	14.57±0.05	13.94±0.05			1985 Sep 23	Mt. Lemmon	12″
Q0804+761	13.41±0.06	12.49±0.06	11.18±0.06	9.36±0.17		1984 Sep 14	MMT	5″
	13.38±0.05	12.47±0.05	11.20±0.05	9.60±0.05		1986 Feb 23	MMT	5″
Q0837-120	14.50±0.05	13.74±0.05	12.63±0.05			1985 Apr 12	Mt. Lemmon	12″
	14.83±0.06	14.07±0.06	12.86±0.06	11.30±0.09		1988 Feb 1	MMT	5″
Q0844+349	13.28±0.04	12.63±0.04	11.89±0.04		10.30±0.04	1988 Apr 25	IRTF	6″
Q0923+129	12.88±0.05	12.02±0.05	11.32±0.05			1985 May 2	MMT	5″
	12.86±0.06	12.05±0.05	11.33±0.06	10.07±0.06		1985 May 4	MMT	5″
	12.77±0.04	11.92±0.04	11.29±0.04		10.07±0.05	1986 Feb 4	IRTF	6″
	12.57±0.07	11.72±0.07	11.06±0.07			1986 Feb 27	MMT	9″
Q1028+313	14.48±0.05	13.85±0.05	12.92±0.05	11.33±0.14		1985 Jun 2	MMT	9″[a]
		13.93±0.05		11.87±0.15		1985 Jun 3	MMT	5″
Q1100+772	14.66±0.05	13.93±0.05	12.92±0.05	11.36±0.11		1988 Feb 1	MMT	5″
Q1116+215	13.70±0.04	12.73±0.04	11.61±0.04		10.01±0.04	1986 Feb 4	IRTF	6″
	13.53±0.07	12.66±0.07	11.42±0.07			1986 Feb 27	MMT	9″
	13.48±0.05	12.51±0.05	11.30±0.05	9.70±0.05		1988 Apr 8	MMT	5″
	13.45±0.04	12.44±0.04	11.35±0.04		9.51±0.04	1988 Apr 25	IRTF	6″
Q1137+660	14.93±0.05	14.75±0.05	13.86±0.05		11.95±0.08	1986 Feb 4	IRTF	6″
Q1146−037	16.35±0.05	15.49±0.05	14.68±0.05			1986 Feb 23	MMT	9″
	16.42±0.13	15.77±0.08	14.78±0.05			1988 Apr 25	IRTF	6″
Q1202+281	14.87±0.05	14.05±0.05	12.77±0.05	11.14±0.13		1985 May 4	MMT	5″
	14.95±0.04	13.96±0.04	12.78±0.04		11.16±0.05	1986 Feb 4	IRTF	6″
Q1211+143	12.97	12.19	11.04			1985 Apr 11	Mt. Lemmon	12″
	12.97	12.24	11.10			1985 Apr 12	Mt. Lemmon	12″
	13.25±0.04	12.36±0.04	11.21±0.04		9.49±0.04	1986 Feb 4	IRTF	6″
	13.10±0.05	12.32±0.05	11.16±0.05	9.56±0.06		1986 Feb 23	MMT	9″
	13.27±0.04	12.47±0.04	11.35±0.04		9.27±0.04	1988 Apr 25	IRTF	6″
	13.45±0.05	12.56±0.05	11.36±0.05	9.73±0.07		1988 Apr 8	MMT	5″
Q1219+755	13.18±0.05	12.40±0.05	11.60±0.05	10.46±0.09		1985 Jun 1	MMT	9″
	13.24±0.07	12.40±0.07	11.58±0.07			1986 Feb 27	MMT	9″
Q1226+023	11.71±0.06	10.84±0.06	9.71±0.06	8.23±0.06		1988 Apr 7	MMT	5″
	11.78±0.04	10.87±0.04	9.78±0.04		7.91±0.04	1988 Apr 25	IRTF	6″
Q1244+026	14.69±0.06	13.86±0.04	13.09±0.04		11.74±0.08	1983 Feb 6	IRTF	6″
Q1307+085	14.12±0.06	13.56±0.04	12.63±0.04		10.81±0.06	1988 Apr 25	IRTF	6″
	14.08±0.05	13.51±0.05	12.56±0.05	11.19±0.12		1988 Apr 8	MMT	5″
Q1352+183	14.97±0.05	14.22±0.05	13.01±0.05	11.43±0.09		1986 Feb 23	MMT	5″
Q1407+265	14.86±0.06	14.49±0.06	13.84±0.08	12.21±0.17		1988 Apr 7	MMT	5″
	14.85±0.04	14.39±0.05	13.88±0.05		11.74±0.06	1988 Apr 25	IRTF	6″
	14.86±0.06	14.49±0.06	13.84±0.07	12.21±0.16		1988 Apr 7	MMT	5″
Q1416−129	14.62±0.05	14.01±0.05	13.02±0.06		12.05±0.22	1983 Feb 6	IRTF	6″
	14.44±0.03	13.73±0.03	12.52			1985 Apr 12	Mt. Lemmon	12″
	13.87±0.05	14.05±0.05	12.95±0.05		11.25±0.09	1986 Feb 5	IRTF	6″
	14.87±0.05	14.03±0.05	12.81±0.05			1988 Apr 8	MMT	5″
	14.88±0.07	13.97±0.05	12.83±0.04		11.01±0.04	1988 Apr 25	IRTF	6″
Q1426+015	13.30±0.05	12.50±0.04	11.54±0.04		10.24±0.09	1983 Feb 6	IRTF	6″
	13.03	12.23	11.69			1985 Apr 12	Mt. Lemmon	12″
	13.13±0.06	12.27±0.06	11.21±0.06	9.76±0.06		1985 May 5	MMT	5″
	13.09±0.07	12.19±0.07	11.18±0.07			1986 Feb 27	MMT	9″
	13.43±0.04	12.59±0.04	11.59±0.04		9.73±0.04	1988 Apr 25	IRTF	6″

TABLE 6—*Continued*

Object	J 1.2μm	H 1.65μm	K 2.2μm	3.4μm $\Delta\lambda = 0.2\mu$m	L′ 3.8μm	Date UT	Telescope	Beam arcsec
Q1501+106	12.96±0.07	12.12±0.08	11.19±0.05		9.84±0.07	1983 Feb 6	IRTF	6″
	12.93±0.05	12.17±0.05	11.23±0.05	9.82±0.05		1986 Feb 23	MMT	9″
		12.13±0.07				1986 Feb 27	MMT	9″
	13.38±0.04	12.65±0.04	11.82±0.04		9.89±0.04	1988 Apr 25	IRTF	6″
Q1545+210	14.79±0.06	14.03±0.06	12.98±0.06	>10.96		1985 May 5	MMT	5″
	14.74±0.05	14.00±0.05	13.11±0.04		11.16±0.04	1988 Apr 25	IRTF	6″
Q1613+658	14.03±0.05	12.77±0.05	11.86±0.05	$11.50\pm^{0.55}_{0.37}$		1984 Sep 15	MMT	9″[a]
	13.55±0.06	12.77±0.06	11.79±0.06	10.37±0.06		1985 May 5	MMT	5″
	13.55±0.06	12.73±0.06	11.72±0.06	10.30±0.07		1988 Apr 7	MMT	5″
	13.64±0.04	12.75±0.04	11.82±0.04		10.05±0.04	1988 Apr 25	IRTF	6″
Q1635+119	15.15±0.06	14.38±0.06	13.61±0.06	>12.79		1986 Feb 22	MMT	9″
	15.51±0.04		14.10±0.07		12.71±0.26	1988 Apr 25	IRTF	6″
Q1704+608	14.45±0.06	13.76±0.05	12.77±0.06	11.02±0.08		1988 Apr 7	MMT	5″
	14.44±0.04	13.73±0.05	12.84±0.04		10.62±0.05	1988 Apr 25	IRTF	6″
Q1721+343	14.37±0.06	13.82±0.06	12.77±0.06	11.60±0.23		1984 Sep 14	MMT	5″
	14.22±0.07	13.74±0.07	12.64±0.07	>10.74		1985 May 31	MMT	9″
	14.22:±0.13	13.67:±0.13	12.82:±0.13	11.33:±0.18		1985 Sep 25	MMT	5″[c]
	14.39±0.05	13.77±0.04	12.75±0.045		10.87±0.05	1988 Apr 25	IRTF	6″
Q1803+676	14.48±0.06	13.56±0.06	12.42±0.05	$11.18\pm^{0.52}_{0.35}$		1984 Sep 14	MMT	5″
	14.40±0.05	13.50±0.05	12.37±0.05	10.83±0.09		1985 Sep 27	MMT	5″
	14.52±0.04	13.56±0.04	12.45±0.04		10.73±0.05	1988 Apr 25	IRTF	6″
Q2128-123	14.97±0.08	14.39	13.51			1982 Jun 14	Mt. Lemmon	12″
	14.56	14.06	13.33			1984 Oct 29	Mt. Lemmon	8″
	14.70	14.10	13.32			1986 Sep 27	Mt. Lemmon	12″
Q2130+099	12.95±0.06	11.83±0.06	10.72±0.06	9.31±0.06		1984 Sep 14	MMT	5″
	13.25±0.05	12.15±0.05	10.97±0.05	9.38±0.05		1985 Sep 26	MMT	5″
	13.46±0.06	12.17±0.04	11.22			1986 Sep 23	Mt. Lemmon	12″
Q2135-147	14.83	13.81	12.64±0.14			1981 Oct 26	Mt. Lemmon	12″
	14.58±0.07	13.65	12.96			1982 Jun 16	Mt. Lemmon	12″
	14.20±0.07	13.57	12.51			1983 Nov 1	Mt. Lemmon	12″
	14.13	13.57	12.43			1984 Oct 29	Mt. Lemmon	8″
	14.23±0.05	13.50±0.05	12.35±0.05	10.85±0.09		1985 Sep 27	MMT	5″
	14.06	13.45	12.37			1986 Sep 27	Mt. Lemmon	12″
Q2209+184	13.88±0.06	13.14±0.06	12.44±0.06	$11.55\pm^{0.59}_{0.38}$		1984 Sep 14	MMT	5″
Q2251−178	13.30±0.06	12.58±0.06	11.61±0.06	10.07±0.11		1984 Sep 14	MMT	5″
OTHER "IPC" QUASARS								
Q0112−017	16.88±0.08	15.88±0.08	15.45±0.14			1984 Sep 14	MMT	5″
Q0133+207	15.83±0.07	14.88±0.05	13.75±0.05	12.04±0.13		1988 Jan 31	MMT	5″
Q0219+428	13.67±0.05	12.85±0.05	12.02±0.05	10.46±0.07		1984 Sep 15	MMT	5″
Q0323+022	14.78±0.06	14.07±0.06	13.37±0.06			1984 Sep 14	MMT	5″
		14.04±0.06	13.44±0.06			1984 Sep 14	MMT	5″
Q0424−131	15.95±0.06	15.31±0.07	14.50±0.07			1988 Jan 31	MMT	5″
	15.98±0.05	15.41±0.05	14.62±0.05	>12.79		1988 Feb 1	MMT	5″
Q0923+392	15.69±0.05	15.20±0.05	14.16±0.05			1985 Jun 2	MMT	9″
	15.65±0.06	15.11±0.09	14.07±0.08			1985 Sep 27	MMT	5″
Q1012+008	14.12±0.03	13.37	12.52±0.03			1985 Apr 12	Mt. Lemmon	12″
	14.27±0.06	13.45±0.06	12.46±0.06	11.18±0.11		1986 Feb 22	MMT	9″
		13.60±0.05	12.57±0.05	11.17±0.07		1986 Feb 23	MMT	5″
	14.66±0.07	13.78±0.04	12.81±0.04		10.89±0.05	1988 Apr 25	IRTF	6″
Q1121+422	14.68±0.04	14.18±0.04	13.23±0.04			1985 Apr 11	Mt. Lemmon	12″
	15.06±0.05	14.28±0.05	13.21±0.05	11.59±0.07		1986 Feb 26	MMT	9″[a]
Q1217+023	15.07±0.05	14.28±0.05	13.16±0.05			1985 Jun 2	MMT	9″
		14.23±0.05		11.67±0.30		1985 Jun 3	MMT	5″
	15.28±0.05	14.47±0.04	13.41±0.04		11.94±0.06	1986 Feb 4	IRTF	6″
Q1253−055	14.83±0.06	13.84±0.06	12.87±0.06	11.33±0.09		1986 Feb 22	MMT	9″
Q1346−036	15.60±0.06	15.04±0.06	14.22±0.06			1986 Feb 22	MMT	9″
Q1517+239	16.90±0.10	16.17±0.10	15.46±0.12			1986 Feb 26	MMT	9″
Q2112+059	14.45±0.05	13.71±0.05	12.59±0.05	10.94±0.11		1986 Sep 20	MMT	9″[a]
Q2126−158	15.50±0.06	14.93±0.06	14.25±0.06			1984 Sep 14	MMT	5″
Q2233+134	15.61±0.06	14.86±0.05	13.59±0.06	12.19±0.24		1986 Sep 20	MMT	9″[a]
Q2214+139	13.26±0.05	12.43±0.05	11.58±0.05	10.30±0.06		1986 Sep 20	MMT	9″[a]
Q2251+113	14.60	13.58	12.55			1981 Oct 26	Mt. Lemmon	12″
	14.31±0.07	13.73	12.50			1982 Dec 21	Mt. Lemmon	12″
	14.35±0.04	13.43	12.42			1984 Oct 28	Mt. Lemmon	8″
	14.20±0.04	13.41±0.03	12.44±0.03			1986 Sep 15	Mt. Lemmon	12″
	14.27±0.05	13.42±0.05	12.34±0.05	10.75±0.08		1986 Sep 20	MMT	9″[a]
Q2254+023	16.37±0.05	15.75±0.05	14.89±0.06	>11.80		1986 Sep 20	MMT	9″[a]
Q2304+042	13.51	12.75	12.18			1986 Sep 27	Mt. Lemmon	12″

[a] A 5″ aperture was used for the 3.4 μm band measurement.
[b] Magnitudes are on the instrumental system and Vega is defined to have magnitude zero in all bands. See Table 14 for adopted zero points.
[c] Possible clouds; uncertainties believed adequate.

TABLE 7

N-H AND Q-BAND INFRARED PHOTOMETRY

Object	N (mag) 10.2μm	Q (mag) 20μm	Date	Telescope	Aperture
		UVSX SAMPLE QUASARS			
Q0003+199	5.52±0.08	>3.85	1984 Sep 23	IRTF	6″
	5.56±0.09	3.66±0.16	1985 Aug 28	IRTF	6″
Q0026+129	7.76±0.11		1985 Aug 29	IRTF	6″
Q0050+124	4.74±0.05		1984 Sep 23	IRTF	6″
Q0054+144	7.24±0.17		1985 Aug 28	IRTF	6″
Q0205+024	7.09±0.12		1985 Aug 28	IRTF	6″
Q0923+129	6.55±0.18		1985 Apr 4	IRTF	6″
	6.40±0.09	4.19±0.22	1986 Feb 1,2,5	IRTF	6″
Q1116+215	6.85±0.09	>5.02	1986 Feb 1,5	IRTF	6″
Q1202+281	7.37±0.15		1986 Feb 1	IRTF	6″
Q1211+143	6.1±0.11	3.75±0.12	1986 Feb 1	IRTF	6″
Q1426+015	6.80±0.18	$4.41\pm^{0.54}_{0.36}$	1984 Mar	UKIRT	5″
	6.72±0.13		1985 Apr 2	IRTF	4″
Q1501+106	6.06±0.08	3.60±0.24	1984 Mar 6	UKIRT	5″
Q1545+210	$8.31\pm^{0.76}_{0.44}$		1985 Apr 3	IRTF	6″
Q1613+658	6.86±0.15		1985 Apr 2	IRTF	4″
	6.27±0.24		1985 Aug 27	IRTF	6″
	6.65±0.10		1985 Aug 28	IRTF	6″
Q1721+343	7.84±0.17		1985 Aug 29	IRTF	6″
Q2130+099	6.10:±0.10		1984 Sep 23	IRTF	6″
	6.18±0.08	3.68±0.15	1985 Aug 28	IRTF	6″
Q2135-147	$7.80\pm^{0.48}_{0.33}$		1985 Aug 28	IRTF	6″
	7.93±0.18		1985 Aug 29	IRTF	6″
Q2251-178	6.61:±0.20		1984 Sep 23	IRTF	6″
		OTHER "IPC" QUASARS			
Q0219+428	>6.8:		1984 Sep 23	IRTF	6″
Q1217+023	$8.62\pm^{0.87}_{0.48}$		1986 Feb 1	IRTF	6″

NOTE.—Magnitudes given correspond to a system in which Vega has magnitude zero. See Table 14 for adopted zero points.

given preference to infrared estimates of the galaxy luminosity over optical measurements. We have not attempted to model the dust emission from the host galaxy, although far-infrared observations of RSA spirals (de Jong et al. 1984) and submillimeter observations of normal galaxies (Thronson et al. 1990) indicate that the 60 and 100 μm contribution of the host galaxy to the energy distribution may be significant even in the absence of a starburst; the dashed line in Figure 4 shows an estimate of the mean normal spiral dust emission, but we emphasize that the dispersion in the shape is too large to make this a useful template. If a starburst is also present, the far-infrared contribution will be even larger, and, as Edelson (1987) and Condon & Broderick (1988) have shown, the radio may also be contaminated.

Rather than attempt an independent fit, we have chosen to use direct measurements of the host galaxy luminosities for the individual objects as found in the literature. Where possible, we have used the quoted total apparent magnitudes at the observed wavelengths to calculate the appropriate normalization of the template, rather than the reported absolute magnitudes which usually depend on the template model assumed by the authors in question. This normalization is expressed as L_H, the monochromatic luminosity at H band in the rest frame, where the host galaxy SED peaks. We have also attempted to estimate the model-independent half-light radius r_e for each galaxy.

Neugebauer et al. (1985) present observed frame H-band annular photometry of quasars and estimate total magnitudes assuming that, first, the radial light distribution follows a modified Hubble law with a fixed ratio of core radius to half-light radius as found by Kormendy (1977) and a corresponding outer cutoff; and, second, that the half-light radius is related to the total absolute H magnitude by a universal relation based on the results of Binggeli, Sandage, & Tarenghi (1984) and the assumption of a constant $B - H$ color for the galaxies. They then solve iteratively for the total magnitude. We have adopted their scheme and recalculated the results for our cosmological assumptions. We are unable to reproduce the exact results in their paper; however, direct measurements of the host galaxy luminosities from CCD imaging should be available soon. The surface brightness versus radius relation we adopt is a modified Hubble law,

$$\Sigma(r) = \frac{\Sigma(0)}{[1 + (r/0.093r_e)]^2}$$

cut off at $r_0 = 5.4r_e$; experiments with a de Vaucouleurs law

TABLE 8

IRAS FLUXES

Object	12μm[a]	25μm[a]	60μm[a]	100μm[a]	Obs[b]
		UVSX SAMPLE QUASARS			
Q0003+158	<0.04	<0.08	<0.07	<0.23	AO
Q0003+199	0.30 ±0.01	0.41 ±0.02	0.43 ±0.02	<0.19	AO
Q0007+106	0.10 ±0.01	0.15 ±0.01	0.22 ±0.01	1.40 ±0.04	AO
Q0026+129	<0.06	<0.04	<0.03	<0.11	AO
Q0049+171	< 0.15	< 0.12	< 0.14	< 0.46	LA
Q0050+124	0.53 ±0.01	1.05 ±0.02	2.39 ±0.02	3.56 ±0.06	AO
Q0052+251	0.06 ±0.01	0.09 ±0.02	0.10 ±0.02	0.45 ±0.07	AO
Q0054+144	0.06 ±0.01	0.09 ±0.01	0.30 ±0.01	0.77 ±0.03	AO
Q0121−590	0.369 ±0.005	0.54 ±0.01	0.62 ±0.02	0.89 ±0.06	AO
Q0134+329	0.048 ±0.006	0.15 ±0.01	0.78 ±0.01	1.14 ±0.03	AO
Q0205+024	0.05 ±0.01	0.12 ±0.02	0.10 ±0.02	<0.15	AO
Q0312−770	<0.04	<0.04	<0.07	< 0.49	AO
Q0414−060	< 0.09	< 0.11	< 0.10	< 0.38	LA
Q0637−752	< 0.07	0.13±0.02	0.20±0.03	< 0.39	LA
Q0804+761	0.17±0.02	0.25±0.03	0.16±0.04	< 0.51	LA
Q0837−120	<0.03	<0.05	0.071 ±0.016	<0.05	AO
Q0844+349	0.10±0.03	0.18±0.04	0.14±0.03	< 0.29	LA
Q0915+165	0.37	0.59	<0.48	< 1.00	PSC
Q0923+129	0.17±0.04	0.27±0.07	0.58±0.04	1.21±0.15	LA
Q1028+313	< 0.10	< 0.12	< 0.14	< 0.39	LA
Q1100+770	<0.02	0.040 ±0.006	0.07 ±0.01	<0.11	AO
Q1137+660	<0.04	<0.05	<0.07	<0.25	AO
Q1146−037	< 0.11	< 0.32	< 0.22	< 0.70	LA
Q1202+281	< 0.10	0.21±0.05	0.20±0.04	0.37±0.12	LA
Q1211+143	0.28±0.06	0.29±0.08	0.32±0.06	0.69±0.12	LA
Q1219+755	< 0.08	< 0.08	< 0.34	< 2.15	AO
Q1226+023	0.40 ±0.01	0.95 ±0.03	1.89 ±0.01	3.41 ±0.05	AO
Q1244+026	< 0.14	< 0.25	0.29±0.06	< 0.47	LA
Q1307+085	< 0.15	< 0.23	0.19±0.04	< 0.57	LA
Q1351+695	< 0.25	0.26	1.08	2.28	L88
Q1352+183	< 0.09	< 0.11	< 0.13	< 0.43	LA
Q1407+265	< 0.12	0.11±0.04	< 0.15	< 0.43	LA
Q1416−129	< 0.11	< 0.22	< 0.12	< 0.37	LA
Q1426+015	0.14±0.03	0.23±0.05	0.27±0.04	< 0.26	LA
Q1501+106	0.24 ±0.03	0.50±0.05	0.45 ±0.03	<0.37	LA
Q1545+210	<0.03	<0.04	0.08 ±0.02	<0.10	AO
Q1613+658	0.08 ±0.01	0.21 ±0.01	0.65 ±0.02	1.30 ±0.08	AO
Q1635+119	< 0.08	< 0.11	< 0.11	< 0.81	LA
Q1704+608	0.06 ±0.01	0.18 ±0.01	0.17 ±0.03	<0.17	LA
Q1721+343	0.08±0.02	0.12±0.02	0.14±0.03	< 0.92	LA
Q1803+676	<0.03	<0.03	<0.06	<0.21	AO
Q2128−123	<0.04	<0.09	0.08 ±0.02	0.95 ±0.08	AO
Q2130+099	0.17 ±0.01	0.31 ±0.01	0.47 ±0.02	0.25 ±0.05	AO
Q2135−147	< 0.11	0.14±0.03	0.17±0.05	< 0.52	LA
Q2209+184	0.04 ±L	<0.05	<0.07	0.34 ±0.07	AO
Q2251−178	0.09 ±0.01	0.15 ±0.02	0.32 ±0.02	<0.78	AO
		OTHER "IPC" QUASARS			
Q0112-017	< 0.14	< 0.21	< 0.27	Cirrus	LA
Q0133+207	< 0.11	< 0.17	0.17±0.05	0.40±0.13	LA
Q0923+392	<0.02	<0.03	<0.03	<0.10	AO
Q1012+008	< 0.16	< 0.16	< 0.14	< 0.2	LA
Q1048-090	< 0.14	< 0.11	< 0.12	< 0.2	LA
Q1121+422	< 0.12	< 0.07	< 0.10	< 0.29	LA
Q1217+023	< 0.23	< 0.26	0.21±0.03	< 0.31	LA
Q1253-055	0.10±0.03	0.29±0.07	0.24±0.05	< 0.46	LA
Q1351+640	0.17±0.03	0.63±0.03	0.82±0.04	1.33±0.07	LA
Q1435-067	< 0.11	< 0.17	< 0.09	< 0.46	LA
Q2126−158	<0.04	<0.07	0.09 ±0.02	<0.23	AO
Q2304+042	< 0.12	< 0.26	0.15±0.04	< 0.6	LA

[a] Flux in Jy.

[b] LA = Line add from survey; AO = Additional Observation; PSC = Point Source Catalog; L88 = Low et al. 1988.

TABLE 9

RADIO FLUXES

Object	ν(GHz)	S_{core}(mJy)[a]	S_{ext}(mJy)[a]	Date	Telescope[b]	Resolution (")	Ref
Q0003+158	5	130±0.07	199	1983 Nov	VLA	0.5	1
Q0003+199	1.5	4.1±0.9		1983 Jul	VLA	90	26
	5	3.0±0.07	0.89	1983 Nov	VLA	0.5	1
	5	3.30±0.18		1983 Jul	VLA	15	26
	20	<1.7		1983 Jul	OVRO	90	26
Q0007+106	1.5	296±15	8±1	1983 Aug	VLA	1.0	4
	1.5	340±1		1982 Apr	VLA	1.0	3
	5	470±1		1982 Apr	VLA	0.5	3
	5	184±10		1983 Aug	VLA	0.3	4
	5	151±0.07	170±0.07	1983 Nov	VLA	0.5	1
Q0026+129	1.4		1.2±0.2	1982 Oct	VLA	6	7
	5		2.9±0.4	1982 Oct	VLA	16	7
	5	0.2±0.07	4.9±0.07	1983 Nov	VLA	0.5	1
	15		4.6±0.7	1982 Oct	VLA	58	7
Q0049+171	5	0.65±0.1	<0.2	1983 Nov	VLA	0.5	1
Q0050+124	5	1.80±0.07	0.80	1983 Nov	VLA	0.5	1
Q0052+251	5	0.42±0.07	0.32±0.07	1983 Nov	VLA	0.5	1
Q0054+144	5	1.0±0.2	< 1	1986	VLA	5	2
Q0121-590	8.4	<10	<10	1986 Jun	PKS	162	4
Q0134+329	2.3	210±50		1976	VLBI	<<1	5
	5		5510±280	1982 Jun	VLA	0.5	12
	15		2290±114	1982 Jun	VLA	0.15	12
Q0205+024	1.4	1.2±0.2	3.3±0.5	1982 Mar	VLA	2.0	7
	5	0.8±0.15	<0.3	1982 Mar	VLA	0.3	7
	15	< 0.8		1982 Oct	VLA	5	7
Q0312-770	0.4	<1500	<1500	1965?	PKS	2880	22
	1.4	600	<600	1965?	PKS	840	22
	2.7	500±20		1970	PKS	474	24
	5.0	560±30		1971 Jan	PKS	240	23
Q0414-060	0.4		3000±150	1970 Oct	PKS	2880	31
	1.4		800±40	1966?	PKS	840	32
	2.7		480±24	1966?	PKS	474	32
	2.7	480		1973 May	NRAO	1?	14
Q0637-752	0.6	6510±300		1965-9	PKS	1830	21
	1.4	5330±160		1965-9	PKS	930	21
	2.7	4510 ±120		1970	PKS	474	24
	2.7	5900±180		1973 Jan	PKS	474	20
	5.0	6190±190		1971 Jan	PKS	240	23
	5.0	5490±160		1973 Apr	PKS	240	20
	8.9	5530±200		1974 Mar	PKS	151	19
Q0804+761	5	0.97±0.07	1.41	1983 Nov	VLA	0.5	1
Q0837-120	0.6	<700	3510±200	1973/4	WSRT	49	8
	1.4	165±10	1374±45	1971/4	WSRT	21	8
	5	160±10	672±50	1973/4	WSRT	6	8
	5	181±10		1987 Jan	VLA		17
	15	221±11		1987 Jan	VLA		17
	22.5	199.2±20		1987 Jan	VLA		17
Q0844+349	5	<0.25	0.31±0.1	1983 Nov	VLA	0.5	1
Q0915+165	1.4	6.8±0.7		1977-8	WSRT	25	25
Q0923+129	5.0	<10		1983 Nov	VLA	0.5	1
Q0923+129	1.4	<2		1977-8	WSRT	25	25
Q1028+313	1.4	< 100	124±50	1982 Oct	VLA	13	6
	1.5	89±1		1982 Apr	VLA	1.0	3
	5	110±1		1982 Apr	VLA	0.5	3
	5	91±13	54±8	1982 Oct	VLA	4.0	6
Q1100+772	1.4		2350±75	1974	WSRT	26	8
	5	75±20	1398±30	1974	WSRT	6	8
	5	100	856	1981 Mar	VLA	0.4	13
	5	76±0.07	584±0.1	1983 Nov	VLA	0.5	1
	5	78±10		1987 Jan	VLA		17
	15	78±4		1987 Jan	VLA		17
	22.5	68.6±6		1987 Jan	VLA		17
Q1116+215	5	1.9±0.07	0.86±0.07	1983 Nov	VLA	0.5	1
Q1137+660	1.4		2915±58	1974	WSRT	26	8
	2.7	94±32	1610	1975-6	NRAO	0.2	15
	5	130		1973	OMT	2	10
	5	162±8	913±40	1974	WSRT	6	8
	5	169	840	1981	VLA	0.4	13
	8.1	153±19	545	1975-6	NRAO	0.2	15

TABLE 9—*Continued*

Object	ν(GHz)	S_{core}(mJy)[a]	S_{ext}(mJy)[a]	Date	Telescope[b]	Resolution (")	Ref
Q1146-037	1.4	115	199	1980/1	VLA	2	16
	2.7	180		1973 May	NRAO		14
	8.1	190		1973 May	NRAO		14
Q1202+281	5	0.65±0.07	0.18±0.07	1983 Nov	VLA	0.5	1
Q1211+143	5	1.2±0.07	155.8±0.1	1983 Nov	VLA	0.5	1
Q1219+755	5	1.2±0.1	<1.2	1986	VLA	5	2
Q1244+026	5.0	0.47±0.07	0.36	1983 Nov	VLA	0.5	1
Q1226+023	5	30500		1980 Nov	VLA	0.4	11
	5	41500±2100		1974	WSRT	6	8
	5	26400	10600	1983 Nov	VLA	0.5	1
Q1307+085	5	<0.35	0.35±0.1	1983 Nov	VLA	0.5	1
Q1351+695	1.5	22.4±1.4		1983 Jul	OVRO	90	26
	5	7.4±0.4		1983 Jul	VLA	15	26
	20	<3.3		1983 Jul	VLA	90	26
Q1352+183	5	<0.25		1983 Nov	VLA	0.5	1
Q1407+265	5	2.9±0.07	5.0±0.1	1983 Nov	VLA	0.5	1
Q1416-129	5	0.8±0.07	2.8±0.1	1983 Nov	VLA	0.5	1
Q1426+015	5	0.93±0.07	0.28±0.1	1983 Nov	VLA	0.5	1
Q1501+106	1.5	<14.8		1983 Jul	VLA	90	26
	5	0.50±0.10	1.0±0.1	1983 Nov	VLA	0.5	1
	20.0	<2.2		1983 Jul	VLA	90	26
Q1545+210	0.6		4667±250	1974	WSRT	50	8
	1.4		2284±114	1974	WSRT	26	8
	1.5	35±1		1982 Apr	VLA	0.5	3
	5	30±6	794±40	1974	WSRT	6	8
	5	45	631	1981	VLA	0.4	13
	5	32±0.07	688	1983 Nov	VLA	0.5	1
Q1613+658	1.5	4.26±0.42		1986 Nov	VLA	9	33
	5	0.78±0.07	2.25±0.1	1983 Nov	VLA	0.5	1
	5	2.19±0.11		1986 Oct	VLA	3	33
	14.9	1.51±0.23		1985 Jul	VLA	1	33
	40	<237		1985 Jul	FCRAO		33
Q1635+119	1.4		129	1983	GB	700	28
	1.5	16		1983 Apr	VLA	1.0	3
	5		51±9	1987	GB	210	27
	5	17		1983 Apr	VLA	0.5	3
Q1704+608	0.6		6050± 320	1974	WSRT	50	8
	1.4	<700	3142±157	1974	WSRT	21	8
	2.7		1502	1975-6	NRAO		15
	5	18±2	1042±53	1974	WSRT	6	8
	5	8.0±0.07	1230	1983 Nov	VLA	0.5	1
	5	17.7±0.9		1987 Jan	VLA		17
	8.1		624	1975-6	NRAO		15
	15	8.2 ±0.4		1987 Jan	VLA		17
	22.5	4.8±0.8		1987 Jan	VLA		17
Q1721+343	1.5	610±30	1010±80	1976	WSRT	1000	30
	1.5	450±1		1982 Apr	VLA	1.0	3
	5	440±30	640±40	1979	WSRT	300	30
	5	370±1		1982 Apr	VLA	0.5	3
Q1803+676		< 0.35	<0.35		VLA	0.5	18
Q2128-123	8.4	3340±230		1989	PKS	160	29
Q2130+099	1.5	4.71±0.32		1986 Nov	VLA	9	33
	5	1.3±0.07	0.75±0.1	1983 Nov	VLA	0.5	1
	5	2.09±0.11		1986 Oct	VLA	3	33
	14.9	1.47±0.23		1985 Jul	VLA	1	33
	40	<258		1985 Jul	FCRAO		33
Q2135-147	0.6	<600	6991±350	1974	WSRT	19	8
	1.4	<75	3268±163	1974	WSRT	21	8
	1.5	87±1		1982 Apr	VLA	1.0	3
	5	97±10	1049±70	1974	WSRT	6	8
	5	126±1		1982 Apr	VLA	0.5	3
Q2209+184	1.4		212	1983	GB	700	28
	5		116±16	1987	GB	210	27
	5	280±0.07	10±0.07	1983 Nov	VLA	0.5	1
Q2251-178	5	0.26		1984?	VLA	0.5	18

[a] The division of fluxes into core and extended is arbitrary when only low-resolution observations are available. In such cases the presence of a flux in the "core" column indicates we have chosen to use it in the construction of the energy distribution.

[b] Telescope acronyms are FCRAO: Five College Radio Astronomy Observatory, MA; GB: Green Bank 300 foot (91 m) telescope; NRAO: NRAO Green Bank Interferometer, WVA; OVRO: Owens Valley Radio Observatory, CA; PKS: Parkes 64 m DSN telescope, NSW, Australia; VLA: Very Large Array, NM; VLBI: Goldstone and Madrid DSN telescopes; WSRT: Westerbork Synthesis Radio Telescope, Netherlands.

REFERENCES.—(1) Kellerman et al. 1989; (2) I. Gioia, private communication; (3) Gower & Hutchings 1984; (4) Unger et al. 1987; (5) Preston et al (1985); (6) Feigelson, Isobe & Kembhavi 1984; (7) Rudnick, Sitko, & Stein 1984; (8) Miley & Hartsuijker 1978; (9) Price & Milne 1965; (10) Pooley & Henbest 1974; (11) Perley 1982; (12) Spencer et al. 1989; (13) Swarup, Sinha, & Hilldrup 1984; (14) Wills 1979; (15) Owen, Porcas, & Neff 1978b; (16) Hintzen, Ulvestad, & Owen 1983; (17) Antonucci & Barvainis 1988; (18) Hutchings & Gower 1985; (19) Shimmins & Bolton 1981; (20) Bolton & Butler 1975; (21) Wills 1975; (22) Ekers (1969); (23) Shimmins & Bolton 1972a; (24) Shimmins & Bolton 1972b; (25) Meurs & Wilson 1981; (26) Edelson 1987; (27) Gregory & Condon 1991; (28) White & Becker 1992; (29) Wright et al. 1991; (30) Jagers et al. 1982; (31) Bolton et al. 1971; (32) Shimmins et al. 1966; (33) Barvainis & Antonucci 1989.

TABLE 10

MILLIMETER FLUXES

Object	λ(mm)	S(mJy)	Date	Telescope	Ref
Q0003+199	1.3	<852	1983	NRAO	5
Q0007+106	3.3	1600±100	1979	NRAO	8
	3.3	2600±400	1978	NRAO	8
	1.0	800±200	1979	Hale	7
Q0026+129	1.0	<1600	1982	UKIRT	11
	1.0	<1000	1979	Hale	7
	3.3	190±40	1980	NRAO	10
Q0050+124	1.3	<672	1983	NRAO	5
	1.3	<222	1986	NRAO	2
	3.3	<141	1986	NRAO	2
	0.15	1900±0.8	1987	KAO	6
Q0054+144	3.3	<360	1980	NRAO	10
	1.3	<3.0	1988	IRAM	3
Q0134+329	1.0	<700	1979	Hale	7
	3.3	300	1986	IRAM	12
Q0205+024	3.3	<60	1984	UKIRT	11
Q0837-120	1.3	55.0±6.3	1989	IRAM	1
Q0844+349	1.3	<3.4	1988	IRAM	3
Q1028+313	3.3	140±30	1980	NRAO	10
Q1100+772	1.3	4.2±1.8	1989	IRAM	1
Q1137+660	3.3	140±90	1980	NRAO	10
Q1202+281	3.3	<210	1980	NRAO	10
Q1211+143	1.3	<2.8	1988	IRAM	3
Q1219+755	3.3	<90	1980	NRAO	10
	1.0	<900	1978	Hale	7
Q1226+023	3.3	20280±1960	1977	VLA	9
	3.3	12900±1000	1978	NRAO	8
	3.3	14800±900	1979	NRAO	8
	3.3	16320±1640	1980	NRAO	10
	3.3	31300±400	1982	NRAO	4
	1.9	19000±2000	1982	NRAO	4
	1.1	11000±1000	1982	UKIRT	4
	1.0	10200±2100	1977	Hale	7
	0.8	8700±1500	1982	UKIRT	4
	0.4	4900±900	1982	UKIRT	4
Q1351+695	1.3	<1548	1983	NRAO	5
Q1426+015	1.3	<4.3	1988	IRAM	3
Q1613+658	1.3	<3.1	1988	IRAM	3
Q1704+608	3.3	<180	1980	NRAO	10
	1.3	<6.0	1989	IRAM	1
	1.0	<1000	1979	Hale	7
Q2128-123	3.3	1.3±0.1	1986	IRAM	5
	1.3	0.35±0.1	1986	IRAM	5
Q2130+099	1.3	2.1±0.7	1988	IRAM	12
Q2135-147	3.3	230±50	1980	NRAO	10
	1.0	<800	1979	Hale	7

REFERENCES.—(1) Antonucci, Barvainis, & Alloin 1990; (2) Barvainis & Antonucci 1989; (3) Chini, Kreysa, & Biermann 1989; (4) Clegg et al. 1983; (5) Edelson, Malkan, & Rieke 1987; (6) Engargiola et al. 1988; (7) Ennis, Neguebauer, & Werner 1982; (8) Landau, Epstein, & Rather 1980; (9) Owen et al. 1978a; (10) Owen & Puschell 1982; (11) Robson et al. 1985; (12) Steppe et al. 1988.

gave similar results, but the de Vaucouleurs law was a worse fit to a few of the objects for which detailed profiles were available—although we might expect the law to be a better representation for those objects whose host galaxies are elliptical. The same scheme can be used to estimate total magnitudes for the off-nuclear slit photometry of Boroson, Oke, & Green (1982), Boroson & Oke (1984), and Boroson, Persson, & Oke (1985); for these data we conducted a numerical integration of the modified Hubble law over the area of the slit, replacing the analytic expression possible in the annular case. We note that our derived fractional luminosities in the slit ranged from 0.07 to 0.14 in reasonable agreement with the simple assumption of 0.10 used by Boroson et al. Similarly, the scheme can be adapted for photometry in two annuli, as in Neizvestnii (1986) and MacKenty (1990).

For some of our objects, more detailed CCD PSF-subtracted profiles are available. In these cases (Gehren et al. 1984; Smith et al. 1986; Yee & Green 1987) we have calculated the half-light radius and total magnitude directly from the published profile graphs; the modified Hubble law was used to estimate the contribution within the innermost point at which the profile departed from the point spread function.

The total apparent magnitude and half-light radius of Fairall 9 were taken directly from Griersmith & Visvanathan (1979).

TABLE 11

MAGNITUDE SCALE ZERO POINTS[a]

Band	Reference λ (μm)	Zero pt (Jy) (Vega)	Zero pt (Jy) ($\alpha = 1$)
U	0.36	1317	1779
B	0.44	4333	4047
V	0.54	3647	3536
R	0.70	2791	2869
I	0.90	1871	2339
J	1.25	1567	1657
H	1.65	1016	1053
K	2.20	687	710
N34	3.40	325	321
L'	3.80	256	270
M	4.8	161	167
N	10.1	39	38
Q	20.25	9.8	11

[a] The zero points correspond to a system in which the magnitude of Vega is exactly zero. Values are given for an object with the same spectrum as Vega and for an object with a flat energy distribution (power-law spectrum $F_\nu \sim \nu^{-\alpha}$ of slope unity).

In two cases where only absolute magnitudes were given (Q1352+183, Q2251−178; Hutchings, Crampton, & Campbell 1984) we took the tabulated values directly, correcting only for cosmology.

In total, estimates of host galaxy luminosity and half-light radius were obtained for 29 of the 47 UVSX sample objects. Where no error bar was directly available from the fitting process, we assumed an uncertainty of 10% in the luminosity. Values for the remaining 18 objects were adopted by the crude expedient of taking the median luminosity and half-light radius of the other hosts and using error bars corresponding to the observed 75 percentile range; thus $L_H = 5(+3, -4) \times 10^{44}$ ergs s^{-1} and $r_e = 10(+3, -6)$ kpc. The upper error bars were modified by the constraint that the predicted near-IR flux should not exceed that actually observed for the quasar plus host; in only one cases, Q1244+026, was the adopted luminosity altered to satisfy this constraint.

Figure 5 shows the adopted host luminosities and half-light radii for our sample. The well known galaxies M31 and M87 are marked on the diagram to orient the reader. Where no radial profile was available, we adopted an iterative method similar to that of Neugebauer et al. (1985) and using the mean relationship (*solid line*) between half-light radius and total lu-

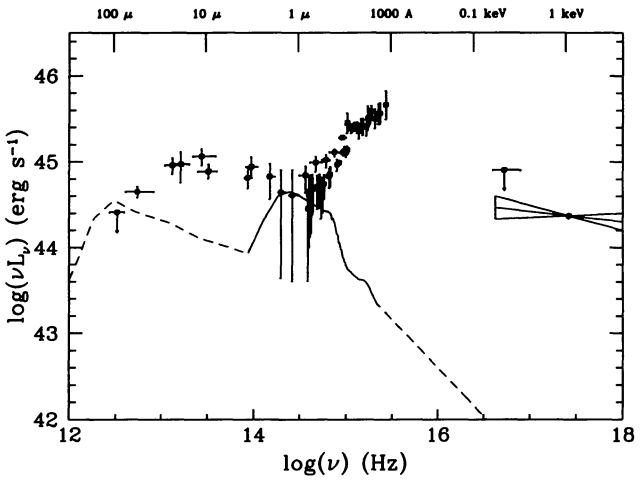

FIG. 4.—Starlight template used for host galaxy subtraction. Template is shown with energy distribution of PG 1426+015 for comparison, with relative normalization appropriate for the limit of large aperture. Dashed lines illustrate mean IR and X-ray colors of galaxy, not used in subtraction.

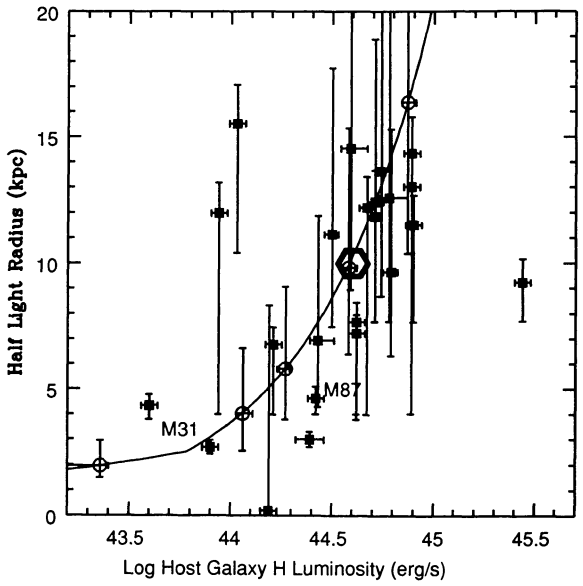

FIG. 5.—Adopted host galaxy luminosities and radii. The solid curve indicates the Bingelli et al. (1984) relation. Points marked by open circles are constrained to lie on the curve, while radii for other points are derived using radial profile information as described in the text. The median host galaxy normalization used where specific information is lacking is indicated by the large solid symbol and represents the median of the other points. The well-known galaxies M31 and M87 are also plotted on the figure for comparison.

TABLE 12

ADOPTED HOST GALAXY PARAMETERS

Object	Log Luminosity H band	Half-Light Radius kpc	Ref
Q0003+158	$44.60\pm^{0.30}_{0.60}$	10.00	(0)
Q0003+199	$43.90\pm^{0.04}_{0.04}$	2.69	(13)
Q0007+106	$44.43\pm^{0.08}_{0.04}$	6.95	(1)
Q0026+129	$44.27\pm^{0.02}_{0.04}$	5.81	(6)
Q0049+171	$43.60\pm^{0.04}_{0.04}$	4.34	(3)
Q0050+124	$44.62\pm^{0.04}_{0.04}$	7.68	(3)
Q0052+251	$44.78\pm^{0.09}_{0.05}$	12.60	(1)
Q0054+144	$44.71\pm^{0.04}_{0.04}$	12.44	(2)
Q0121-590	$44.90\pm^{0.04}_{0.04}$	11.53	(9)
Q0134+329	$45.44\pm^{0.04}_{0.04}$	9.24	(2)
Q0205+024	$44.19\pm^{0.04}_{0.04}$	0.19	(3)
Q0312-770	$44.60\pm^{0.30}_{0.60}$	10.00	(0)
Q0414-060	$44.60\pm^{0.30}_{0.60}$	10.00	(0)
Q0637-752	$44.60\pm^{0.30}_{0.60}$	10.00	(0)
Q0804+761	$44.60\pm^{0.30}_{0.60}$	10.00	(0)
Q0837-120	$44.60\pm^{0.30}_{0.60}$	10.00	(0)
Q0844+349	$44.60\pm^{0.25}_{0.60}$	10.00	(0)
Q0915+165	$44.39\pm^{0.07}_{0.07}$	3.00	(13)
Q0923+129	$44.59\pm^{0.08}_{0.05}$	14.55	(12)
Q1028+313	$44.60\pm^{0.30}_{0.60}$	10.00	(0)
Q1100+772	$44.50\pm^{0.03}_{0.04}$	11.15	(4)
Q1116+215	$44.74\pm^{0.04}_{0.03}$	13.65	(4)
Q1137+660	$44.60\pm^{0.30}_{0.60}$	10.00	(0)
Q1146-037	$44.60\pm^{0.24}_{0.60}$	10.00	(0)
Q1202+281	$44.71\pm^{0.03}_{0.04}$	11.87	(4)
Q1211+143	$43.36\pm^{0.04}_{0.23}$	1.96	(6)
Q1219+755	$44.60\pm^{0.10}_{0.60}$	10.00	(0)
Q1226+023	$44.79\pm^{0.03}_{0.04}$	9.66	(4)
Q1244+026	$44.23\pm^{0.04}_{0.23}$	10.00	(0)
Q1307+085	$44.60\pm^{0.30}_{0.60}$	10.00	(0)
Q1351+695	$44.60\pm^{0.30}_{0.60}$	10.00	(0)
Q1352+183	$44.21\pm^{0.04}_{0.04}$	6.78	(8)
Q1407+265	$44.60\pm^{0.30}_{0.60}$	10.00	(0)
Q1416-129	$44.60\pm^{0.15}_{0.60}$	10.00	(0)
Q1426+015	$44.60\pm^{0.30}_{0.60}$	10.00	(0)
Q1501+106	$44.06\pm^{0.05}_{0.03}$	4.02	(6)
Q1545+210	$44.87\pm^{0.04}_{0.03}$	16.38	(6)
Q1613+658	$44.89\pm^{0.04}_{0.04}$	13.04	(7)
Q1635+119	$44.03\pm^{0.04}_{0.04}$	15.52	(10)
Q1704+608	$44.58\pm^{0.04}_{0.04}$	9.82	(6)
Q1721+343	$44.60\pm^{0.30}_{0.60}$	10.00	(0)
Q1803+676	$43.94\pm^{0.04}_{0.04}$	11.98	(11)
Q2128-123	$44.60\pm^{0.30}_{0.60}$	10.00	(0)
Q2130+099	$44.42\pm^{0.04}_{0.04}$	4.64	(2)
Q2135-147	$44.89\pm^{0.04}_{0.04}$	14.36	(3)
Q2209+184	$44.62\pm^{0.04}_{0.04}$	7.23	(3)
Q2251-178	$44.67\pm^{0.04}_{0.04}$	12.21	(8)

NOTE.—Adopted luminosities and half-light radii for host galaxies, derived as discussed in the text. No spatial information was available for objects marked with reference (0), and they have been assigned the median luminosity of the remainder of the sample.

REFERENCES.—(1) Boroson, Oke, & Green 1982; (2) Gehren et al. 1984; (3) Smith et al 1986; (4) Boroson & Oke 1984; (5) McAlary et al. 1983; (6) Neugebauer et al. 1985; (7) Yee & Green 1987; (8) Hutchings, Crampton & Campbell 1984; (9) Griersmith & Visvanathan 1979; (10) Hutchings, Janson, & Pike 1988; (11) Hutchings, Johnsonn, & Neff 1989; (12) Neizvestnii 1986; (13) MacKenty 1990.

minosity found for ellipticals by Binggeli, Sandage, & Tarenghi (1984) as its starting point.

The observed SEDs were then corrected for host galaxy emission, using the fixed spectral host galaxy template, the tabulated normalization and errors, and the modified Hubble law, which was used to determine the fraction of the host flux within the aperture separately for each data point. Uncertainties in the half-light radius were, however, ignored in the calculation of the final errors.

Table 12 gives the adopted normalizations at rest frame H for the host galaxy luminosities; most are a few times 10^{44} ergs s^{-1}. We also present the adopted half-light radii in kiloparsecs. The size of the correction at H is shown as a function of absolute magnitude in Figure 6. Corrections can be important up to $M_V = -25.5$ or more (e.g., 3C 48), while quasars as faint as $M_V = -23.5$ can show negligible host galaxy contamination (e.g., Kaz 102).

5.5. *Variability and Averaging*

A potentially severe limitation on our dataset is that the observations are typically not simultaneous, although the optical and ground-based IR data were generally obtained within about 1 month. This problem is worst in the ultraviolet since the amount of variability increases with frequency throughout the UVOIR region (Cutri et al. 1985). Edelson, Krolik, & Pike (1990) reported that the degree of variability was smaller in the higher luminosity sources that form the bulk of the present sample, than in low-luminosity Seyferts. However, the variations are still enough to contribute to the scatter in our ultraviolet energy distributions.

For about one-third of the objects, we have observations at two epochs (occasionally more) in a given waveband, so we can make a crude estimate of the degree of variability. In Table 13 we list the observed range of variability, F_{max}/F_{min}, and the associated timescale, at rest wavelengths in the near-infrared, optical, mid-ultraviolet and far-ultraviolet. It can be seen that in the optical and infrared variability is not a serious problem for these "normal" quasars, but that in the ultraviolet the variability is significant on timescales of a few years (median timescale samples is 4 yr), although typically (13 of 18 cases) it is less than a factor of 2. These results indicate somewhat less variability than found by Kinney et al. (1991), and this is probably an artifact of the small number of observations of our objects (more observations would tend to increase the observed range of variability).

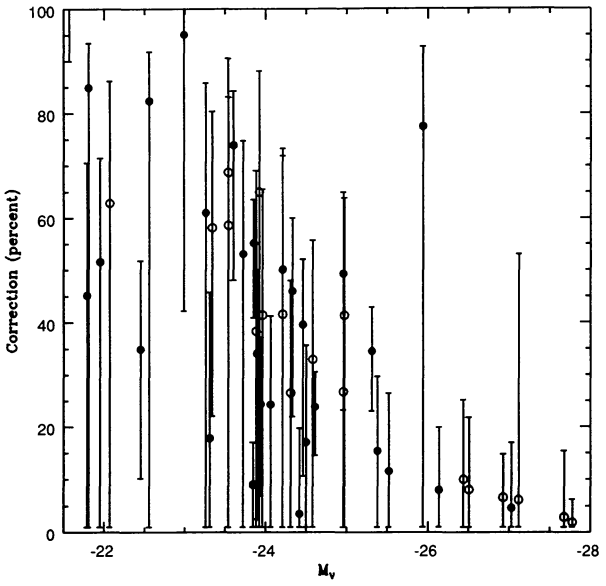

FIG. 6.—Host galaxy flux corrections at rest frame H (percent) as a function of absolute visual magnitude. Solid circles indicate corrections made using data on the specific host galaxy, while open circles indicate use of the median normalization.

To generate a single mean energy distribution for each quasar, we have taken an average [in log $\nu F(\nu)$] of all the data in each frequency bin. However, for the *IUE* data, because of the increased problem of variability and also the widely different S/N among observations, we have been selective in the exposures from Table A2 we chose to include in the average. Specifically, where simultaneous data from the long- (LWP/LWR) and short- (SWP) wavelength cameras were available, we have included them and excluded "orphan" LWP/LWR or SWP exposures. This avoids spurious steps in the UV data due to variability. Objects where "orphans" were excluded are Q0007+106, Q1100+772, Q1146–037, Q1202+281, Q1407+265, and Q1613+658. Further, when one exposure had significantly lower signal-to-noise ratio than the others, it was omitted (Q1545+210, Q1613+658, and Q1721+343).

5.6. *PG 1407+265*

The redshift of PG 1407+265 (=2E 3196) is uncertain; the object has very weak emission lines, the only certain feature coming at 5500 Å. An identification of this as Mg II and the weak presence of a feature at C III] led Schmidt & Green (1983) to propose the redshift as $z = 0.944$. The near infrared to ultraviolet spectrum of PG 1407+265 is presented in Figure 7. The absence of a clear Lyman-alpha line in the *IUE* spectrum caused us to consider lower redshift identifications, including blueshifts, but no choice of redshift allows normal quasar line ratios. We have adopted the high redshift given by Schmidt & Green because of the position of a prominent continuum feature, namely the near-infrared inflection. The rest wavelength of this feature lies between 1.0 and 1.5 μm for all our other objects, and in this object occurs at an observed wavelength between 2.0 and 2.4 μm, which lends support to the high-redshift estimate.

We continue to adopt the Schmidt & Green value despite the absence of definitely observed hydrogen lines. We note that the broad width of the one line clearly detected, the overall continuum shape, the lack of strong optical variability, and the X-ray–to–optical flux ratio indicate that the object is indeed a quasar rather than, for instance, a star, a BL Lac object, or some more exotic object. Note the good agreement in flux level at the overlap between the two optical spectra and the smooth continuation of the spectrum made by the infrared photometry, implying a lack of variability at longer wavelengths. Comparison with the data in Neugebauer et al. (1987) indicates that the optical has varied by less than 10% over an 8 yr interval. A 1986 LWP spectrum shows a lower flux level than the other ultraviolet data, implying significant variability in the

TABLE 13

VARIABILITY ESTIMATES

Object	Var(2 μm)	Var(5000Å)	Var(2500Å)	Var(1350Å)
Q0003+158				
Q0003+199				
Q0007+106			<1.2 (6 yr)	4.1 (6 yr)
Q0026+129	<1.1 (1 yr)	<1.1 (1 yr)	<1.2 (6 yr)	
Q0049+171	2.2 (3.3 yr)			
Q0050+124				
Q0052+251				
Q0054+144	1.1 (1 yr)	1.1 (1 yr)		
Q0121-590	2.6 (9 yr)	2.8 (6 yr)	1.7 (4 yr)	1.8 (4 yr)
Q0134+329				
Q0205+024	<1.1 (1 yr)			
Q0312-770				2.3 (0.8 yr)
Q0414-060				
Q0637-752				1.2 (0.5yr)
Q0804+762				
Q0837-120	1.3 (2 yr)	1.6 (1 yr)		
Q0844+349			1.3 (1 yr)	1.3 (1 yr)
Q0915+165				
Q0923+129				
Q1028+313				
Q1100+772				
Q1116+215	1.3 (2 yr)			1.5 (2 yr)
Q1137+660				
Q1146-037	1.1 (2 yr)			
Q1202+281	<1.1 (1 yr)		1.5 (6 yr)	2.8 (6 yr)
Q1211+143	1.2 (2 yr)		<1.2 (1 yr)	1.6 (1 yr)
Q1219+755	<1.1 (0.8 yr)	1.2 (1 yr)	2.4 (5 yr)	1.5 (5 yr)
Q1226+023	1.2 (2 yr)	1.3 (2 yr)	1.6 (11 yr)	2.2 (11 yr)
Q1244+026				
Q1307+085				
Q1351+695				
Q1352+183				
Q1407+265				
Q1416-129	1.2 (5 yr)			<1.2 (8 yr)
Q1426+015	1.5 (5 yr)	1.1 (1 yr)	1.3 (2 yr)	1.8 (2 yr)
Q1501+106	1.8 (5 yr)			
Q1545+210	1.1 (2 yr)	1.3 (1 yr)		
Q1613+658	1.1 (4 yr)		<1.2 (1.6yr)	1.2 (1.6 yr)
Q1704+608			<1.2 (7 yr)	<1.2 (4 yr)
Q1721+343	<1.1 (4 yr)		<1.2 (3 yr)	<1.2 (3 yr)
Q1803+676	<1.1 (4 yr)			
Q2128-123				
Q2130+099	1.2 (1 yr)	1.1 (1 yr)	<1.2 (7 yr)	1.7 (7 yr)
Q2135-147	1.2 (2 yr)	1.1 (1 yr)	<1.2 (4 yr)	1.3 (4 yr)
Q2209+184				
Q2251-178				

NOTE.—Estimates of variability at four wavelengths. The quantity given is the observed range of variability (maximum value over minimum) followed by the corresponding observational interval in years.

UV (at least 30%). These variability properties are all consistent with normal quasar behavior.

6. PROPERTIES OF THE ENERGY DISTRIBUTIONS

In Figures 8 and 9 we present two energy distributions for each object in the UVSX sample, an overall view and a closeup of the infrared to ultraviolet region. The overall view covers a fixed flux range of 10 decades and illustrates the radio-loudness and X-ray properties of each quasar. The closeup view covers two decades in flux and illustrates the near-infrared inflection, and the strength of the blue bump. For objects in which host galaxy subtraction makes a significant difference (>5%) to the energy distribution, the starlight-subtracted energy distribution is also shown.

6.1. *Luminosities: Bolometric and Individual Bands*

To characterize the large-scale distribution of the energy output of the quasars, we calculate integral luminosities in a set of broad bands. The integrals are calculated by running a simple linear interpolation through the data points in log νL_ν space, i.e., connecting the individual points with a power law. The errors indicated in the tables are estimated by performing the integrals using the 1 σ high and 1 σ low flux values instead of the nominal values. For upper limits we interpolate between

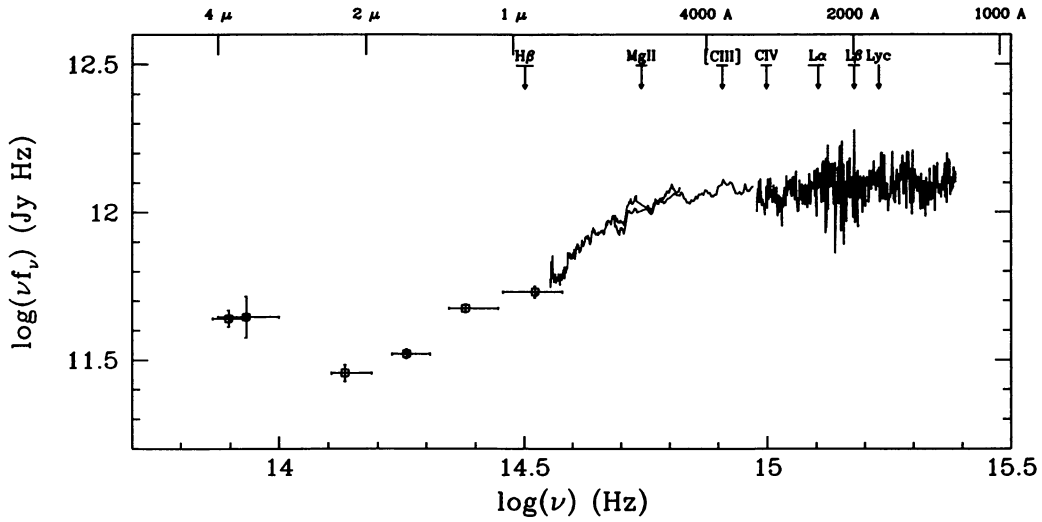

FIG. 7.—The observed energy distribution of PG 1407+265 from the near-infrared to the far-ultraviolet. The expected positions of prominent quasar emission lines are indicated for an assumed redshift $z = 0.94$.

detections on either side. The lower of the interpolated value and the upper limit is used as the nominal flux estimate, but the errors are estimated using zero as the lower error bar and the upper limit as the upper error bar.

The logarithms of the calculated integral luminosities in units of ergs s^{-1} are tabulated in Tables 14–16.

1. *Bolometric.*—The bolometric luminosity is typically well defined except for contributions from two regions of the spectrum: the mostly unobservable EUV region and the as yet unobserved hard X-ray and gamma-ray region. Indications are strong that the gap in the 0.1–10.0 mm wavelength range is energetically negligible. As a first crude estimate of the EUV luminosity, we simply make a linear interpolation (in the log-log space of Fig. 8; i.e., a power-law interpolation in flux space) between the ends of the *IUE* and *Einstein* ranges. We note, however, that in contrast to the claim of Padovani & Rafanelli (1988), the lack of EUV data does introduce a major uncertainty into the final bolometric luminosity. An upper limit to the physically reasonable EUV luminosity can be made by finding the maximum blackbody curve which does not exceed the observed data; however, this limit is not strong, as the luminosity implied is typically 10–100 times the luminosity observed in the rest of the spectrum.

We perforce neglect the unknown luminosity above 10 keV ($10^{18.4}$Hz). *Compton Observatory* observations will provide some constraints in this region. The number of ionizing photons is somewhat better determined than the luminosity, since the photon spectrum is rapidly falling in the ultraviolet. However, our estimate of this quantity is still very speculative since it is based on our linear interpolation across the EUV gap. We tabulate the total estimated ionizing photon rate multiplied by 1 rydberg, $N_{\rm Ion}R$, to give the quantity the same units as the luminosities for easy comparison. Since 1 ryd = $R = 2.18 \times 10^{-11}$ ergs, if $N_{\rm Ion}R = 10^{44}N_{44}$ ergs s^{-1}, then $N_{\rm Ion} = 4.6 \times 10^{54} N_{44}$ photons s^{-1}. The mean ionizing photon energy in rydbergs is then simply $L_{\rm Ion}/(N_{\rm Ion}R)$.

2. *UVOIR.*—The three decades between 100 μm and 0.1 μm (the ultraviolet/optical/infrared or "UVOIR" region) are relatively well sampled, so the corresponding UVOIR luminosity can be calculated much more accurately. This luminosity accounts for most of that which is directly observed, and so is a useful fiducial luminosity for a quasar.

3. *Decades.*—We also tabulate the luminosity in individual decades across the electromagnetic spectrum. Outside the range 1–0.1 μm, these are often estimates from only one or two points, and the errors are correspondingly large (typically 25% in the far-IR).

4. *Octaves.*—In order to describe the shape of the ultraviolet bump component, we define a set of narrower octave-wide bands. We call the four bands IR (0.8–1.6 μm), VIS (4000–8000 Å), NUV (2000–4000 Å), and UV (1000–2000 Å). The IR band gives the luminosity just shortward of the near-infrared inflection, where the bump starts. The UV band measures the luminosity in the bluest observed part of the bump, while the VIS band samples the early part of the bump's rise. The NUV band covers the near-ultraviolet region of the spectrum dominated by the "small bump" of blended Fe II and Balmer continuum emission (Wills, Netzer, & Wills 1985). Further discussion and interpretation of the octave colors of our sample may be found in Siemiginowska et al. (1994).

6.2. *The Mean and Dispersion of the Spectral Energy Distributions*

We have also derived mean bolometric corrections and mean energy distributions for the sample. We have excluded four objects (Q0923+129, Q1244+026, Q1351+695, and Q2209+184) from these calculations because of the large uncertainties in the starlight subtraction for those objects. In Table 17, the median, mean, and standard deviation of the bolometric corrections at a given band are given, followed by the minimum and maximum values found in the sample. Errors in the determination of individual energy distributions have been ignored for the purposes of this table. To estimate bolometric luminosity from a rest frame luminosity at B, the value

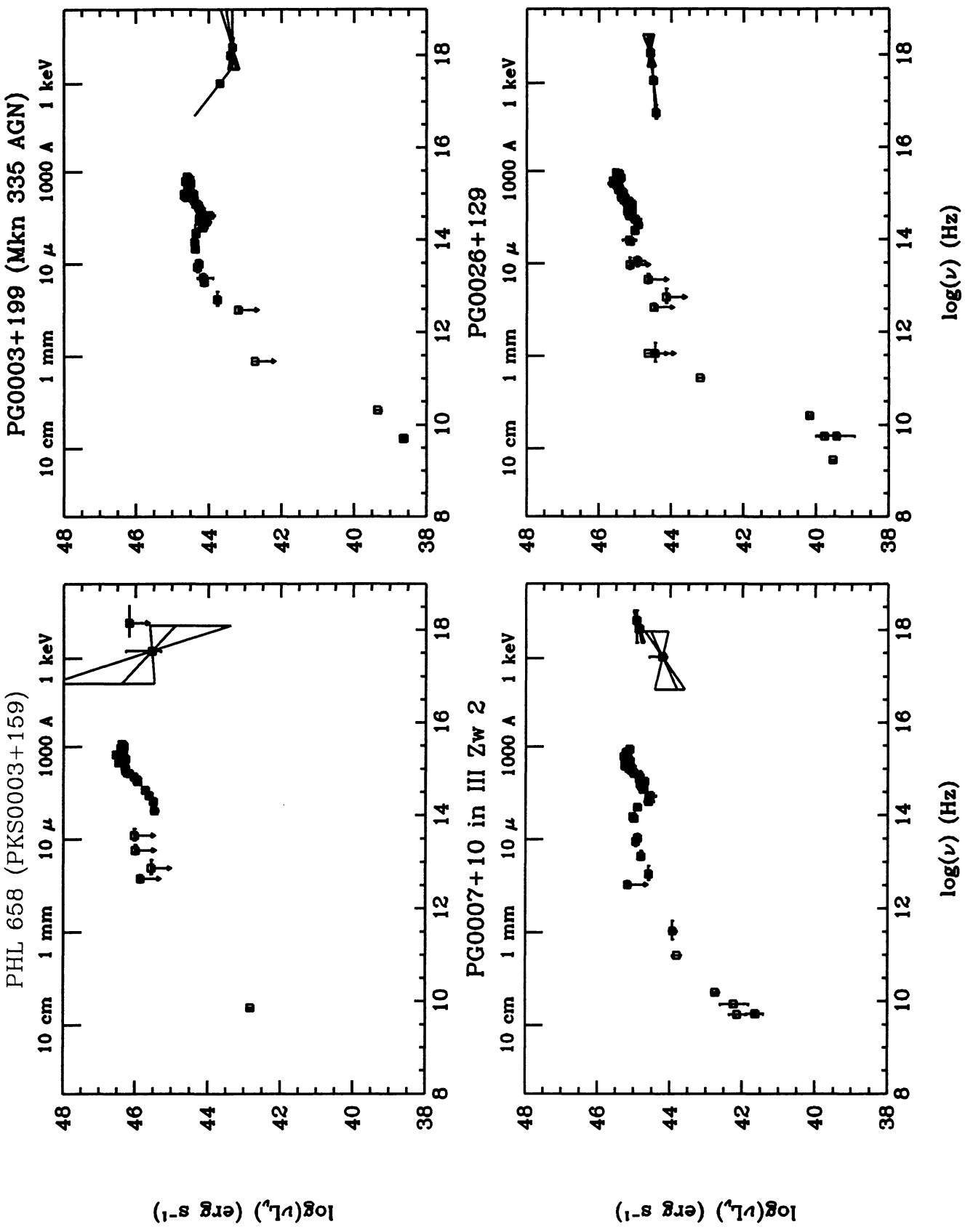

FIG. 8.—Rest frame, dereddened continuum energy distributions of the quasar sample. For each object, the panel shows the overall radio to X-ray energy distribution.

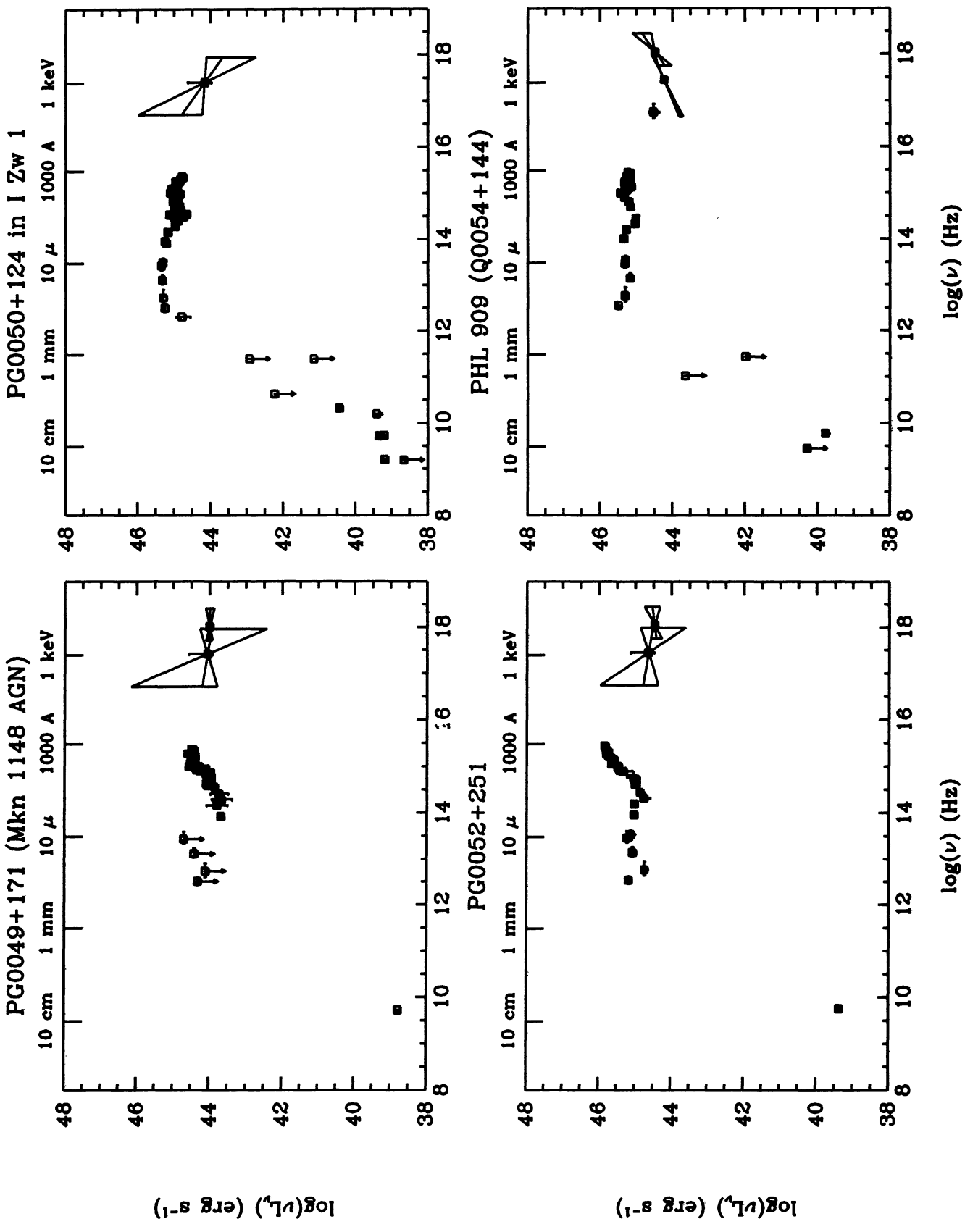

FIG. 8—*Continued*

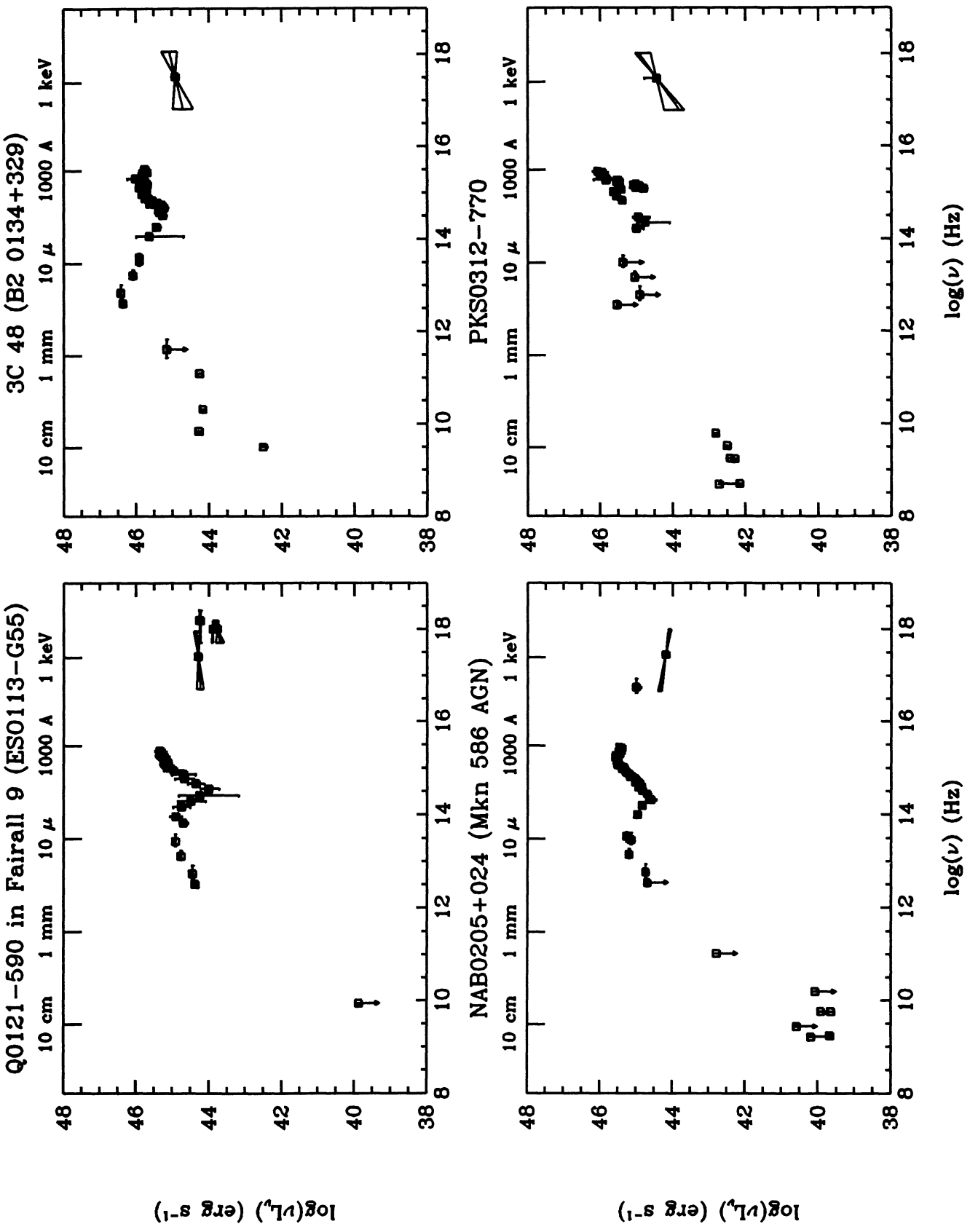

FIG. 8—*Continued*

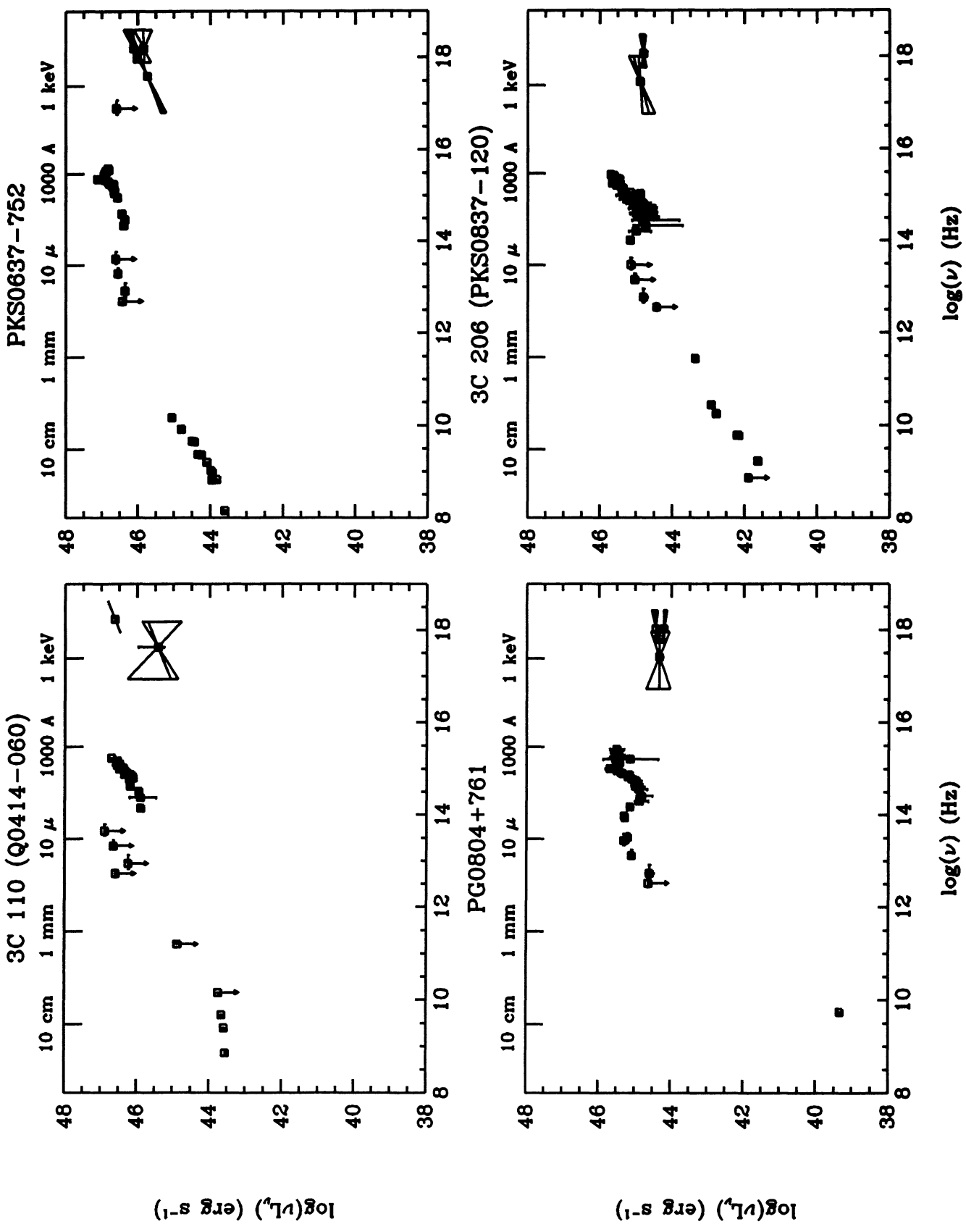

FIG. 8—*Continued*

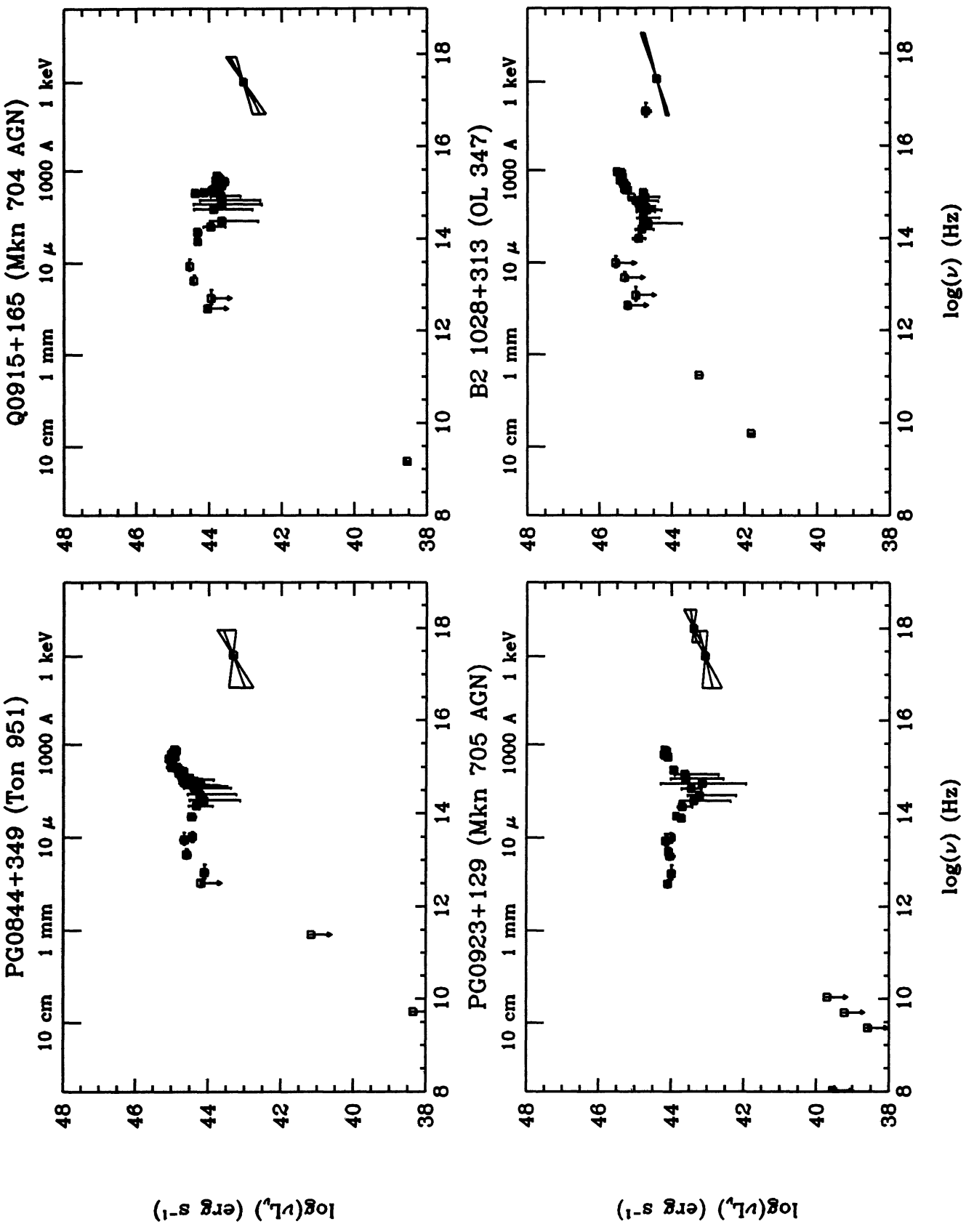

FIG. 8—*Continued*

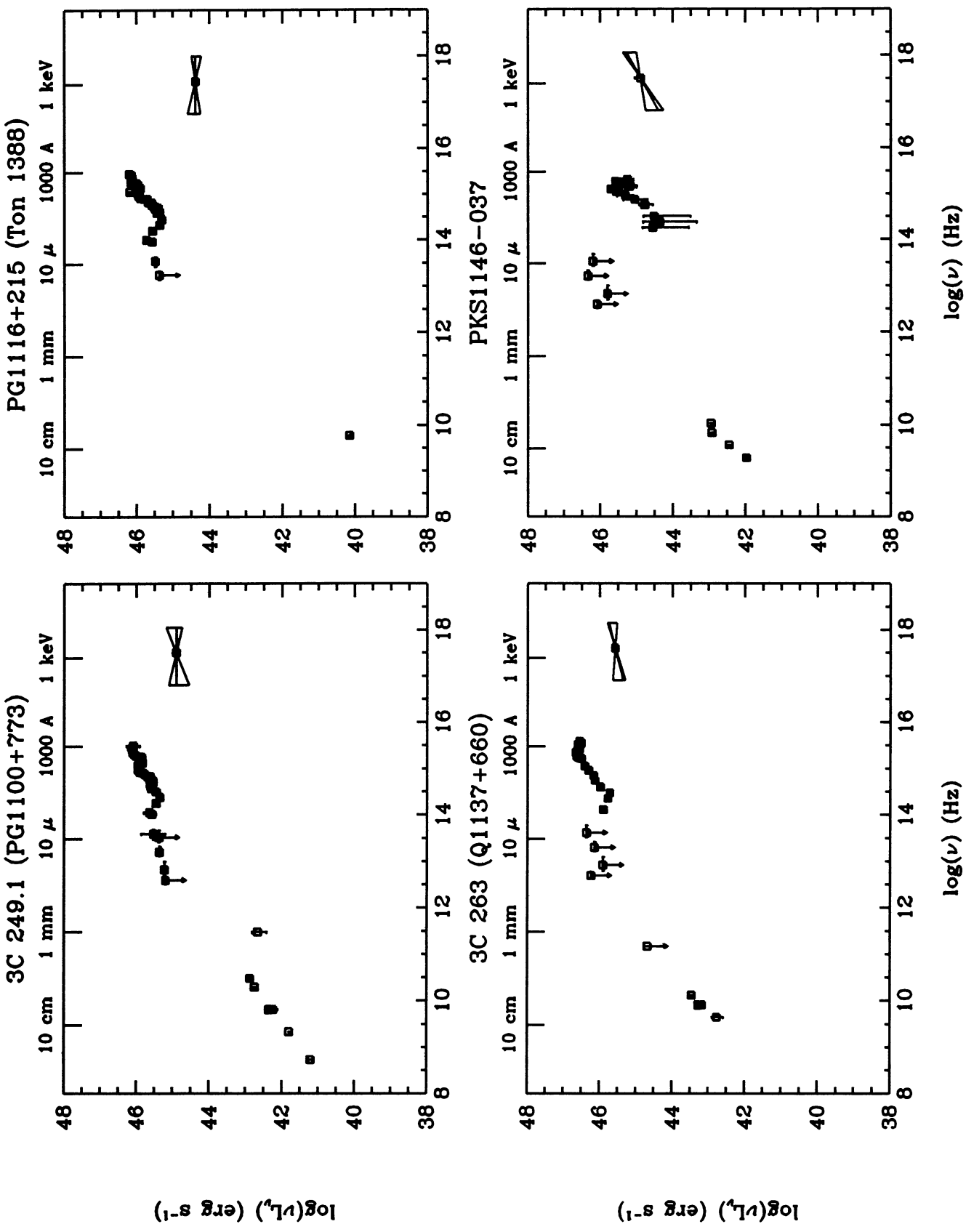

FIG. 8—*Continued*

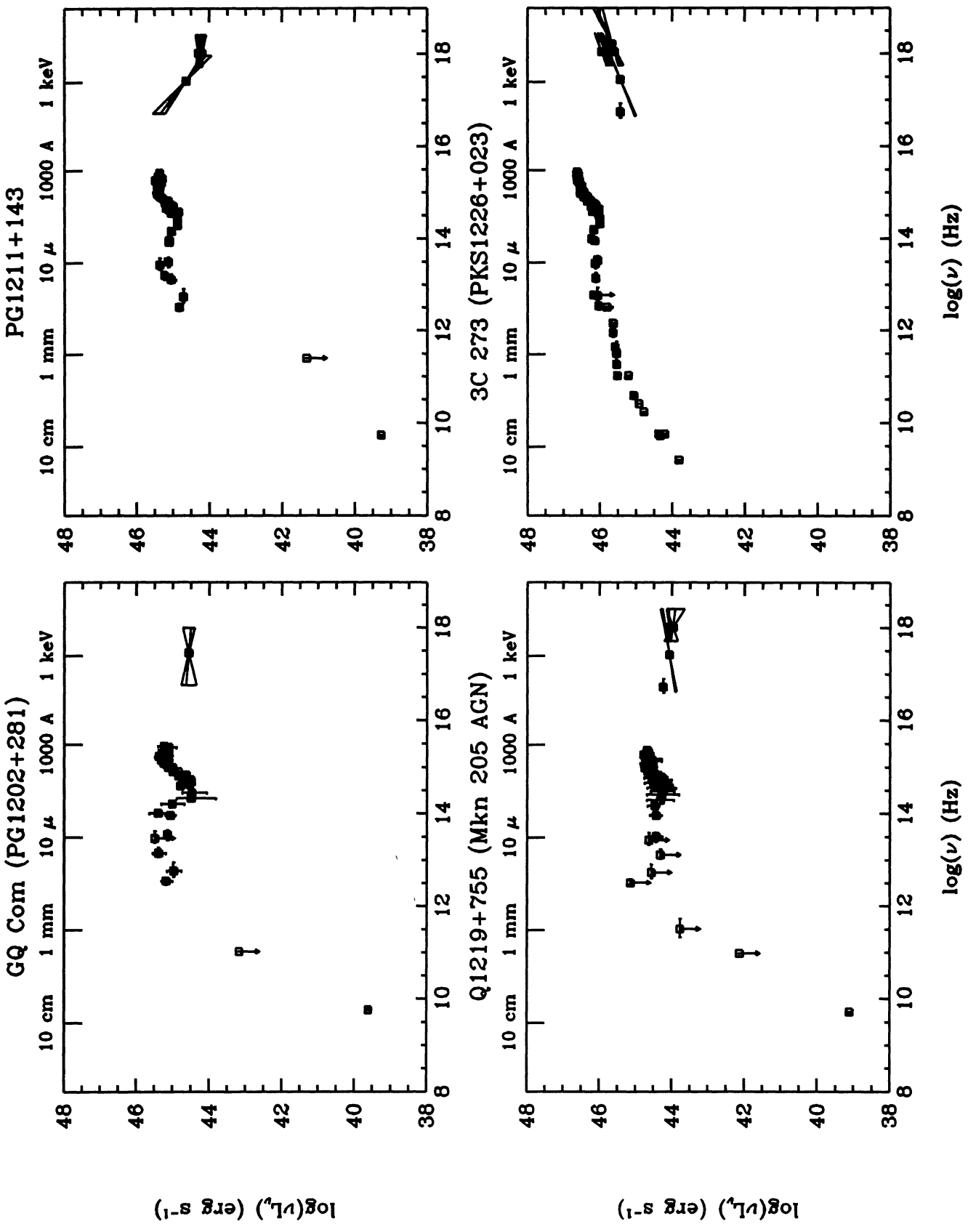

FIG. 8—*Continued*

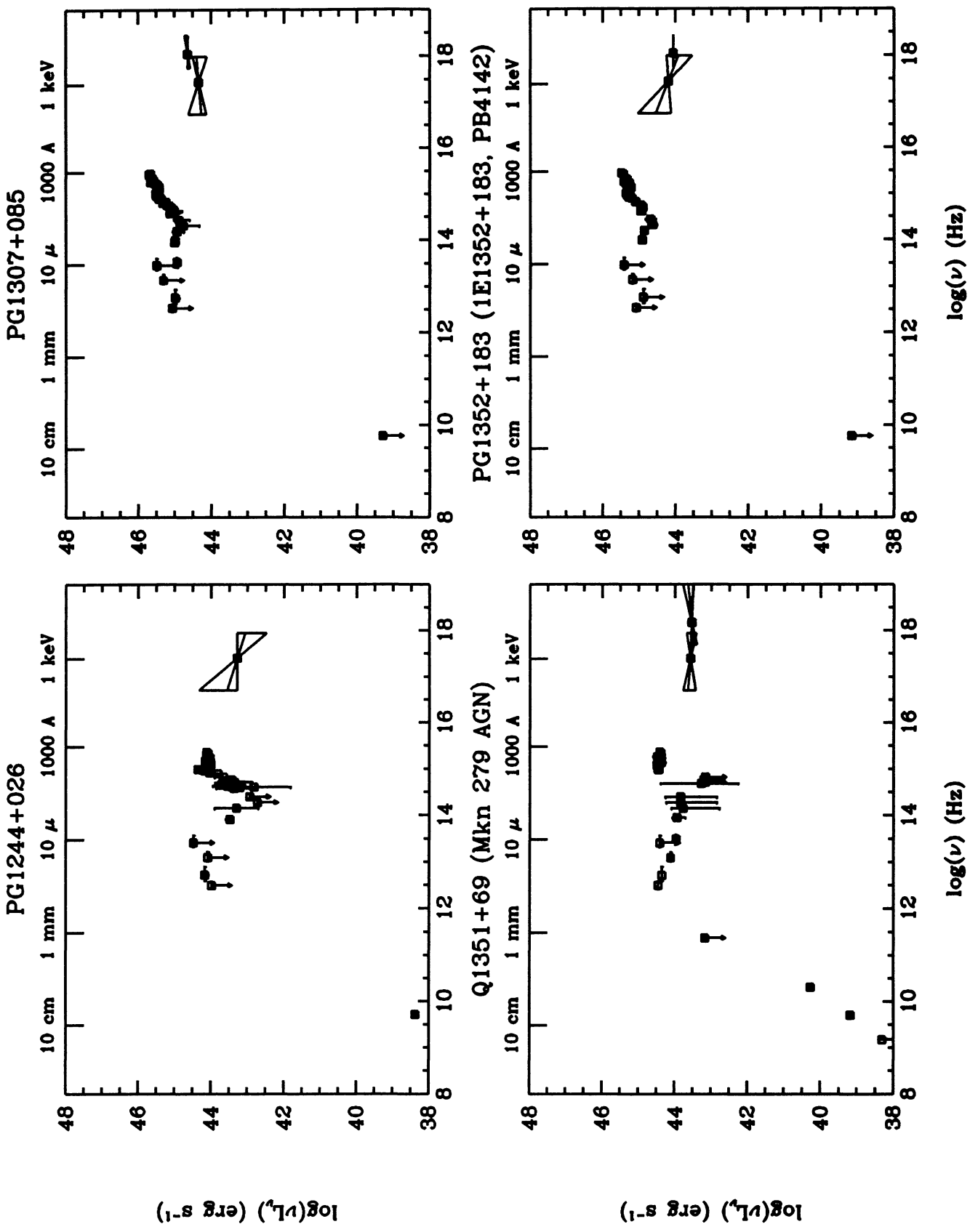

FIG. 8—*Continued*

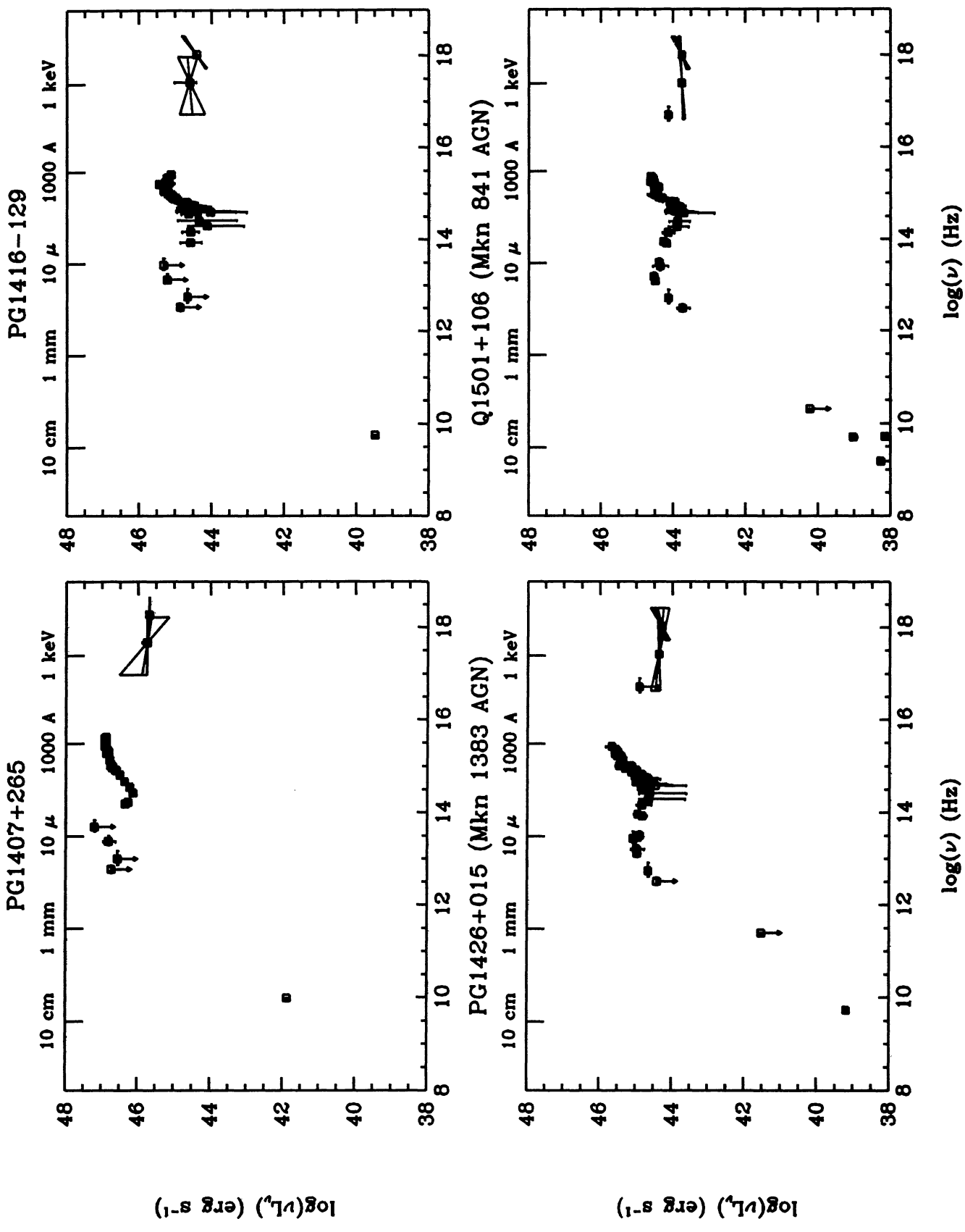

FIG. 8—*Continued*

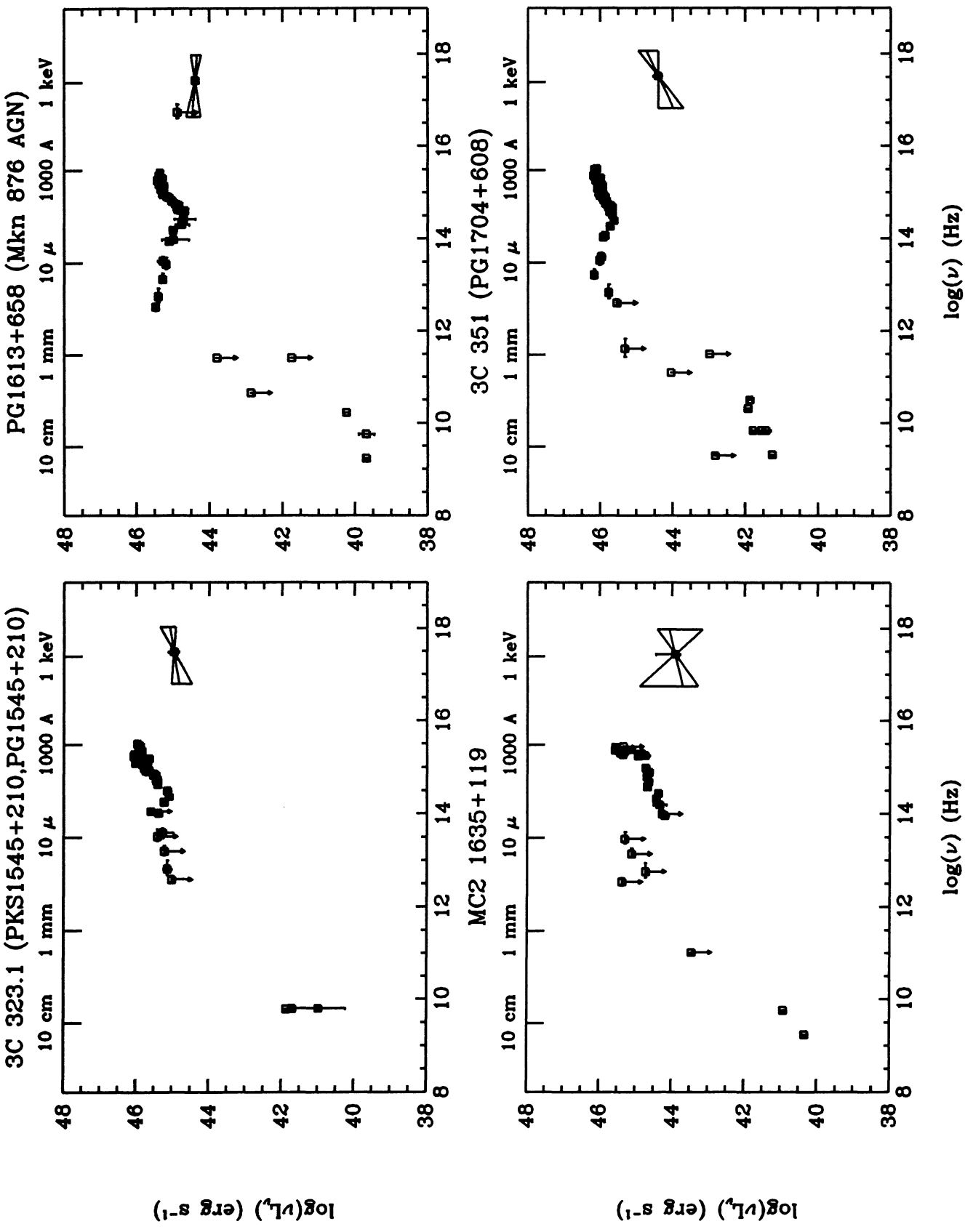

FIG. 8—*Continued*

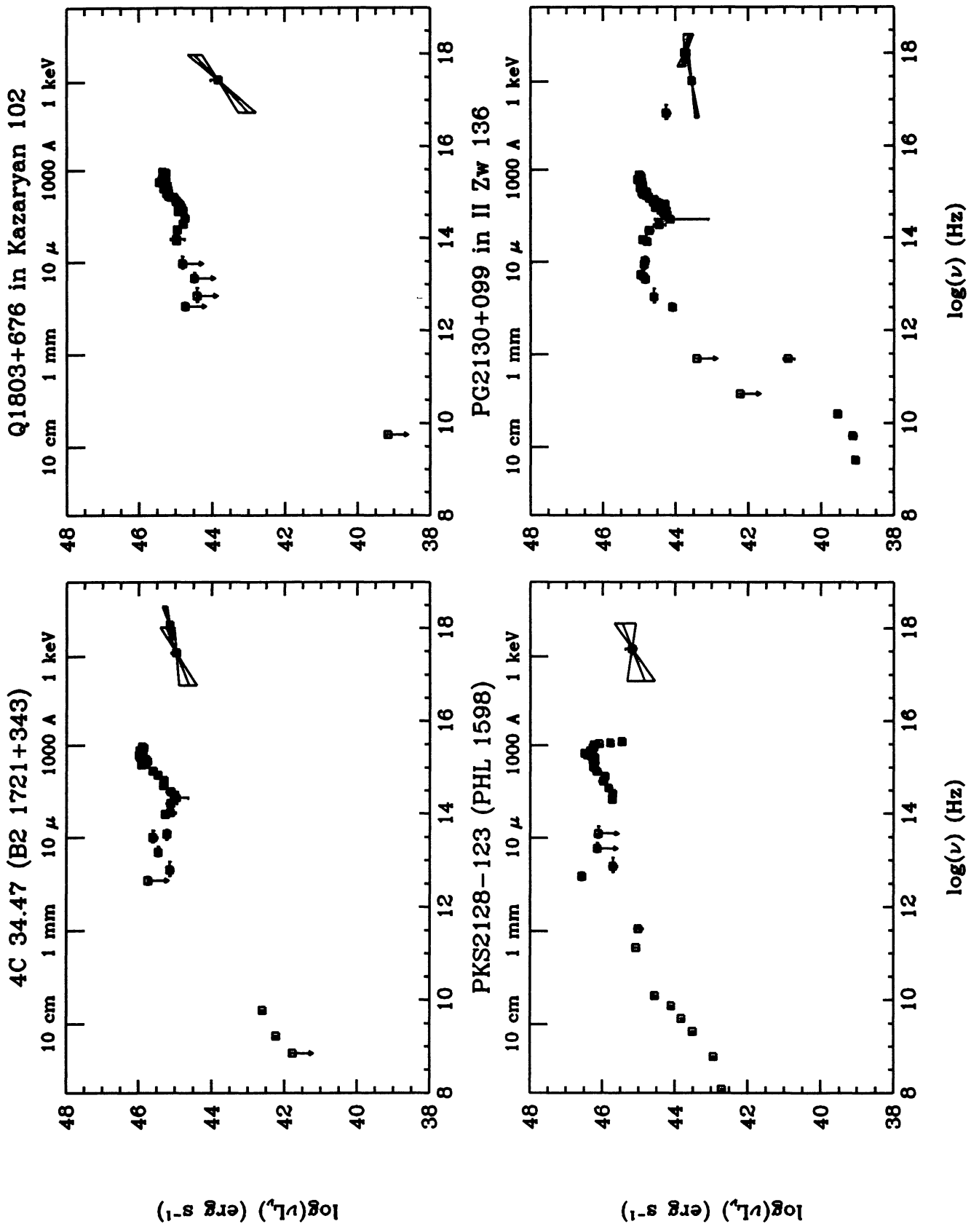

FIG. 8—*Continued*

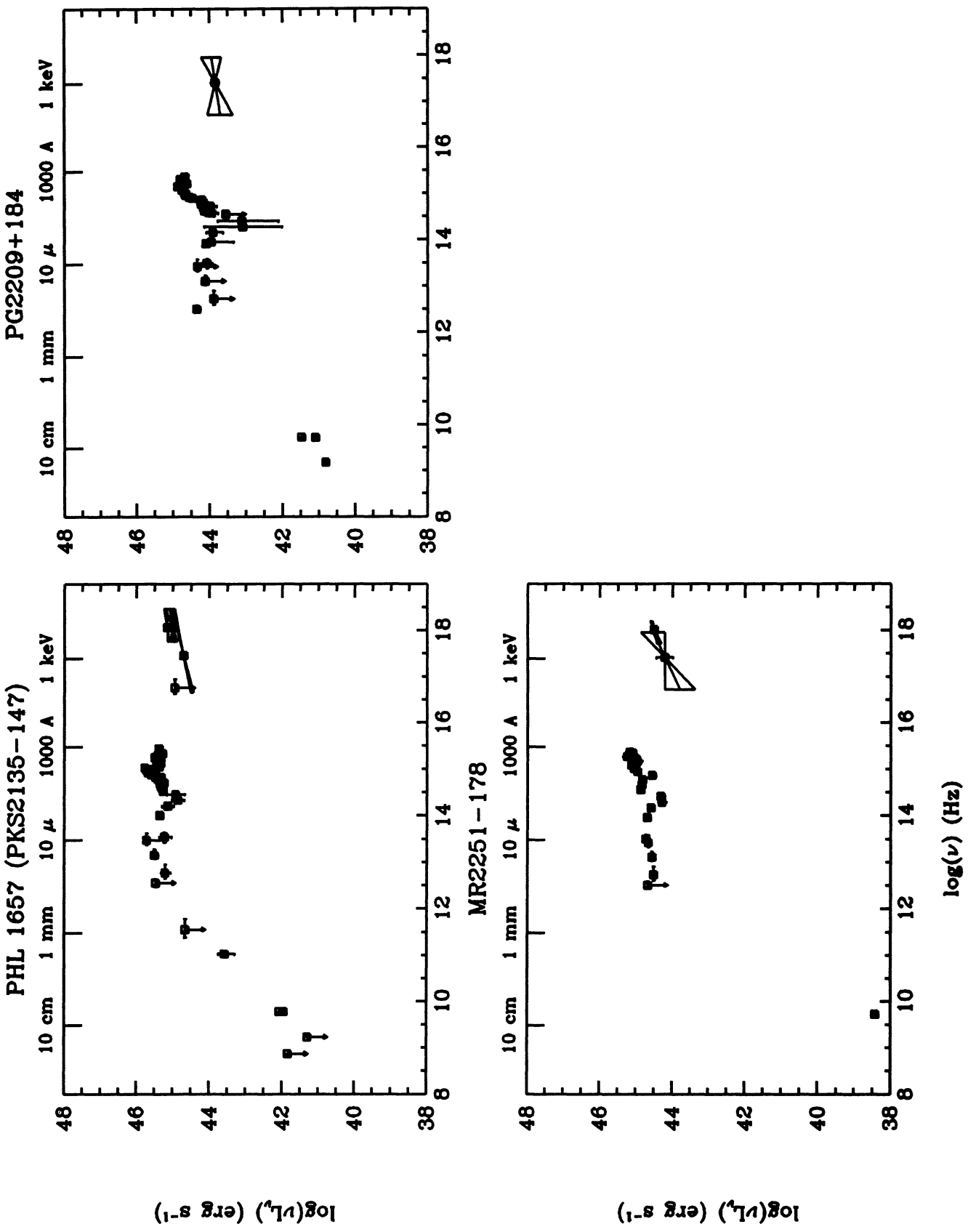

FIG. 8—*Continued*

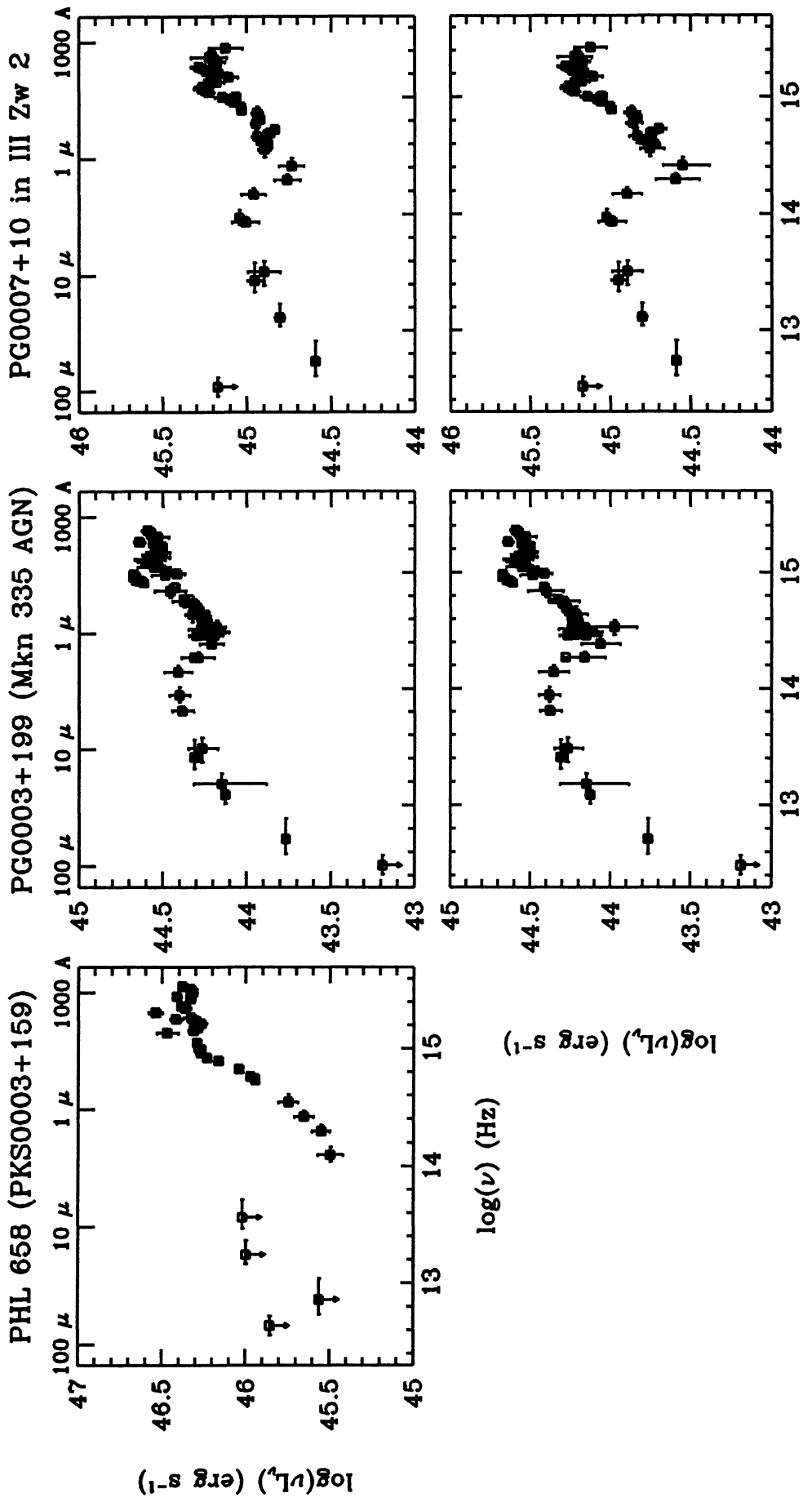

FIG. 9.—Rest frame, dereddened continuum energy distributions of the quasar sample, showing the details of the UVOIR (100 μm to 1000 Å) region. When two panels are present for an object, the upper panel shows the data before host galaxy subtraction, and the lower panel shows the same region after host galaxy subtraction (see text).

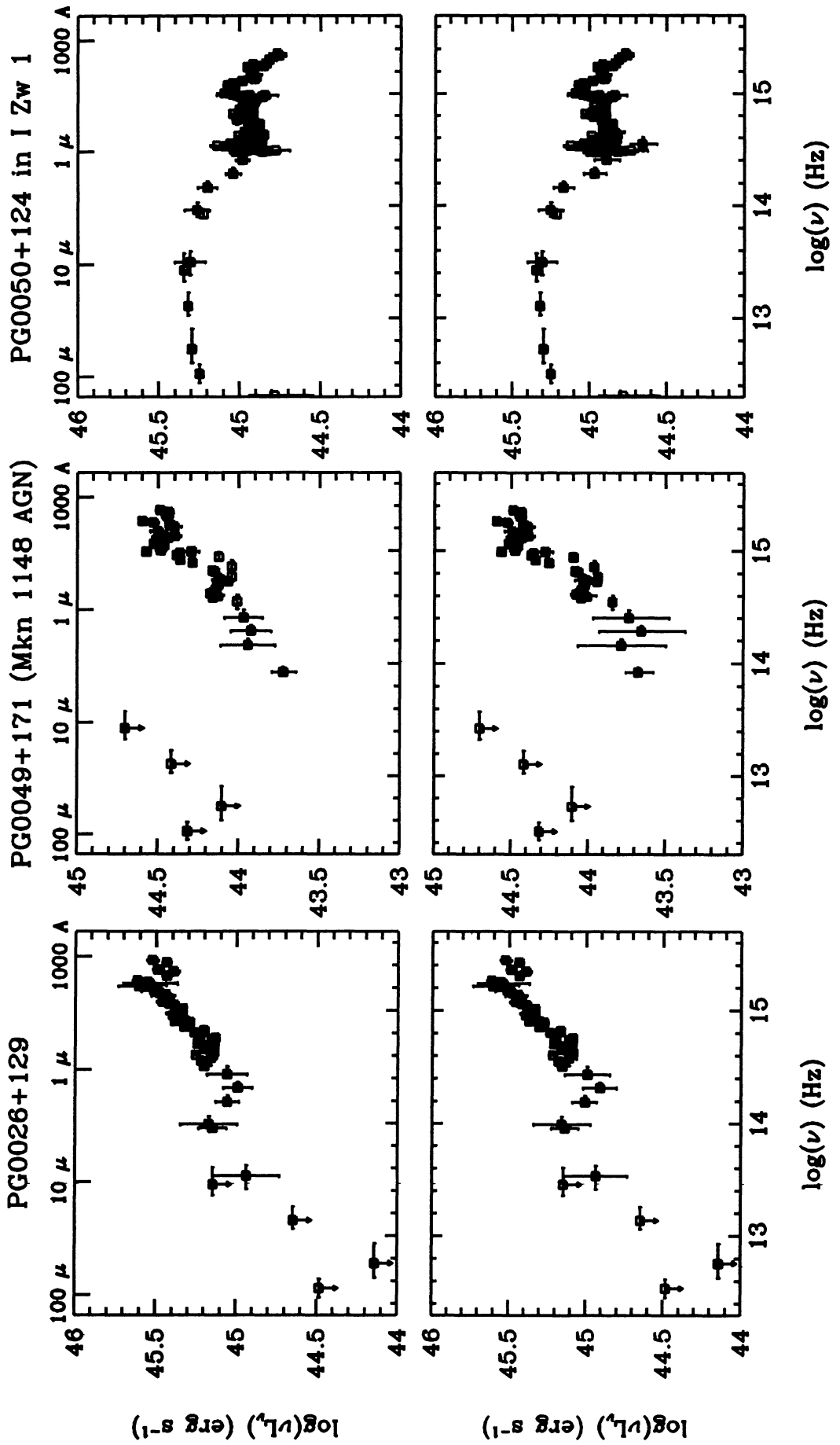

FIG. 9—*Continued*

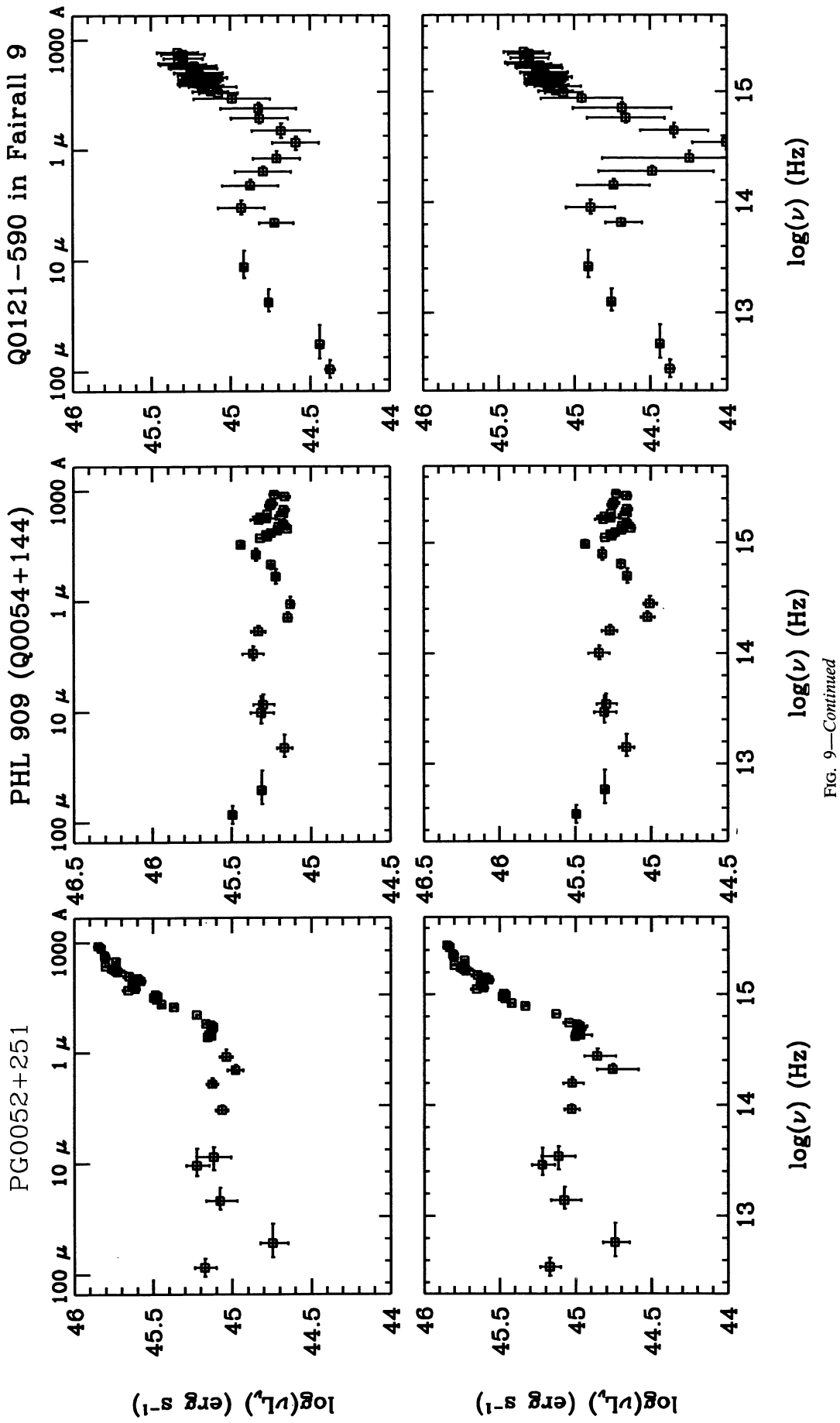

FIG. 9—*Continued*

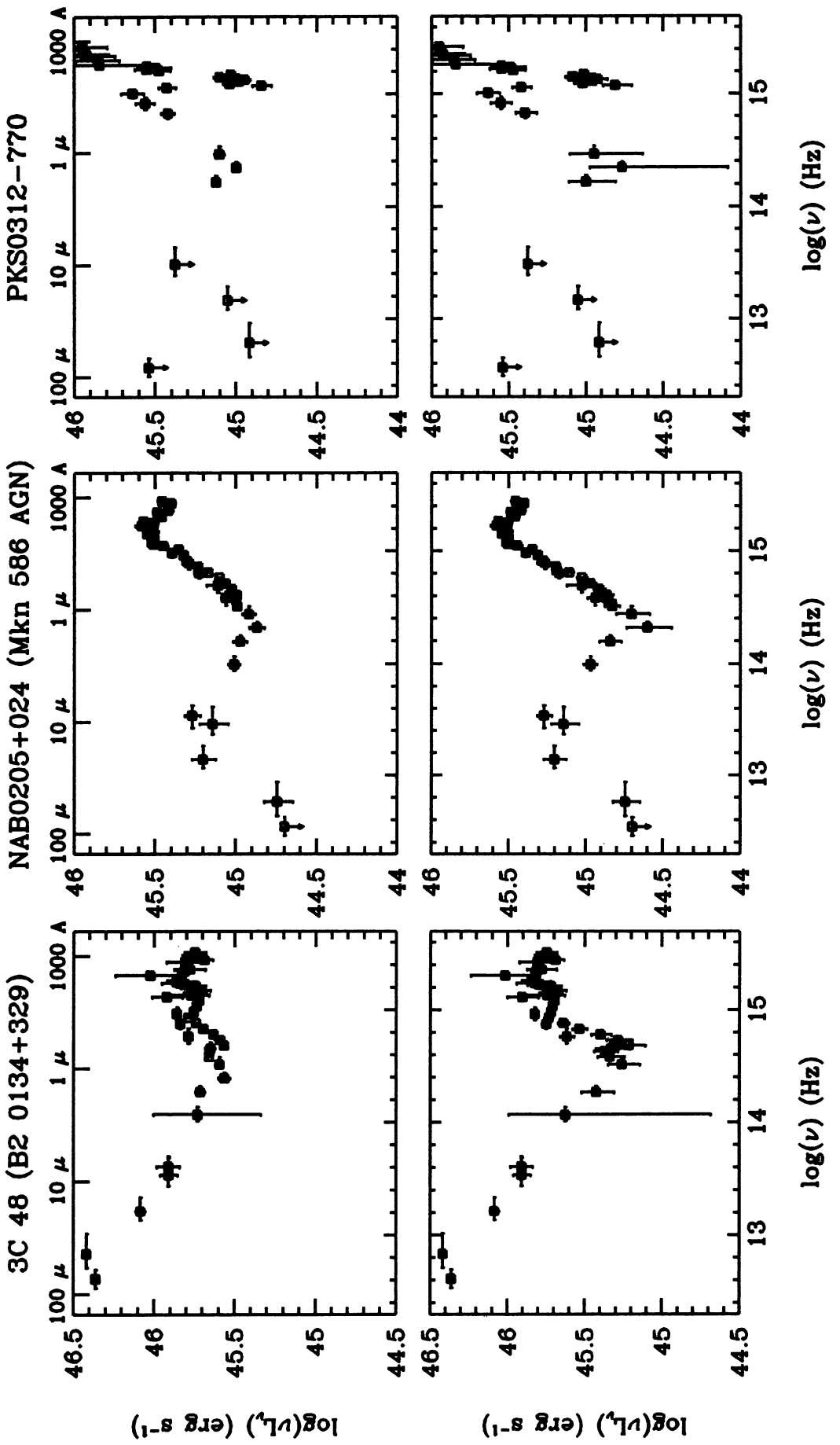

FIG. 9—*Continued*

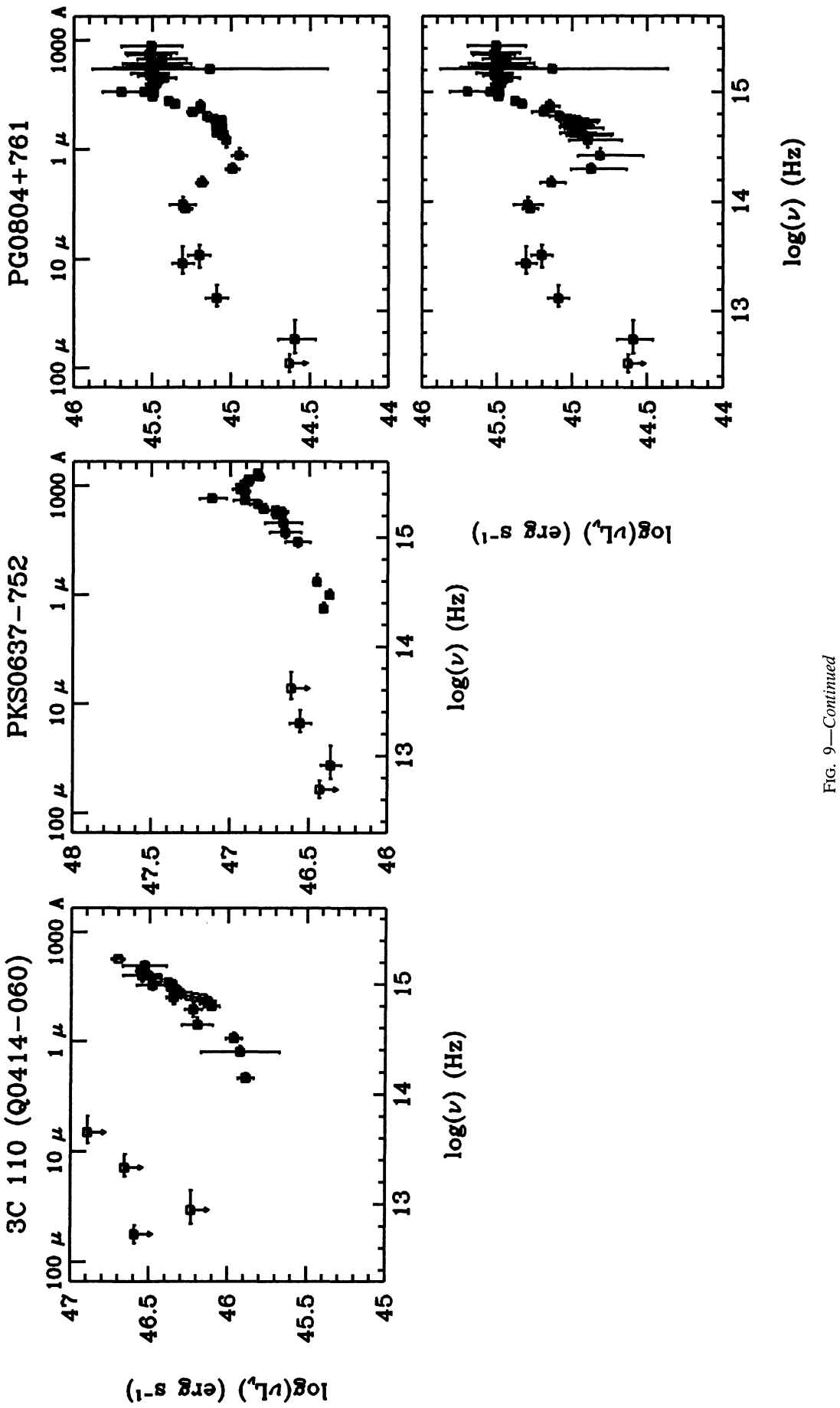

FIG. 9—*Continued*

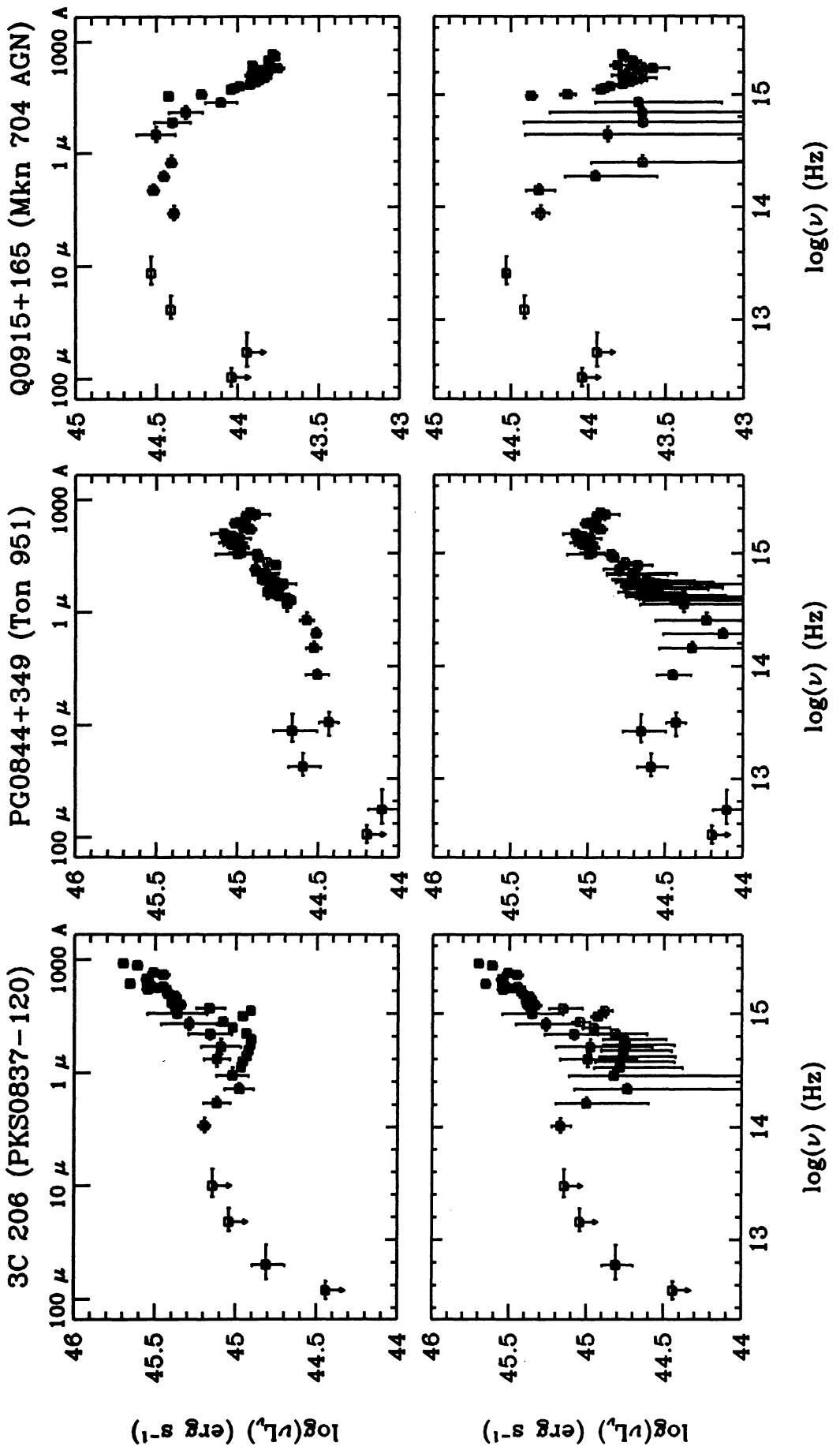

FIG. 9—*Continued*

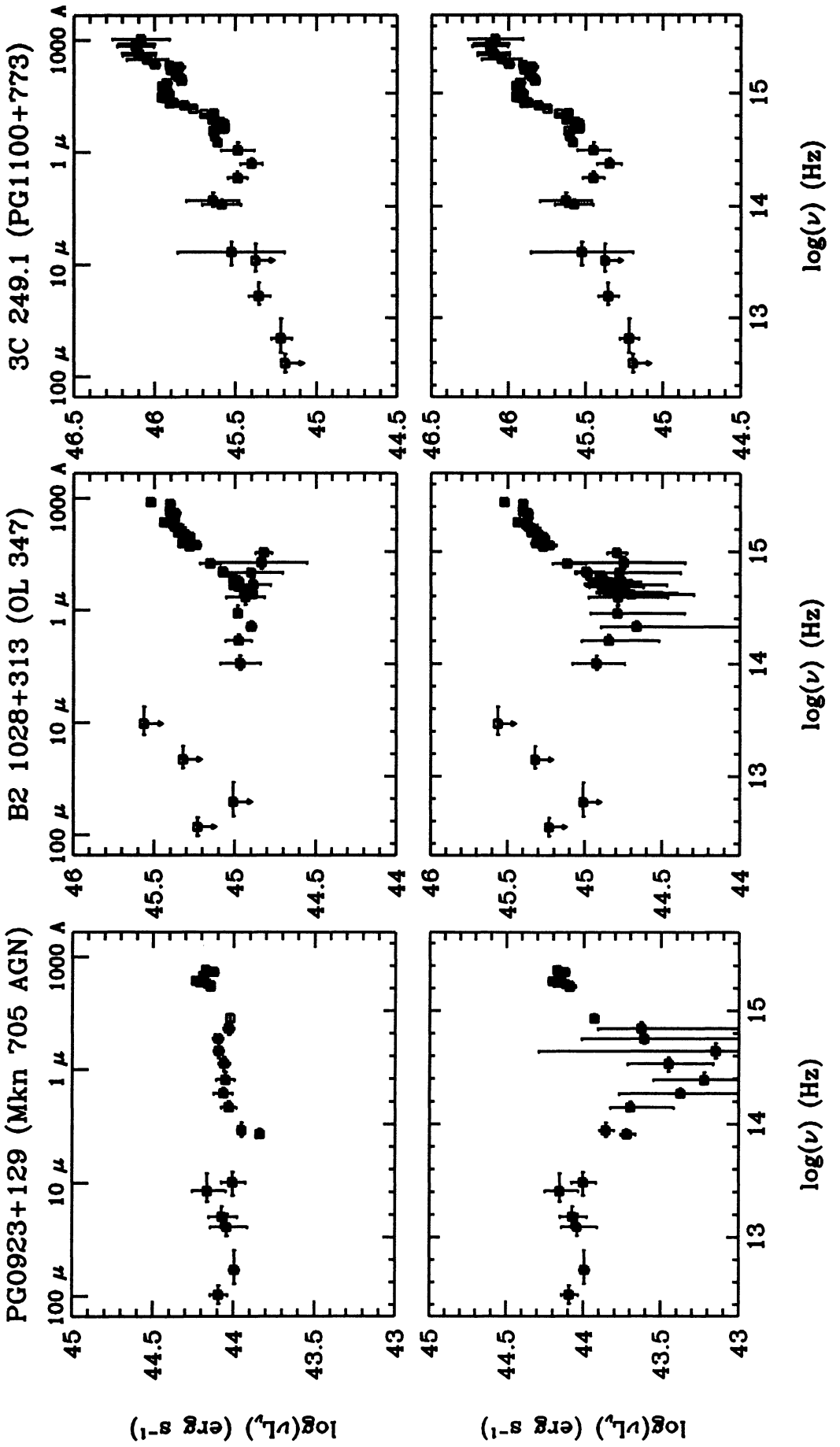

FIG. 9—*Continued*

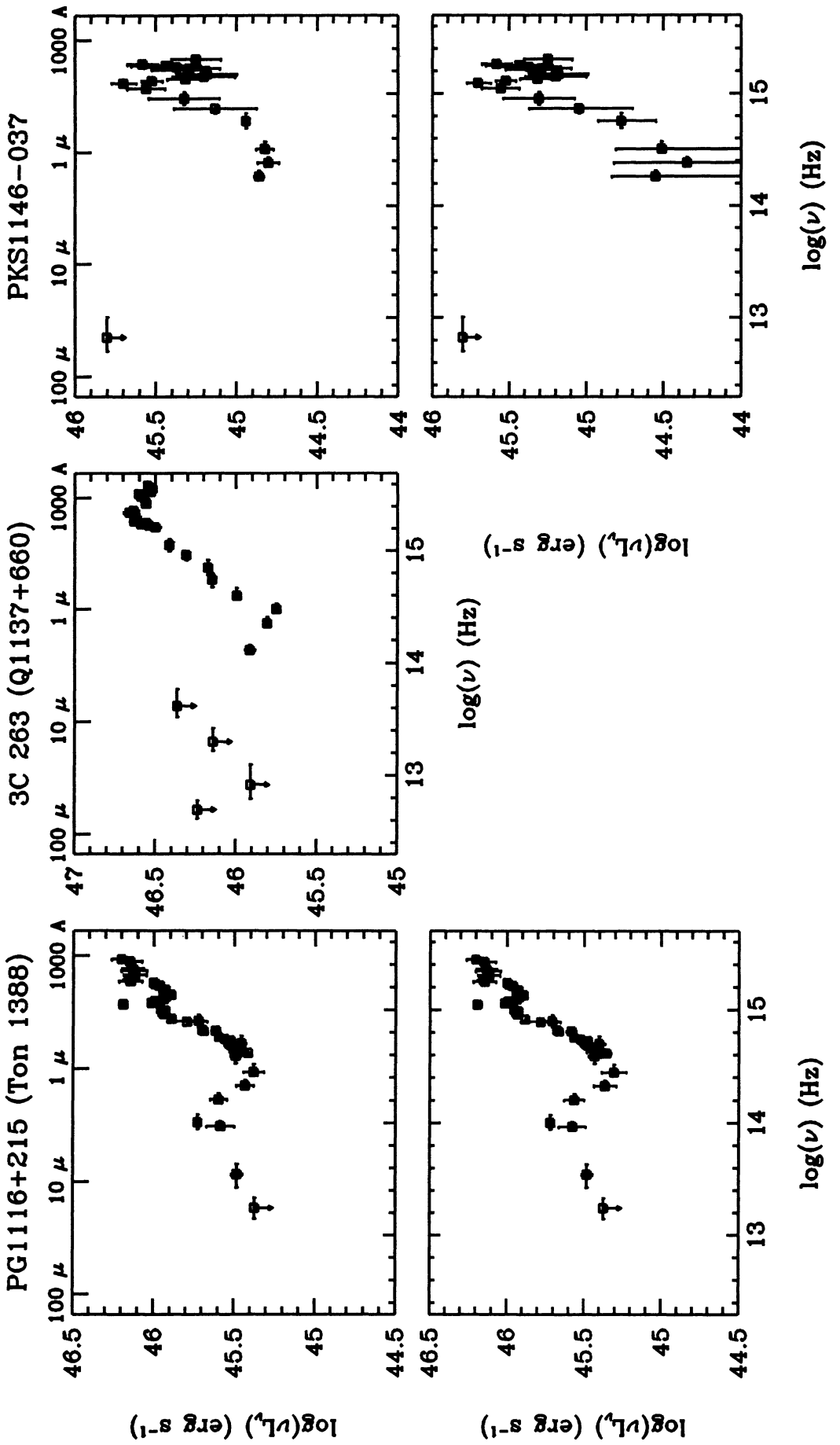

FIG. 9—*Continued*

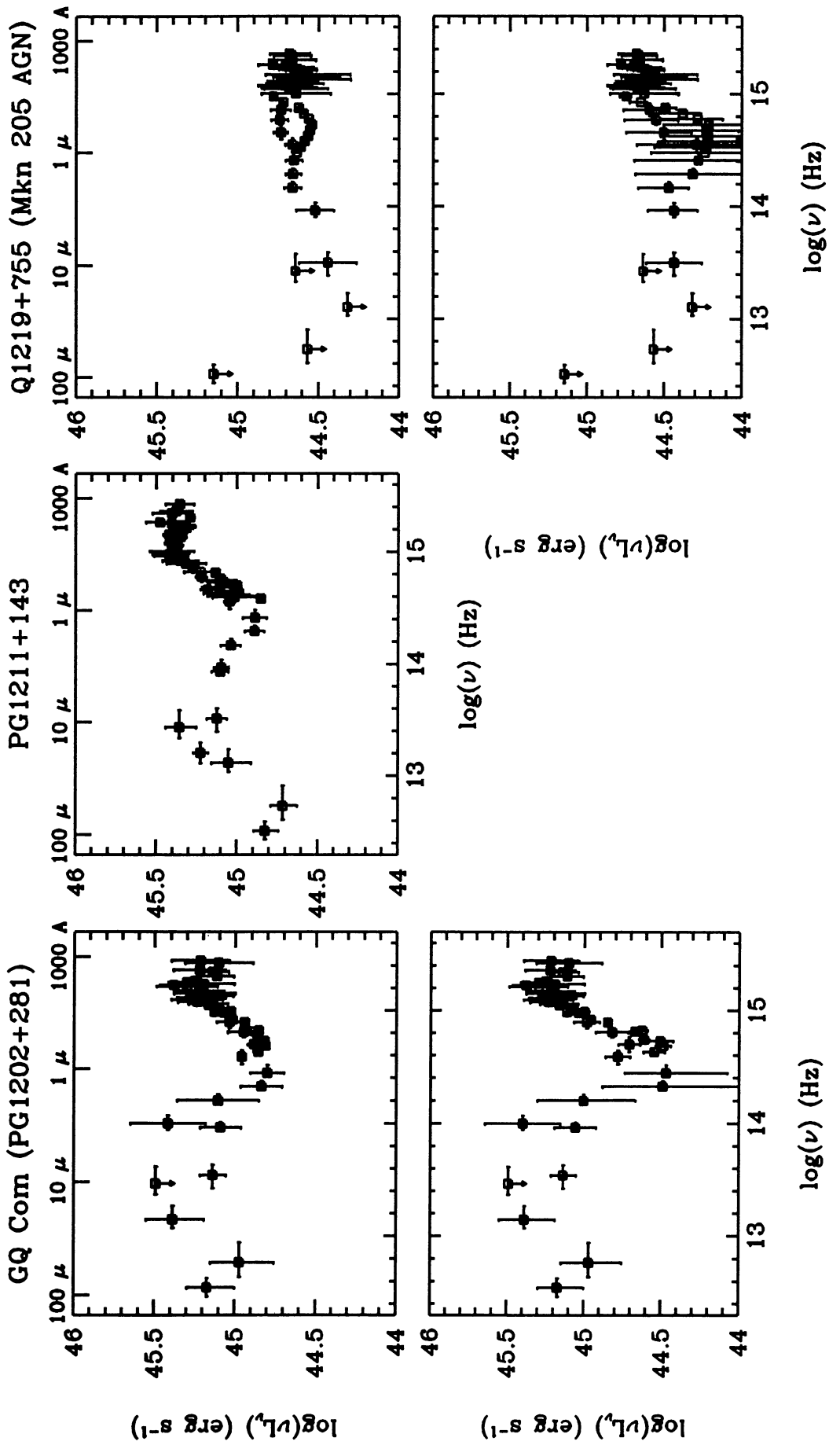

FIG. 9—*Continued*

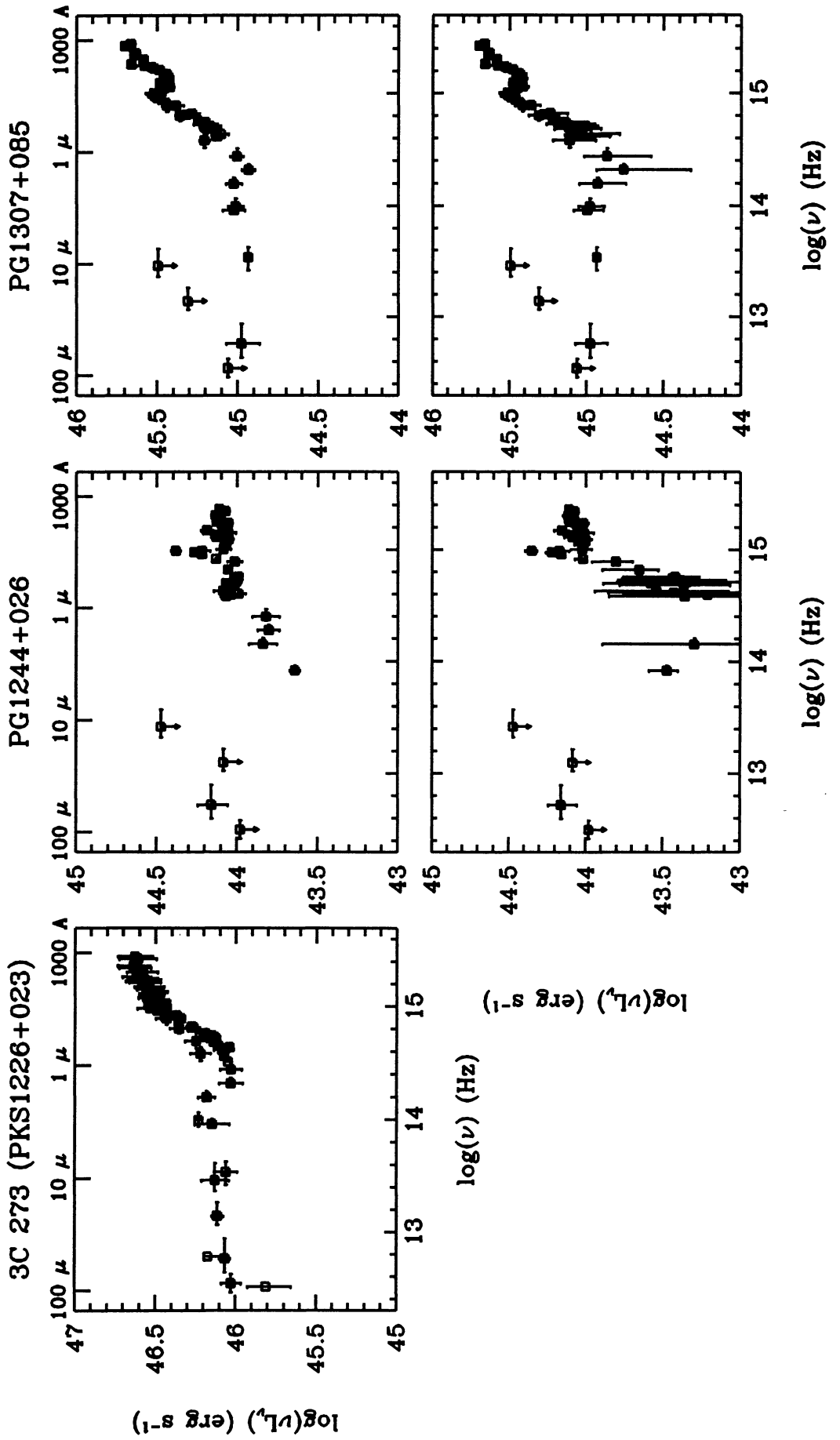

FIG. 9—*Continued*

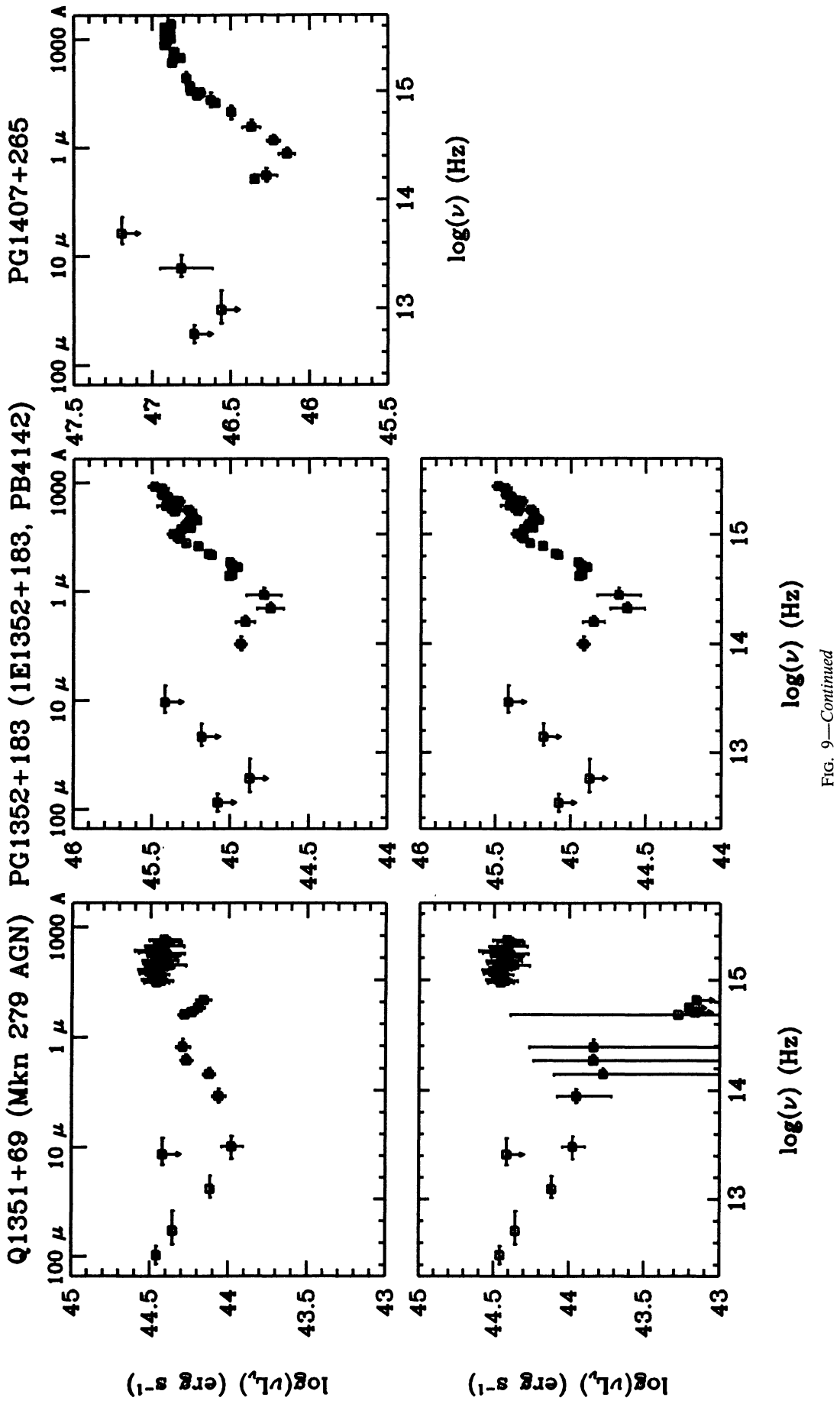

FIG. 9—*Continued*

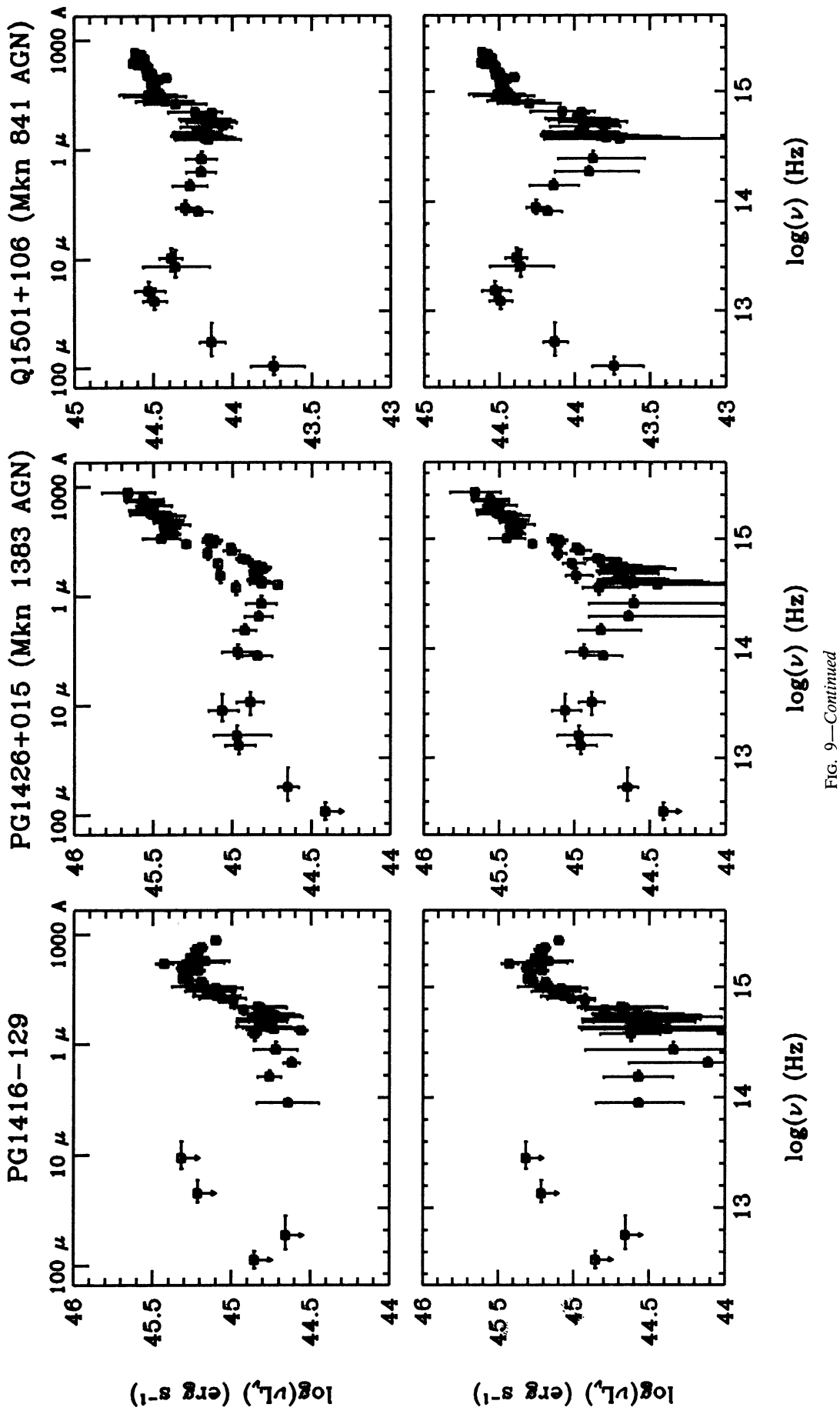

FIG. 9—*Continued*

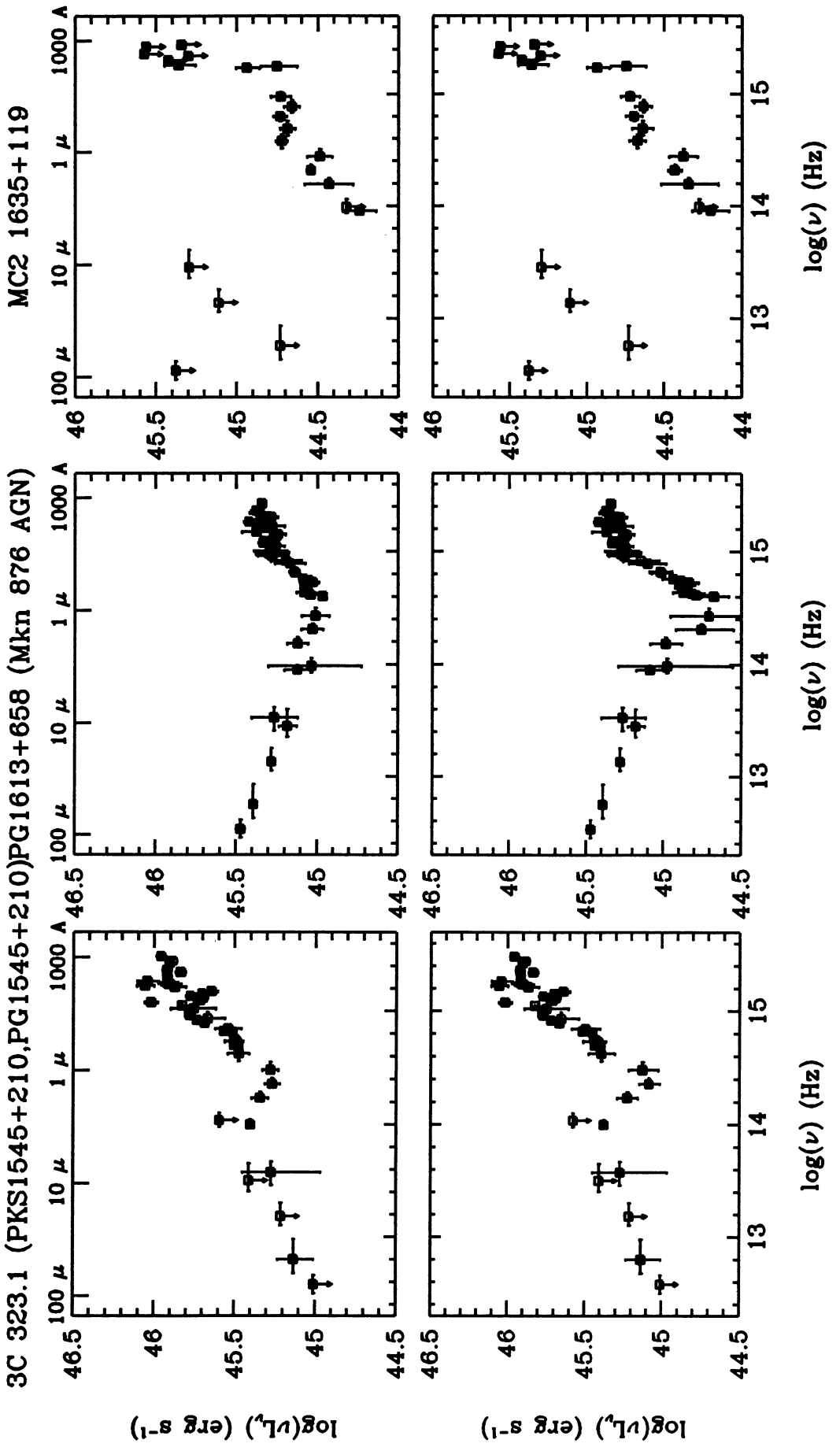

FIG. 9—*Continued*

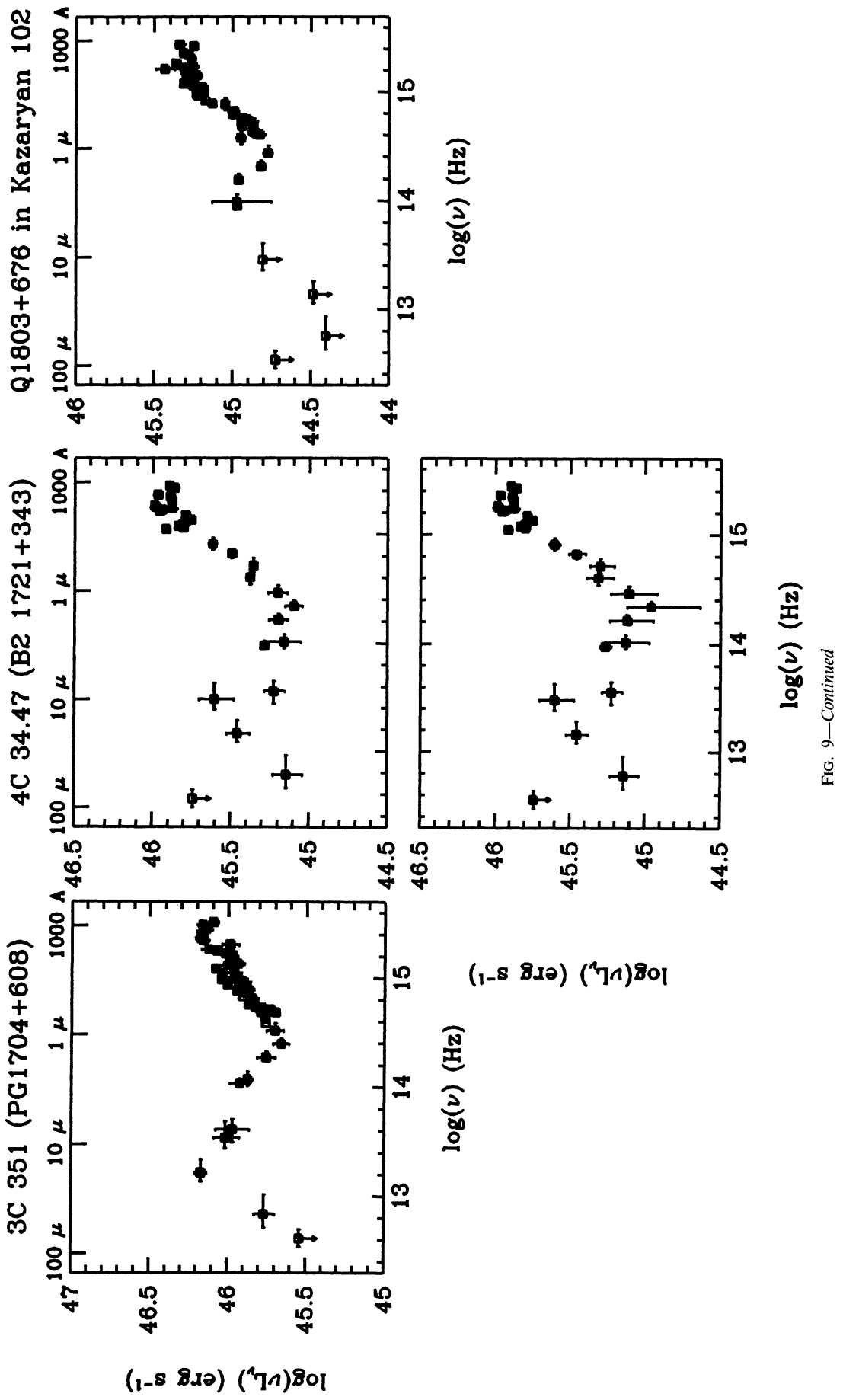

FIG. 9—*Continued*

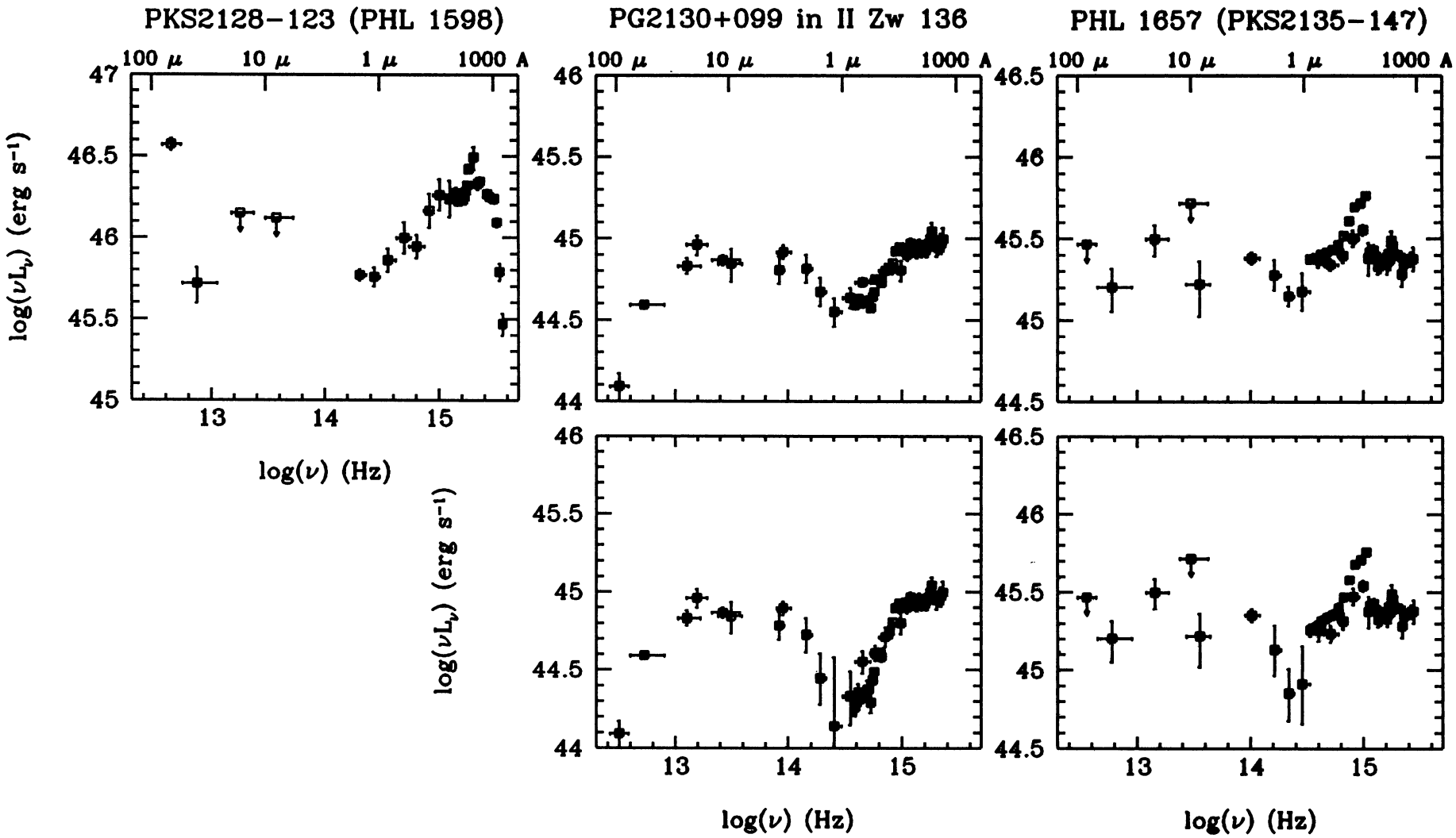

FIG. 9—*Continued*

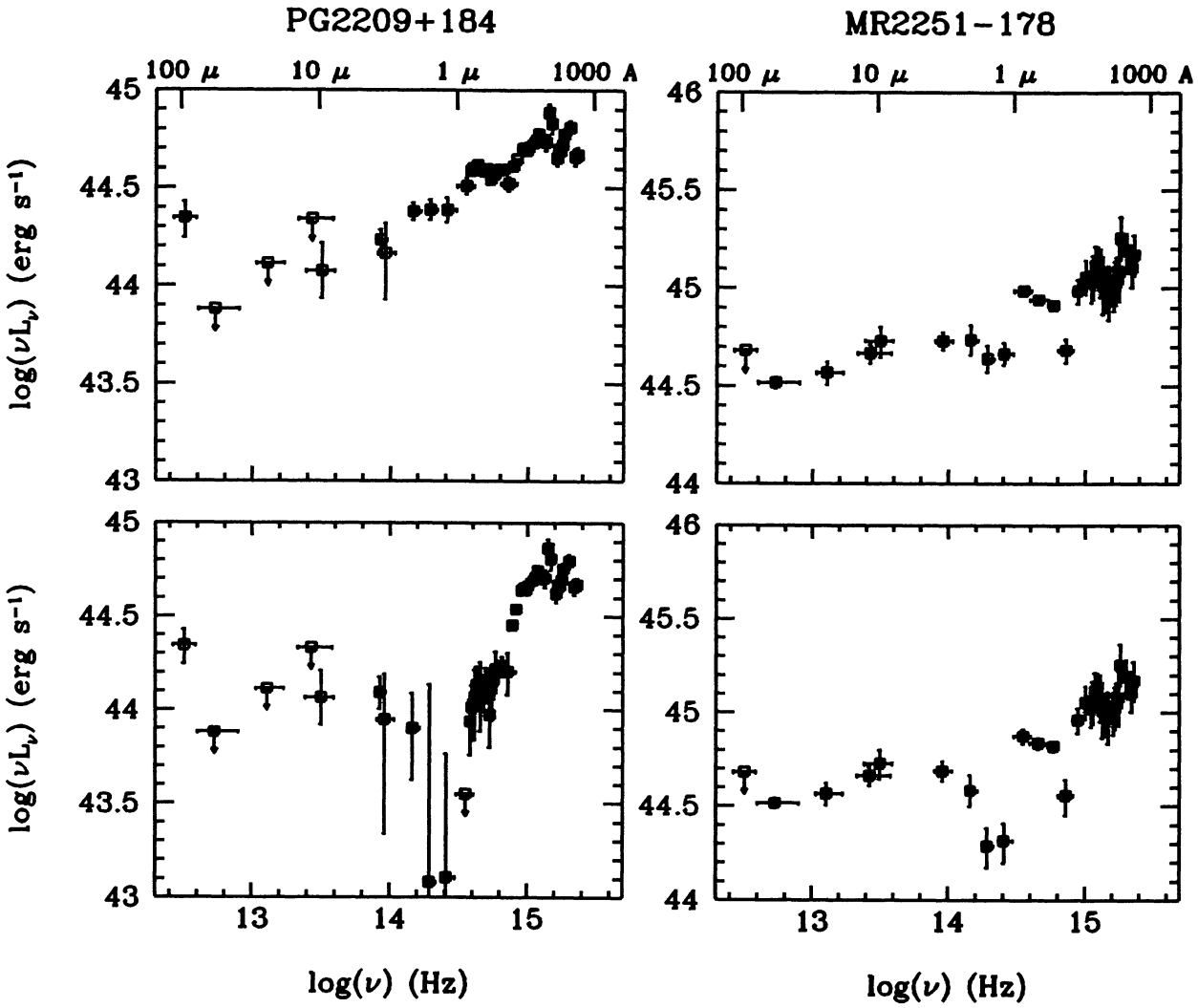

FIG. 9—*Continued*

of νL_ν at B may be multiplied by the median derived visual bolometric correction in Table 17, approximately a factor of 12. This is somewhat smaller than the value of 16.5 derived by Sanders et al. (1989) in their study, and the range of actual values of the correction covers a factor of 5. The median value of $N_{\rm Ion}R/L_{\rm Bol}$ found in our sample is 0.12. This means that for a quasar of bolometric luminosity of 10^{44} ergs s^{-1}, the corresponding median rate of emission of ionizing photons is $N_{\rm Ion} = 5.5 \times 10^{53}$ photons s^{-1}. The median value of the mean ionizing photon energy is found to be 2.8 rydberg.

In Figure 10 we present the quasar mean energy distribution (MED). This distribution is obtained by normalizing the individual starlight-subtracted energy distributions and smoothing them with a $\Delta \log(\nu) = 0.2$ boxcar. The mean of $\log(\nu L\omega)$ is then calculated using the Kaplan-Meier estimator (Feigelson & Nelson 1985). Figure 10 shows the MED for radio-quiet and radio-loud quasars separately, over the full frequency range we have studied. Note that the different X-ray slopes for radio-loud and radio-quiet quasars show up clearly, but that the MED for radio-loud and radio-quiet quasars is indistinguish-

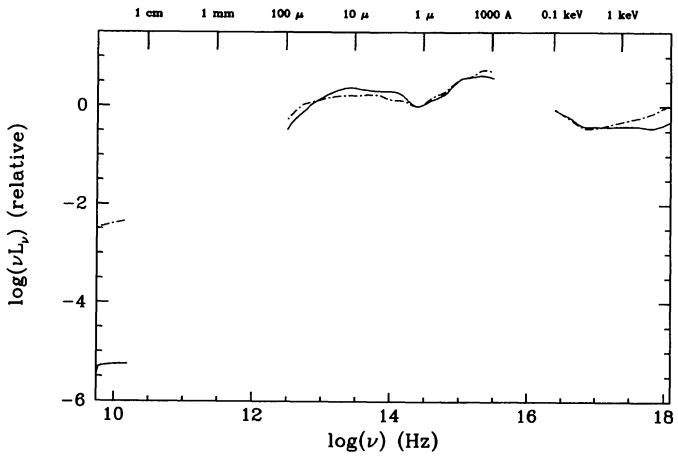

FIG. 10.—The mean quasar energy distribution, normalized at 1.25 μm, for radio-loud (*dashed line*) and radio-quiet (*solid line*) quasars. Spectral regions where few or no data are available are omitted. The radio-loud distribution has a rising X-ray spectrum in this plot, while the radio-quiet X-ray spectrum is horizontal.

TABLE 14

BOLOMETRIC AND MULTIWAVEBAND LUMINOSITIES

Name	UVOIR (0.1 – 100μm)	Bolometric (1 m-10 keV)	Ly cont (912Å-10 keV)	Ionizing Photon Rate
Q0003+158	$46.65^{+0.19}_{-0.08}$	$47.14^{+1.22}_{-0.28}$	$46.97^{+1.38}_{-0.43}$	$46.37^{+0.91}_{-0.23}$
Q0003+199	$45.20^{+0.05}_{-0.06}$	$45.48^{+0.03}_{-0.04}$	$45.14^{+0.01}_{-0.01}$	$44.68^{+0.01}_{-0.01}$
Q0007+106	$45.75^{+0.06}_{-0.06}$	$45.92^{+0.12}_{-0.08}$	$45.32^{+0.23}_{-0.11}$	$44.73^{+0.23}_{-0.12}$
Q0026+129	$45.92^{+0.09}_{-0.11}$	$46.12^{+0.09}_{-0.09}$	$45.64^{+0.05}_{-0.05}$	$45.20^{+0.05}_{-0.05}$
Q0049+171	$44.76^{+0.38}_{-0.08}$	$45.21^{+1.07}_{-0.16}$	$45.01^{+1.23}_{-0.21}$	$44.37^{+0.97}_{-0.16}$
Q0050+124	$46.00^{+0.03}_{-0.03}$	$46.10^{+0.30}_{-0.08}$	$45.32^{+0.82}_{-0.34}$	$44.69^{+0.59}_{-0.22}$
Q0052+251	$46.09^{+0.05}_{-0.05}$	$46.34^{+0.33}_{-0.11}$	$45.92^{+0.58}_{-0.17}$	$45.53^{+0.36}_{-0.11}$
Q0054+144	$46.10^{+0.04}_{-0.06}$	$46.22^{+0.05}_{-0.08}$	$45.49^{+0.07}_{-0.08}$	$45.00^{+0.05}_{-0.06}$
Q0121-590	$45.68^{+0.14}_{-0.12}$	$45.86^{+0.13}_{-0.11}$	$45.36^{+0.11}_{-0.10}$	$44.95^{+0.12}_{-0.12}$
Q0134+329	$46.79^{+0.06}_{-0.12}$	$46.92^{+0.07}_{-0.18}$	$45.93^{+0.15}_{-0.14}$	$45.49^{+0.11}_{-0.10}$
Q0205+024	$45.97^{+0.05}_{-0.06}$	$46.17^{+0.06}_{-0.07}$	$45.72^{+0.06}_{-0.07}$	$45.29^{+0.05}_{-0.06}$
Q0312-770	$46.01^{+0.25}_{-0.23}$	$46.24^{+0.27}_{-0.20}$	$45.78^{+0.22}_{-0.15}$	$45.51^{+0.19}_{-0.14}$
Q0414-060	$46.94^{+0.41}_{-0.13}$	$47.26^{+0.36}_{-0.09}$	$46.94^{+0.29}_{-0.06}$	$46.38^{+0.22}_{-0.08}$
Q0637-752	$47.37^{+0.07}_{-0.06}$	$47.55^{+0.16}_{-0.21}$	$46.92^{+0.37}_{-0.50}$	$46.56^{+0.23}_{-0.55}$
Q0804+761	$46.02^{+0.11}_{-0.10}$	$46.16^{+0.15}_{-0.14}$	$45.55^{+0.24}_{-0.22}$	$45.15^{+0.23}_{-0.22}$
Q0837-120	$45.92^{+0.09}_{-0.29}$	$46.22^{+0.09}_{-0.19}$	$45.87^{+0.08}_{-0.07}$	$45.39^{+0.07}_{-0.06}$
Q0844+349	$45.43^{+0.11}_{-0.15}$	$45.49^{+0.13}_{-0.13}$	$44.61^{+0.18}_{-0.11}$	$44.32^{+0.14}_{-0.09}$
Q0915+165	$45.00^{+0.11}_{-0.07}$	$45.05^{+0.12}_{-0.15}$	$43.89^{+0.10}_{-0.09}$	$43.37^{+0.08}_{-0.06}$
Q0923+129	$44.76^{+0.11}_{-0.10}$	$45.28^{+0.26}_{-0.50}$	$44.22^{+0.12}_{-0.11}$	$43.73^{+0.10}_{-0.09}$
Q1028+313	$45.73^{+0.35}_{-0.23}$	$46.04^{+0.24}_{-0.15}$	$45.72^{+0.05}_{-0.06}$	$45.27^{+0.04}_{-0.05}$
Q1100+772	$46.44^{+0.09}_{-0.08}$	$46.63^{+0.13}_{-0.13}$	$46.15^{+0.18}_{-0.22}$	$45.78^{+0.18}_{-0.21}$
Q1116+215	$46.44^{+0.06}_{-0.08}$	$46.58^{+0.07}_{-0.08}$	$45.98^{+0.10}_{-0.08}$	$45.72^{+0.09}_{-0.08}$
Q1137+660	$46.85^{+0.21}_{-0.11}$	$47.11^{+0.18}_{-0.08}$	$46.72^{+0.10}_{-0.05}$	$46.32^{+0.06}_{-0.03}$
Q1146-037	$45.65^{+1.01}_{-0.27}$	$45.96^{+0.82}_{-0.22}$	$45.63^{+0.21}_{-0.15}$	$44.95^{+0.22}_{-0.15}$
Q1202+281	$45.94^{+0.17}_{-0.19}$	$46.11^{+0.17}_{-0.21}$	$45.55^{+0.15}_{-0.20}$	$45.02^{+0.17}_{-0.21}$
Q1211+143	$45.98^{+0.07}_{-0.07}$	$46.26^{+0.11}_{-0.09}$	$45.92^{+0.15}_{-0.11}$	$45.33^{+0.13}_{-0.11}$
Q1219+755	$45.20^{+0.31}_{-0.22}$	$45.45^{+0.30}_{-0.16}$	$45.07^{+0.08}_{-0.09}$	$44.50^{+0.10}_{-0.10}$
Q1226+023	$47.08^{+0.07}_{-0.06}$	$47.28^{+0.07}_{-0.07}$	$46.69^{+0.08}_{-0.09}$	$46.28^{+0.09}_{-0.09}$
Q1244+026	$44.66^{+0.12}_{-0.08}$	$44.87^{+0.25}_{-0.15}$	$44.39^{+0.42}_{-0.16}$	$43.90^{+0.30}_{-0.11}$
Q1307+085	$46.00^{+0.07}_{-0.11}$	$46.16^{+0.11}_{-0.07}$	$45.66^{+0.12}_{-0.06}$	$45.27^{+0.10}_{-0.05}$
Q1351+695	$44.97^{+0.12}_{-0.10}$	$45.18^{+0.13}_{-0.15}$	$44.64^{+0.11}_{-0.13}$	$44.13^{+0.11}_{-0.13}$
Q1352+183	$45.87^{+0.13}_{-0.25}$	$45.94^{+0.30}_{-0.09}$	$45.59^{+0.22}_{-0.17}$	$45.19^{+0.16}_{-0.13}$
Q1407+265	$47.38^{+0.14}_{-0.17}$	$47.58^{+0.18}_{-0.13}$	$47.11^{+0.23}_{-0.06}$	$46.71^{+0.11}_{-0.04}$
Q1416-129	$45.50^{+0.40}_{-0.16}$	$45.81^{+0.33}_{-0.16}$	$45.50^{+0.22}_{-0.15}$	$44.91^{+0.13}_{-0.12}$
Q1426+015	$45.87^{+0.11}_{-0.17}$	$46.09^{+0.17}_{-0.32}$	$45.64^{+0.26}_{-0.72}$	< 45.53
Q1501+106	$45.13^{+0.10}_{-0.10}$	$45.35^{+0.08}_{-0.08}$	$44.93^{+0.04}_{-0.05}$	$44.42^{+0.04}_{-0.05}$
Q1545+210	$46.28^{+0.05}_{-0.06}$	$46.50^{+0.08}_{-0.10}$	$46.06^{+0.11}_{-0.14}$	$45.66^{+0.07}_{-0.09}$
Q1613+658	$46.04^{+0.07}_{-0.09}$	$46.17^{+0.09}_{-0.19}$	$45.48^{+0.18}_{-0.69}$	< 45.19
Q1635+119	$45.36^{+0.46}_{-0.13}$	$45.57^{+0.56}_{-0.51}$	$45.10^{+0.59}_{-0.91}$	< 45.19
Q1704+608	$46.75^{+0.06}_{-0.07}$	$46.82^{+0.09}_{-0.08}$	$45.91^{+0.12}_{-0.09}$	$45.67^{+0.08}_{-0.06}$
Q1721+343	$46.31^{+0.09}_{-0.07}$	$46.51^{+0.12}_{-0.09}$	$46.01^{+0.11}_{-0.07}$	$45.53^{+0.08}_{-0.06}$
Q1803+676	$45.87^{+0.07}_{-0.28}$	$45.74^{+0.17}_{-0.05}$	$45.05^{+0.11}_{-0.09}$	$44.76^{+0.07}_{-0.06}$
Q2128-123	$46.87^{+0.13}_{-0.18}$	$47.01^{+0.13}_{-0.34}$	$45.98^{+0.24}_{-0.17}$	$45.38^{+0.14}_{-0.10}$
Q2130+099	$45.60^{+0.07}_{-0.07}$	$45.73^{+0.07}_{-0.08}$	$45.11^{+0.08}_{-0.09}$	$44.72^{+0.08}_{-0.08}$
Q2135-147	$46.16^{+0.09}_{-0.11}$	$46.32^{+0.14}_{-0.19}$	$45.72^{+0.17}_{-0.35}$	< 45.28
Q2209+184	$45.08^{+0.07}_{-0.06}$	$45.31^{+0.11}_{-0.15}$	$44.80^{+0.19}_{-0.17}$	$44.33^{+0.13}_{-0.13}$
Q2251-178	$45.59^{+0.09}_{-0.08}$	$45.75^{+0.13}_{-0.12}$	$45.20^{+0.20}_{-0.17}$	$44.71^{+0.19}_{-0.19}$

NOTE.—Values are logarithm of luminosity in units of ergs s^{-1}; the ionizing photon rate is the number of photons emitted per unit time, multiplied by 1 rydberg to give it the units of luminosity.

TABLE 15

DECADE LUMINOSITIES

Name	(10-100 μm)	(1-10 μm)	(0.1-1μm)	(0.1-1 keV)	(1-10 keV)
Q0003+158	< 46.20	$45.77^{+0.37}_{-0.38}$	$46.57^{+0.03}_{-0.03}$	$46.83^{+2.41}_{-1.00}$	$45.52^{+0.87}_{-0.39}$
Q0003+199	$44.39^{+0.06}_{-0.11}$	$44.67^{+0.07}_{-0.08}$	$44.94^{+0.03}_{-0.03}$	$44.66^{+0.00}_{-0.00}$	$43.77^{+0.05}_{-0.04}$
Q0007+106	$45.11^{+0.05}_{-0.05}$	$45.24^{+0.08}_{-0.09}$	$45.41^{+0.05}_{-0.05}$	$44.30^{+0.54}_{-0.18}$	$44.97^{+0.08}_{-0.07}$
Q0026+129	< 45.02	$45.39^{+0.14}_{-0.13}$	$45.72^{+0.04}_{-0.04}$	$44.79^{+0.01}_{-0.01}$	$44.92^{+0.05}_{-0.04}$
Q0049+171	< 44.77	$43.98^{+0.49}_{-0.09}$	$44.67^{+0.04}_{-0.03}$	$44.52^{+2.01}_{-0.35}$	$44.37^{+0.20}_{-0.14}$
Q0050+124	$45.67^{+0.01}_{-0.01}$	$45.54^{+0.06}_{-0.06}$	$45.27^{+0.03}_{-0.03}$	$45.07^{+1.25}_{-0.53}$	–
Q0052+251	$45.40^{+0.08}_{-0.09}$	$45.38^{+0.08}_{-0.09}$	$45.88^{+0.03}_{-0.03}$	$45.12^{+1.18}_{-0.37}$	$44.89^{+0.25}_{-0.16}$
Q0054+144	$45.66^{+0.03}_{-0.08}$	$45.63^{+0.06}_{-0.06}$	$45.59^{+0.03}_{-0.03}$	$44.24^{+0.04}_{-0.04}$	$44.82^{+0.09}_{-0.09}$
Q0121-590	$45.05^{+0.01}_{-0.02}$	$45.08^{+0.18}_{-0.17}$	$45.39^{+0.16}_{-0.16}$	$44.61^{+0.09}_{-0.07}$	$44.43^{+0.06}_{-0.06}$
Q0134+329	$46.61^{+0.02}_{-0.09}$	$46.04^{+0.19}_{-0.31}$	$46.02^{+0.08}_{-0.08}$	$45.09^{+0.26}_{-0.24}$	–
Q0205+024	$45.35^{+0.09}_{-0.13}$	$45.37^{+0.06}_{-0.06}$	$45.68^{+0.03}_{-0.03}$	$44.55^{+0.05}_{-0.05}$	–
Q0312-770	< 45.56	$45.21^{+0.36}_{-0.98}$	$45.91^{+0.13}_{-0.13}$	$44.35^{+0.39}_{-0.12}$	–
Q0414-060	< 46.86	$46.14^{+0.71}_{-0.62}$	$46.84^{+0.05}_{-0.05}$	$45.43^{+1.23}_{-0.21}$	$46.63^{+0.07}_{-0.02}$
Q0637-752	$46.77^{+0.09}_{-0.24}$	$46.82^{+0.05}_{-0.05}$	$47.03^{+0.06}_{-0.06}$	$45.88^{+0.22}_{--}$	$46.24^{+0.11}_{-0.13}$
Q0804+761	$45.33^{+0.09}_{-0.08}$	$45.53^{+0.08}_{-0.09}$	$45.70^{+0.13}_{-0.12}$	$44.71^{+0.31}_{-0.26}$	$44.69^{+0.14}_{-0.13}$
Q0837-120	$45.20^{+0.11}_{-0.81}$	$45.40^{+0.14}_{-0.11}$	$45.64^{+0.06}_{-0.08}$	$45.06^{+0.16}_{-0.13}$	$45.22^{+0.05}_{-0.05}$
Q0844+349	$44.80^{+0.10}_{-0.18}$	$44.73^{+0.17}_{-0.22}$	$45.18^{+0.10}_{-0.11}$	$43.47^{+0.33}_{-0.15}$	–
Q0915+165	$44.62^{+0.04}_{-0.20}$	$44.64^{+0.07}_{-0.08}$	$44.16^{+0.33}_{-0.27}$	$43.12^{+0.14}_{-0.10}$	–
Q0923+129	$44.42^{+0.07}_{-0.09}$	$44.10^{+0.11}_{-0.14}$	$44.27^{+0.16}_{-0.10}$	$43.29^{+0.23}_{-0.19}$	$43.69^{+0.08}_{-0.08}$
Q1028+313	< 45.64	$45.16^{+0.41}_{-0.18}$	$45.52^{+0.06}_{-0.07}$	$44.52^{+0.04}_{-0.04}$	$44.97^{+0.05}_{-0.05}$
Q1100+772	$45.59^{+0.09}_{-0.14}$	$45.87^{+0.17}_{-0.16}$	$46.22^{+0.06}_{-0.05}$	$45.26^{+0.20}_{-0.31}$	–
Q1116+215	< 45.47	$45.89^{+0.06}_{-0.08}$	$46.25^{+0.04}_{-0.04}$	$44.74^{+0.19}_{-0.12}$	–
Q1137+660	< 46.46	$46.12^{+0.35}_{-0.44}$	$46.73^{+0.03}_{-0.03}$	$45.73^{+0.28}_{-0.07}$	$45.88^{+0.07}_{-0.11}$
Q1146-037	< 46.49	< 46.01	$45.56^{+0.17}_{-0.18}$	$44.86^{+0.30}_{-0.12}$	–
Q1202+281	$45.56^{+0.18}_{-0.24}$	$45.42^{+0.19}_{-0.19}$	$45.38^{+0.12}_{-0.11}$	$44.98^{+0.13}_{-0.24}$	–
Q1211+143	$45.41^{+0.08}_{-0.10}$	$45.41^{+0.06}_{-0.06}$	$45.64^{+0.07}_{-0.07}$	$45.62^{+0.22}_{-0.14}$	$44.71^{+0.08}_{-0.07}$
Q1219+755	< 45.00	$44.77^{+0.23}_{-0.20}$	$44.91^{+0.17}_{-0.14}$	$44.28^{+0.02}_{-0.02}$	$44.41^{+0.07}_{-0.10}$

TABLE 15—*Continued*

Name	(10-100 μm)	(1-10 μm)	(0.1-1μm)	(0.1-1 keV)	(1-10 keV)
Q1226+023	$46.44^{+0.05}_{-0.05}$	$46.48^{+0.07}_{-0.07}$	$46.79^{+0.07}_{-0.07}$	$45.48^{+0.02}_{-0.02}$	$46.02^{+0.10}_{-0.16}$
Q1244+026	$44.32^{+0.11}_{-0.09}$	$43.79^{+0.19}_{-0.12}$	$44.28^{+0.11}_{-0.06}$	$43.87^{+0.75}_{-0.24}$	–
Q1307+085	$45.32^{+0.12}_{-0.30}$	$45.29^{+0.09}_{-0.13}$	$45.78^{+0.05}_{-0.06}$	$44.64^{+0.30}_{-0.11}$	$44.92^{+0.03}_{-0.03}$
Q1351+695	$44.59^{+0.00}_{-0.01}$	$44.26^{+0.23}_{-0.33}$	$44.56^{+0.17}_{-0.11}$	$43.99^{+0.12}_{-0.16}$	$43.90^{+0.08}_{-0.08}$
Q1352+183	< 45.50	$45.22^{+0.21}_{-0.06}$	$45.58^{+0.03}_{-0.03}$	$44.86^{+0.50}_{-0.38}$	$44.45^{+0.04}_{-0.05}$
Q1407+265	$46.76^{+0.31}_{-0.78}$	$46.85^{+0.14}_{-0.16}$	$47.04^{+0.03}_{-0.03}$	$46.27^{+0.76}_{-0.15}$	$46.08^{+0.12}_{-0.06}$
Q1416-129	< 45.42	$44.75^{+0.57}_{-0.22}$	$45.41^{+0.11}_{-0.09}$	$44.90^{+0.37}_{-0.30}$	$44.88^{+0.17}_{-0.07}$
Q1426+015	$45.19^{+0.10}_{-0.17}$	$45.18^{+0.14}_{-0.21}$	$45.64^{+0.11}_{-0.16}$	$44.83^{+0.01}_{--}$	$44.70^{+0.04}_{-0.04}$
Q1501+106	$44.68^{+0.10}_{-0.12}$	$44.54^{+0.12}_{-0.12}$	$44.72^{+0.09}_{-0.07}$	$44.03^{+0.03}_{-0.03}$	$44.15^{+0.03}_{-0.03}$
Q1545+210	$45.49^{+0.06}_{-0.19}$	$45.64^{+0.07}_{-0.10}$	$46.07^{+0.04}_{-0.04}$	$45.20^{+0.20}_{-0.30}$	–
Q1613+658	$45.69^{+0.02}_{-0.05}$	$45.42^{+0.14}_{-0.16}$	$45.53^{+0.06}_{-0.10}$	$44.83^{+0.02}_{--}$	–
Q1635+119	< 45.47	$44.59^{+0.48}_{-0.05}$	$45.26^{+0.14}_{-0.34}$	$44.12^{+1.09}_{-0.32}$	–
Q1704+608	$46.27^{+0.07}_{-0.11}$	$46.24^{+0.07}_{-0.07}$	$46.31^{+0.04}_{-0.04}$	$44.41^{+0.37}_{-0.23}$	–
Q1721+343	$45.70^{+0.19}_{-0.10}$	$45.56^{+0.08}_{-0.11}$	$46.07^{+0.03}_{-0.04}$	$45.06^{+0.24}_{-0.16}$	$45.47^{+0.06}_{-0.04}$
Q1803+676	< 44.94	$45.28^{+0.01}_{-0.05}$	$45.52^{+0.03}_{-0.03}$	$43.65^{+0.24}_{-0.15}$	–
Q2128-123	$46.43^{+0.14}_{-0.19}$	$46.09^{+0.23}_{-0.85}$	$46.53^{+0.07}_{-0.07}$	$45.24^{+0.46}_{-0.25}$	$45.51^{+0.21}_{-0.23}$
Q2130+099	$45.10^{+0.04}_{-0.05}$	$45.09^{+0.11}_{-0.11}$	$45.16^{+0.05}_{-0.05}$	$43.75^{+0.05}_{-0.05}$	$44.04^{+0.07}_{-0.05}$
Q2135-147	$45.66^{+0.13}_{-0.19}$	$45.57^{+0.10}_{-0.12}$	$45.78^{+0.04}_{-0.05}$	$44.94^{+0.07}_{--}$	$45.34^{+0.07}_{-0.10}$
Q2209+184	$44.39^{+0.02}_{-0.02}$	$44.27^{+0.21}_{-0.21}$	$44.88^{+0.04}_{-0.05}$	$44.10^{+0.29}_{-0.26}$	–
Q2251-178	$44.89^{+0.10}_{-0.05}$	$44.98^{+0.07}_{-0.08}$	$45.33^{+0.09}_{-0.09}$	$44.29^{+0.35}_{-0.33}$	$44.69^{+0.09}_{-0.07}$

NOTE.—Values are logarithm of luminosity in units of ergs s^{-1}.

TABLE 16

OCTAVE LUMINOSITIES

Name	(0.8-1.6 μm)	(0.4-0.8 μm)	(0.2-0.4 μm)	(0.1-0.2 μm)	(0.15-0.3 keV)	(1-2 keV)
Q0003+158	$45.47^{+0.07}_{-0.09}$	$45.77^{+0.03}_{-0.03}$	$46.14^{+0.02}_{-0.02}$	$46.21^{+0.03}_{-0.03}$	$46.40^{+2.26}_{-1.05}$	$45.41^{+0.81}_{-0.34}$
Q0003+199	$44.02^{+0.06}_{-0.06}$	$44.15^{+0.04}_{-0.04}$	$44.46^{+0.04}_{-0.04}$	$44.60^{+0.02}_{-0.02}$	$44.23^{+0.00}_{-0.00}$	$43.40^{+0.03}_{-0.04}$
Q0007+106	$44.47^{+0.10}_{-0.13}$	$44.64^{+0.03}_{-0.04}$	$44.97^{+0.04}_{-0.04}$	$45.02^{+0.06}_{-0.06}$	$43.65^{+0.63}_{-0.21}$	$44.14^{+0.25}_{-0.19}$
Q0026+129	$44.87^{+0.09}_{-0.08}$	$45.01^{+0.02}_{-0.02}$	$45.23^{+0.04}_{-0.04}$	$45.34^{+0.05}_{-0.05}$	$44.25^{+0.03}_{-0.03}$	$44.35^{+0.01}_{-0.01}$
Q0049+171	$43.60^{+0.17}_{-0.16}$	$43.86^{+0.02}_{-0.02}$	$44.24^{+0.02}_{-0.03}$	$44.31^{+0.06}_{-0.04}$	$44.03^{+2.00}_{-0.42}$	$43.87^{+0.40}_{-0.37}$
Q0050+124	$44.77^{+0.06}_{-0.07}$	$44.75^{+0.02}_{-0.02}$	$44.83^{+0.04}_{-0.04}$	$44.65^{+0.04}_{-0.04}$	$44.63^{+1.21}_{-0.57}$	$43.89^{+0.45}_{-0.33}$
Q0052+251	$44.70^{+0.08}_{-0.12}$	$44.90^{+0.02}_{-0.04}$	$45.37^{+0.02}_{-0.02}$	$45.62^{+0.03}_{-0.03}$	$44.63^{+1.24}_{-0.43}$	$44.46^{+0.42}_{-0.26}$
Q0054+144	$44.88^{+0.04}_{-0.04}$	$45.01^{+0.02}_{-0.02}$	$45.15^{+0.02}_{-0.02}$	$45.07^{+0.03}_{-0.04}$	$43.57^{+0.05}_{-0.05}$	$44.12^{+0.03}_{-0.03}$
Q0121-590	$44.09^{+0.43}_{-0.62}$	$44.38^{+0.27}_{-0.27}$	$44.93^{+0.17}_{-0.16}$	$45.12^{+0.13}_{-0.13}$	$44.07^{+0.10}_{-0.09}$	$44.14^{+0.04}_{-0.04}$
Q0134+329	$45.02^{+0.24}_{-0.33}$	$45.26^{+0.06}_{-0.07}$	$45.58^{+0.04}_{-0.04}$	$45.66^{+0.10}_{-0.10}$	$44.51^{+0\ 31}_{-0.31}$	$44.76^{+0.12}_{-0.11}$
Q0205+024	$44.57^{+0.09}_{-0.10}$	$44.87^{+0.04}_{-0.04}$	$45.26^{+0.03}_{-0.03}$	$45.32^{+0.03}_{-0.03}$	$44.11^{+0.05}_{-0.05}$	$44.01^{+0.04}_{-0.05}$
Q0312-770	$44.76^{+0.16}_{-0.38}$	$45.12^{+0.08}_{-0.13}$	$45.26^{+0.06}_{-0.07}$	$45.68^{+0.16}_{-0.15}$	$43.61^{+0.42}_{-0.14}$	$44.35^{+0.31}_{-0.13}$
Q0414-060	$45.77^{+0.18}_{-0.22}$	$46.01^{+0.07}_{-0.07}$	$46.27^{+0.05}_{-0.04}$	$46.58^{+0.05}_{-0.05}$	$44.80^{+1.40}_{-0.22}$	$45.22^{+0.63}_{-0.17}$
Q0637-752	$46.23^{+0.02}_{-0.02}$	$46.33^{+0.05}_{-0.05}$	$46.46^{+0.09}_{-0.09}$	$46.72^{+0.05}_{-0.06}$	< 44.96	$45.54^{+0.03}_{-0.05}$
Q0804+761	$44.70^{+0.13}_{-0.25}$	$44.88^{+0.08}_{-0.13}$	$45.31^{+0.04}_{-0.04}$	$45.31^{+0.22}_{-0.20}$	$44.19^{+0.36}_{-0.32}$	$44.18^{+0.11}_{-0.12}$
Q0837-120	$44.63^{+0.27}_{-0.74}$	$44.69^{+0.15}_{-0.28}$	$45.07^{+0.07}_{-0.07}$	$45.40^{+0.03}_{-0.04}$	$44.47^{+0.20}_{-0.17}$	$44.76^{+0.07}_{-0.06}$
Q0844+349	$44.10^{+0.32}_{-1.00}$	$44.47^{+0.18}_{-0.29}$	$44.77^{+0.07}_{-0.07}$	$44.76^{+0.06}_{-0.05}$	$42.85^{+0.43}_{-0.23}$	$43.23^{+0.12}_{-0.10}$
Q0915+165	$43.61^{+0.35}_{-0.81}$	$43.59^{+0.61}_{-1.06}$	$43.75^{+0.13}_{-0.14}$	$43.57^{+0.04}_{-0.05}$	$42.45^{+0.20}_{-0.16}$	$42.99^{+0.07}_{-0.07}$
Q0923+129	$43.17^{+0.34}_{-0.65}$	$43.33^{+0.59}_{-0.95}$	$43.82^{+0.03}_{-0.06}$	$43.97^{+0.03}_{-0.04}$	$42.71^{+0.29}_{-0.25}$	$42.96^{+0.09}_{-0.10}$
Q1028+313	$44.59^{+0.19}_{-0.52}$	$44.73^{+0.11}_{-0.19}$	$44.96^{+0.07}_{-0.07}$	$45.25^{+0.03}_{-0.03}$	$43.93^{+0.04}_{-0.04}$	$44.30^{+0.04}_{-0.04}$
Q1100+772	$45.27^{+0.08}_{-0.08}$	$45.46^{+0.02}_{-0.02}$	$45.73^{+0.02}_{-0.02}$	$45.87^{+0.09}_{-0.09}$	$44.74^{+0.22}_{-0.38}$	$44.74^{+0.13}_{-0.11}$
Q1116+215	$45.20^{+0.07}_{-0.07}$	$45.39^{+0.03}_{-0.04}$	$45.79^{+0.02}_{-0.02}$	$45.95^{+0.06}_{-0.06}$	$44.22^{+0.22}_{-0.15}$	$44.22^{+0.08}_{-0.06}$
Q1137+660	$45.63^{+0.04}_{-0.05}$	$45.94^{+0.03}_{-0.03}$	$46.21^{+0.02}_{-0.02}$	$46.43^{+0.03}_{-0.03}$	$45.15^{+0.34}_{-0.08}$	$45.40^{+0.09}_{-0.05}$
Q1146-037	$44.31^{+0.36}_{-0.97}$	$44.63^{+0.23}_{-0.36}$	$45.25^{+0.16}_{-0.15}$	$45.13^{+0.16}_{-0.16}$	$44.18^{+0.37}_{-0.15}$	$44.75^{+0.17}_{-0.08}$
Q1202+281	$44.41^{+0.27}_{-0.37}$	$44.50^{+0.06}_{-0.06}$	$44.94^{+0.09}_{-0.09}$	$45.05^{+0.15}_{-0.15}$	$44.47^{+0.14}_{-0.29}$	$44.39^{+0.11}_{-0.11}$
Q1211+143	$44.76^{+0.06}_{-0.06}$	$44.96^{+0.06}_{-0.06}$	$45.22^{+0.07}_{-0.07}$	$45.20^{+0.08}_{-0.08}$	$45.19^{+0.22}_{-0.14}$	$44.37^{+0.06}_{-0.07}$
Q1219+755	$44.12^{+0.38}_{-0.37}$	$44.19^{+0.24}_{-0.17}$	$44.48^{+0.15}_{-0.13}$	$44.50^{+0.13}_{-0.12}$	$43.74^{+0.02}_{-0.02}$	$43.94^{+0.01}_{-0.01}$

TABLE 16—*Continued*

Name	(0.8-1.6 μm)	(0.4-0.8 μm)	(0.2-0.4 μm)	(0.1-0.2 μm)	(0.15-0.3 keV)	(1-2 keV)
Q1226+023	$45.87^{+0.05}_{-0.05}$	$46.03^{+0.03}_{-0.03}$	$46.32^{+0.06}_{-0.05}$	$46.44^{+0.10}_{-0.10}$	$44.85^{+0.02}_{-0.02}$	$45.33^{+0.01}_{-0.01}$
Q1244+026	$42.88^{+0.23}_{-0.20}$	$43.34^{+0.34}_{-0.22}$	$43.89^{+0.06}_{-0.04}$	$43.93^{+0.04}_{-0.03}$	$43.40^{+0.78}_{-0.28}$	$43.07^{+0.10}_{-0.18}$
Q1307+085	$44.74^{+0.14}_{-0.28}$	$45.01^{+0.09}_{-0.13}$	$45.30^{+0.04}_{-0.04}$	$45.45^{+0.03}_{-0.03}$	$44.10^{+0.37}_{-0.14}$	$44.19^{+0.06}_{-0.07}$
Q1351+695	$43.59^{+0.53}_{-1.00}$	$43.15^{+0.70}_{-0.26}$	$44.20^{+0.08}_{-0.09}$	$44.25^{+0.11}_{-0.11}$	$43.48^{+0.14}_{-0.21}$	$43.40^{+0.06}_{-0.05}$
Q1352+183	$44.56^{+0.11}_{-0.11}$	$44.83^{+0.01}_{-0.01}$	$45.12^{+0.02}_{-0.02}$	$45.23^{+0.04}_{-0.04}$	$44.40^{+0.52}_{-0.44}$	$43.99^{+0.08}_{-0.12}$
Q1407+265	$46.02^{+0.06}_{-0.06}$	$46.26^{+0.04}_{-0.04}$	$46.57^{+0.02}_{-0.02}$	$46.71^{+0.02}_{-0.02}$	$45.78^{+0.82}_{-0.17}$	$45.61^{+0.24}_{-0.07}$
Q1416-129	$44.21^{+0.45}_{-0.64}$	$44.45^{+0.29}_{-0.29}$	$45.02^{+0.09}_{-0.08}$	$45.06^{+0.05}_{-0.05}$	$44.36^{+0.35}_{-0.36}$	$44.45^{+0.33}_{-0.17}$
Q1426+015	$44.53^{+0.23}_{-0.64}$	$44.66^{+0.10}_{-0.18}$	$45.12^{+0.06}_{-0.06}$	$45.39^{+0.13}_{-0.22}$	$44.30^{+0.10}_{--}$	$44.20^{+0.04}_{-0.04}$
Q1501+106	$43.68^{+0.31}_{-0.44}$	$43.82^{+0.21}_{-0.21}$	$44.29^{+0.09}_{-0.08}$	$44.41^{+0.02}_{-0.03}$	$43.54^{+0.03}_{-0.03}$	$43.61^{+0.02}_{-0.02}$
Q1545+210	$44.99^{+0.08}_{-0.08}$	$45.27^{+0.04}_{-0.05}$	$45.60^{+0.03}_{-0.03}$	$45.75^{+0.04}_{-0.04}$	$44.64^{+0.22}_{-0.37}$	$44.81^{+0.16}_{-0.14}$
Q1613+658	$44.56^{+0.19}_{-0.24}$	$44.75^{+0.07}_{-0.08}$	$45.09^{+0.07}_{-0.07}$	$45.18^{+0.04}_{-0.12}$	$44.31^{+0.11}_{--}$	$44.22^{+0.05}_{-0.04}$
Q1635+119	$44.31^{+0.07}_{-0.07}$	$44.51^{+0.06}_{-0.06}$	$44.60^{+0.06}_{-0.06}$	$45.01^{+0.19}_{-0.85}$	$43.54^{+1.22}_{-0.43}$	$43.79^{+0.50}_{-0.27}$
Q1704+608	$45.51^{+0.06}_{-0.06}$	$45.64^{+0.02}_{-0.02}$	$45.81^{+0.04}_{-0.04}$	$45.94^{+0.04}_{-0.04}$	$43.75^{+0.46}_{-0.31}$	$44.25^{+0.16}_{-0.12}$
Q1721+343	$44.94^{+0.12}_{-0.21}$	$45.21^{+0.06}_{-0.08}$	$45.60^{+0.03}_{-0.03}$	$45.75^{+0.03}_{-0.03}$	$44.43^{+0.29}_{-0.22}$	$44.85^{+0.13}_{-0.07}$
Q1803+676	$44.64^{+0.04}_{-0.04}$	$44.76^{+0.03}_{-0.03}$	$45.06^{+0.02}_{-0.02}$	$45.15^{+0.03}_{-0.03}$	$42.81^{+0.28}_{-0.21}$	$43.80^{+0.20}_{-0.12}$
Q2128-123	$45.60^{+0.07}_{-0.14}$	$45.79^{+0.09}_{-0.10}$	$46.06^{+0.09}_{-0.09}$	$46.17^{+0.03}_{-0.04}$	$44.61^{+0.55}_{-0.31}$	$45.02^{+0.21}_{-0.14}$
Q2130+099	$44.12^{+0.27}_{-0.43}$	$44.34^{+0.05}_{-0.05}$	$44.74^{+0.03}_{-0.03}$	$44.81^{+0.06}_{-0.06}$	$43.24^{+0.05}_{-0.05}$	$43.42^{+0.03}_{-0.03}$
Q2135-147	$44.86^{+0.13}_{-0.13}$	$45.20^{+0.04}_{-0.04}$	$45.38^{+0.03}_{-0.03}$	$45.22^{+0.05}_{-0.10}$	$44.34^{+0.04}_{--}$	$44.56^{+0.02}_{-0.02}$
Q2209+184	$43.13^{+0.55}_{-0.37}$	$43.98^{+0.09}_{-0.12}$	$44.51^{+0.03}_{-0.03}$	$44.53^{+0.04}_{-0.04}$	$43.54^{+0.35}_{-0.35}$	$43.70^{+0.15}_{-0.14}$
Q2251-178	$44.38^{+0.06}_{-0.08}$	$44.63^{+0.04}_{-0.04}$	$44.83^{+0.10}_{-0.10}$	$44.96^{+0.11}_{-0.11}$	$43.64^{+0.42}_{-0.42}$	$44.13^{+0.21}_{-0.20}$

NOTE.—Values are logarithm of luminosity in units of erg s^{-1}

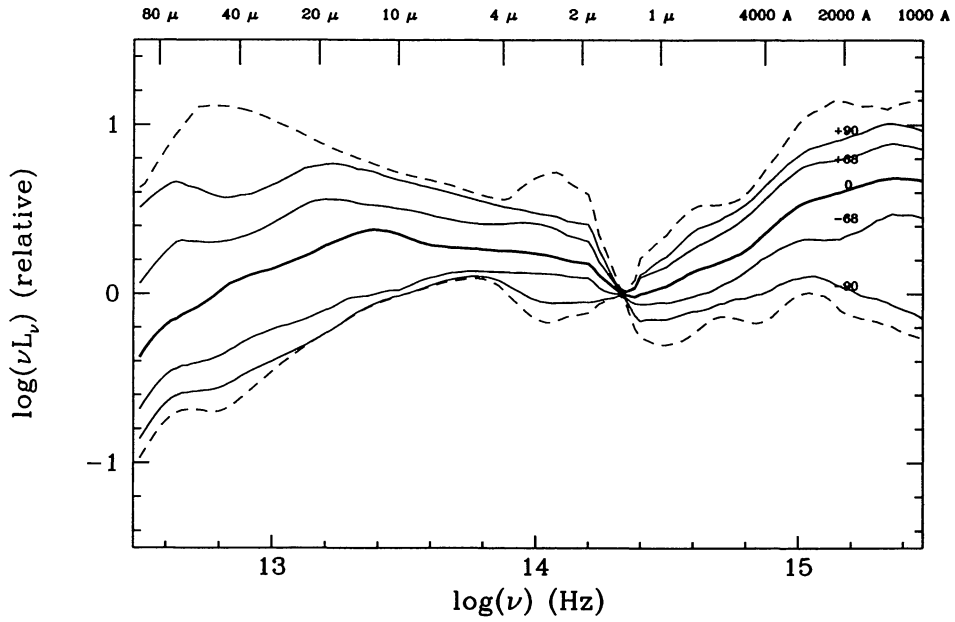

FIG. 11*a*

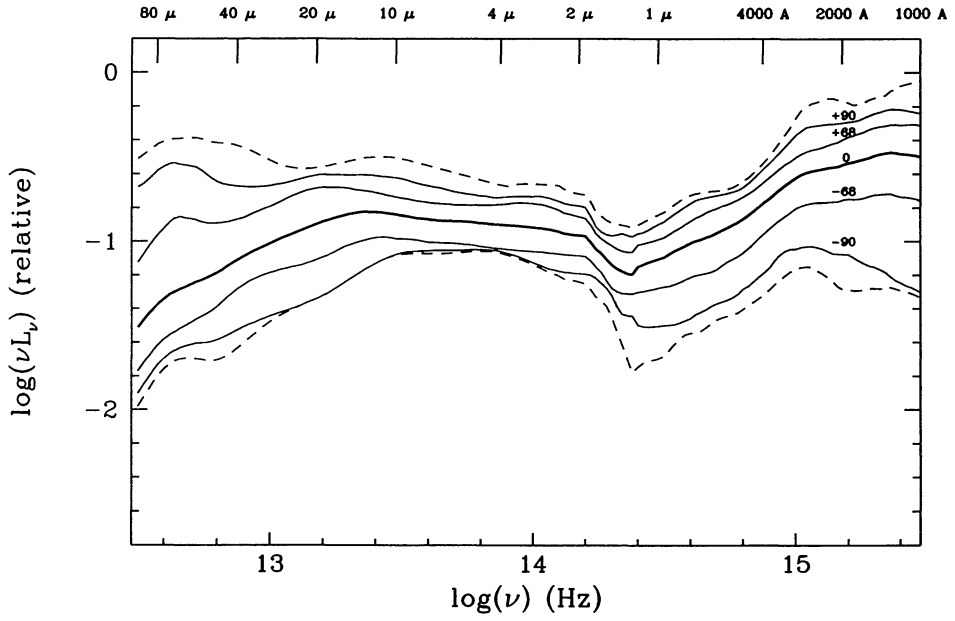

FIG. 11*b*

FIG. 11.—(*a*) The median quasar energy distribution in the *UVOIR* range, normalized at 1.25 μm, and the 68, 90, and 100 (*dashed*) Kaplan-Meier percentile envelopes, showing the large dispersion from the mean in the far-infrared and ultraviolet. (*b*) The median and percentiles when the energy distributions are normalized by their total 100 μm to 1000 Å luminosity rather than the monochromatic 1.25 μm luminosity.

TABLE 17

BOLOMETRIC CORRECTIONS

	Median	Mean, Sigma	Min	Max
$L_{Bol}/L_{2500\,\AA}$	5.6	6.3±3.1	2.4	16.7
L_{Bol}/L_B	10.7	11.8±4.3	5.5	24.7
L_{Bol}/L_V	13.2	14.2±5.1	7.1	29.3
$L_{Bol}/L_{1.5\mu m}$	24.8	25.5±8.4	9.3	41.9
$L_{UVOIR}/L_{2500\,\AA}$	3.5	4.2±2.6	1.2	14.0
L_{UVOIR}/L_B	6.8	7.6±3.5	4.1	22.4
L_{UVOIR}/L_V	8.1	9.2±3.9	4.9	22.7
$L_{UVOIR}/L_{1.5\mu m}$	15.5	16.1±5.3	8.3	28.5
L_{Ion}/L_{Bol}	0.32	0.32±0.13	0.07	0.66
$N_{Ion}R/L_{Bol}$	0.12	0.11±0.04	0.02	0.18
$L_{Ion}/N_{Ion}R$	2.8	3.0±0.8	1.7	4.8

NOTE.—Bolometric correction factors for UV, visible, and infrared monochromatic luminosities. Monochromatic luminosities are defined to be the value of $\nu L(\nu)$ in the rest frame. Mean and standard deviation are given, followed by the minimum and maximum values found in the sample. Errors in the determination of individual energy distributions have been ignored for the purposes of this table. Also listed are estimates of the ionizing flux discussed in the text.

able in the UVOIR region. We have normalized the MEDs at 1.25 μm, the approximate mean location of the near-infrared inflection point. While the MED is a good description of the typical quasar, the full range of SEDs contains considerable variety. Kriss (1988) showed this for a sample of radio-quiet quasars. We have quantified this dispersion in Figure 11*a* which shows the MED for the combined radio-loud and radio-quiet sample in the UVOIR region, together with contours illustrating the dispersion of the actual energy distributions about the median. The Kaplan-Meier median is in very close agreement with the mean calculated in Figure 10. Indicated are 68, 90, and 100 percentile contours on each side of the median, calculated using the smoothed Kaplan-Meier estimate of the survival function (Feigelson & Nelson 1985; Miller 1981). The narrowness at 1.25 μm is an artifact of the normalization there; Figure 11*b* shows the results obtained when the energy distributions are normalized by their total UVOIR (100 μm–1000 Å) luminosity.

The 68 percentile distribution is within a factor of 2–3 of the mean throughout, so the mean is revealing something about the nature of quasars. However, the 90 percentile width is a factor of 20, and the extremes are a factor of 30 in the UV and 60 in the far-IR. The distributions are broader than would be expected from a Gaussian distribution. The MED and its dispersion will be discussed in more detail in a future paper. Here we note that the large dispersion of shapes in individual objects means that the MED should be used only with caution, and that the variety of shapes should contain information about the physics of quasars. Our MED is in good agreement with that of Sanders et al. (1989) except in the far infrared at 60 μm and beyond, where our inclusion of upper limits lowers the estimate of the mean. Our results for radio-quiet quasars are compared with the corresponding Sanders et al. results in Figure 12.

7. CONCLUSIONS

We have collected a set of data useful for many investigations. In particular, these data will serve as a benchmark against which to compare the energy distributions of high redshift quasars. The data are available in FITS BINTABLE for-

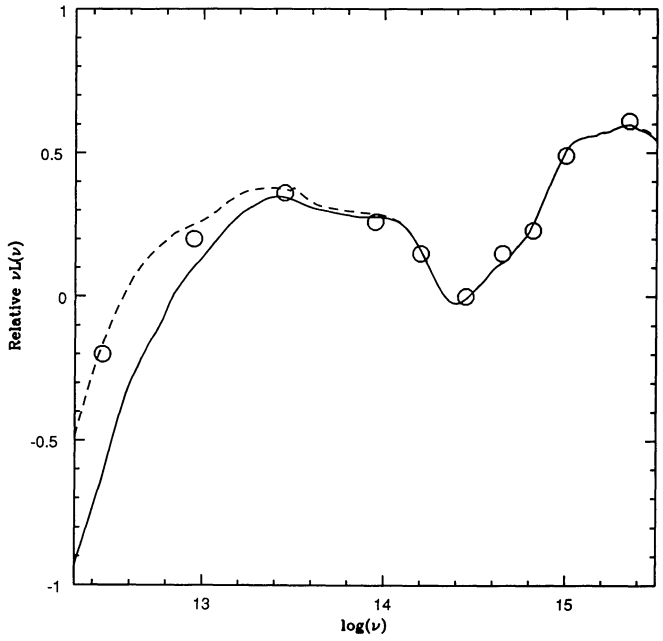

FIG. 12.—Comparison of mean energy distributions for radio-quiet quasars. *Solid line:* UVSX sample using Kaplan-Meier estimator (this paper). *Dashed line:* UVSX sample with conventional mean, excluding upper limits. *Open circles:* PG quasars from Sanders et al. (1989), using conventional mean.

mat by anonymous ftp from sao-ftp.harvard.edu in directory "pub/jcm/qed." The uncorrected, observed frame data are tabulated in Tables B1–B47 in CD-ROM.

This work was carried out as part of NASA Astrophysics Data Program grant NAG8-689 and Long Term Space Astrophysics Research Program grant NAGW-2201, NASA *HEAO* contract NAS 8-30751, and NASA *IUE* grants NAG5-87, NAG5-37. We acknowledge useful discussions with Richard Barvainis, Ski Antonucci, Nat Carleton, Walter Rice, Olga Kuhn, Aneta Siemiginowska, Bożena Czerny, and Diana Worrall. Data for this paper were obtained from the *Einstein* Data Bank, the *IUE* Reduction and Data Analysis Facility, and the *IRAS* data bank at IPAC, and we thank the staff at those facilities for their support. J. C. M. thanks the National Research Council for support as a NAS/NRC Associate during part of this project. B. J. W. acknowledges support from the US *ROSAT* Science Data Center.

REFERENCES

Adam, G. 1978, A&AS, 31, 151
———. 1985, A&AS, 61, 225
Antonucci, R. R. J., & Barvainis, R. 1988, ApJ, 325, L21
Antonucci, R. R. J., Barvainis, R., & Alloin, D. 1990, ApJ, 353, 416
Arnaud, K. A., et al. 1985, MNRAS, 217, 105
Azusienis, A., & Straizys, V. 1969, AZh 46, 2, 402
Barvainis, R., & Antonucci, R. R. J. 1989, ApJS, 70, 257
Bezler, M., Kendziora, E., Stubert, R., Hasinger, G., Pietsch, W., Reppin, C., Truemper, J., & Voges, W. 1984, A&A, 136, 351
Binggeli, B., Sandage, A., & Tarenghi, M. 1984, AJ, 89, 64
Bolton, J. G., & Butler, P. W. 1975, Australian J. Phys. Suppl., 34, 33
Bolton, J. G., Wall, J. V., & Shimmins, A. J. 1971, Australian J. Phys., 24, 889
Boroson, T. A., & Oke, J. B. 1984, ApJ, 281, 535
Boroson, T. A., Oke, J. B., & Green, R. F. 1982, ApJ, 263, 32
Boroson, T. A., Persson, S. E., & Oke, J. B. 1985, ApJ, 293, 120
Brissenden R. J. V. 1989, PhD thesis, Australian National Univ.
Burstein, D., & Heiles, C. 1978, ApJ, 225, 40
Carleton, N. P., Elvis, M., Fabbiano, G., Lawrence, A., Ward, M. J., & Willner, S. P. 1987, ApJ, 318, 595
Chini, R., Kreysa, E., & Biermann, P. L. 1989, A&A, 219, 87
Clegg, P., et al. 1983, ApJ, 273, 58
Coleman, G. D., Wu, C. C., & Weedman, D. W. 1980, ApJS, 43, 393
Comastri, A., Setti, G., Zamorani, G., Elvis, M., Wilkes, B. J., McDowell, J. C., & Giommi, P. 1992, ApJ, 384, 62
Condon, J. J., & Broderick, J. J. 1988, AJ, 96, 30
Condon, J. J., O'Dell, S. L., Puschell, J. J., & Stein, W. 1981, ApJ, 246, 624
Cutri, R. M., Wiśniewski, W. Z., Rieke, G. H., & Lebofsky, M. J. 1985, ApJ, 296, 423
Czerny, B., & Elvis, M. 1987, ApJ, 321, 305
Della Ceca, R., Palumbo, G. G. C., Persic, M., Boldt, E. A., DeZotti, G., & Marshall, F. E. 1990, ApJS, 72, 471
de Jong, et al. 1984, ApJ, 278, L67
de Vaucouleurs, A., & Longo, G. 1988, Catalog of Visual and Infrared Photometry of Galaxies from 0.5 μm to 10 μm (1961–1985), Univ. Texas Mono. Astr., No. 5
Dickey, J. M., Salpeter, E., & Terzian, Y. 1978, ApJS, 36, 77
Edelson, R. A. 1987, ApJ, 313, 651
Edelson, R. A., Krolik, J. H., & Pike, G. F. 1990, ApJ, 359, 86
Edelson, R. A., & Malkan, M. A. 1986, ApJ, 308, 59
Edelson, R. A., Malkan, M. A., & Rieke, G. H. 1987, ApJ, 321, 233
Ekers, J. A. 1969, Australian J. Phys. Suppl., 7, 1
Elias, J. H., Frogel, J. A., Matthews, K., & Neugebauer, G. 1982, AJ, 87, 1029
Elsmore, B., & Ryle, M. 1976, MNRAS, 174, 411
Elvis, M. 1991, in Frontiers of X-Ray Astronomy, ed. Y. Tanaka & K. Koyama (Tokyo: Universal Academic), 567
Elvis, M., Giommi, P., Wilkes, B. J., & McDowell, J. C. 1991, ApJ, 378, 537
Elvis, M., Green, R. F., Bechtold, J., Schmidt, M., Neugebauer, G., Soifer, B. T., Matthews, K., & Fabbiano, G. 1986, ApJ, 310, 291
Elvis, M., Lockman, F., & Wilkes, B. J. 1989, AJ, 97, 777
Engargiola, G., Harper, D. A., Elvis, M., & Willner, S. P. 1988, ApJ, 332, L19
Ennis, D. J., Neugebauer, G., & Werner, M. 1982, ApJ, 262, 460
Feigelson, E. D., Isobe, T., & Kembhavi, A. 1984, AJ, 89, 1464
Feigelson, E. D., & Nelson, P. I. 1985, ApJ, 293, 192
Frogel, J. 1985, ApJ, 298, 528
Gehren, T., Fried, J., Wehinger, P. A., & Wyckoff, S. 1984, ApJ, 278, 11
Giacconi, R., et al. 1979, ApJ, 230, 540
Glass, I. S. 1986, MNRAS, 219, 5P
Gorenstein, P., Harnden, R. F., & Fabricant, D. 1981, IEEE Trans. Nucl. Sci., NS-28, 869
Gower, A. C., & Hutchings, J. B. 1984, AJ, 89, 1658
Gregory, P. C., & Condon, J. J. 1991, ApJS, 75, 1011
Griersmith, D., & Visvanathan, N. 1979, A&A, 79, 329
Harris, D. E., et al. 1991, The Einstein Observatory Catalog of IPC X-Ray Sources, SAO HEAD CD-ROM Series 1 (Einstein), Set 4, Disk 7
Hayes, D. S. 1985, in IAU Symp. 111, Calibration of Fundamental Stellar Quantities, ed. D. S. Hayes, L. R. Pasinetti, & A. D. G. Philip (Dordrecht: Reidel), 225
Heiles, C., & Cleary, M. N. 1979, Australian J. Phys. Suppl., 47, 1
Hintzen, P., Ulvestad, J., & Owen, F. 1983, AJ, 88, 709
Hutchings, J. B., Crampton, D., & Campbell, B. 1984, ApJ, 280, 41
Hutchings, J. B., & Gower, A. C. 1985, AJ, 90, 405
Hutchings, J. B., Janson, T., & Neff, S. G. 1989, ApJ, 342, 660
Hutchings, J. B., Johnson, I., & Pyke, R. 1988, ApJS, 66, 361
Hutchings, J. B., Price, R., & Gower, A. C. 1988, ApJ, 329, 122
Hyland, A. R., & Allen, D. A. 1982, MNRAS, 199, 943
Jagers, W. J., van Breugel, W. J. M., Miley, G. K., Schillizzi, R. T., & Conway, R. G. 1982, A&A, 105, 279
Johnson, H. L. 1965, ApJ, 141, 923
Kellermann, K. I., Sramek, R., Shaffer, D., Green, R., & Schmidt, M. 1989, AJ, 98, 1195
Kinney, A., Bohlin, R. C., Blades, J. C., & York, D. G. 1991, ApJS, 75, 645
Kormendy, J. 1977, ApJ, 218, 333
Kriss, G. A. 1988, ApJ, 324, 809
Kurucz, R. L. 1979, ApJS, 40, 1
Landau R., Epstein, E. E., & Rather, J. D. G. 1980, AJ, 85, 363
Lonsdale, C., & Morison, I. 1983, MNRAS, 203, 833
Low, F. J., Huchra, J. P., Kleinmann, S. G., & Cutri, R. M. 1988, ApJ, 327, L41
MacKenty, J. W. 1990, ApJS, 72, 231
Malkan, M. A. 1983, ApJ, 268, 582
Malkan, M. A., & Sargent, W. L. W. 1982, ApJ, 254, 22
Manduca, A., & Bell, R. A. 1979, PASP, 91, 848
Masnou, J.-L., Wilkes, B. J., Elvis, M., McDowell, J. C., & Arnaud, K. A. 1992, A&A, 253, 35
McAlary, C. W., McLaren, R. A., McGonegal, R. J., & Maza, J. 1983, ApJS, 52, 341
Meurs, E. J. A., & Wilson, A. S. 1981, A&AS, 45, 99
Miley, G. K., & Hartsuijker, A. P. 1978, A&AS, 34, 129
Miller, R. G., Jr. 1981, Survival Analysis (New York: Wiley)
Mountain, C. M., Leggett, S. K., Selby, M. J., & Zadrozny, A. 1985, A&A, 150, 281
Mushotzky, R. F. 1984, Adv. Space Res., 3 (10–13), 312
Neizvestnii, S. I. 1986, Soobshcheniya Spetsial'noi Astrofisicheskoi Observatorii, 51, 5
Neugebauer, G., Green, R. F., Matthews, K., Schmidt, M., Soifer, B. T., & Bennett, J. 1987, ApJS, 63, 615 (N87)
Neugebauer, G., et al. 1984, ApJ, 278, L1
Neugebauer, G., Matthews, K., Soifer, B. T., & Elias, J. H. 1985, ApJ, 298, 275
Neugebauer, G., Miley, G. K., Soifer, B. T., & Clegg, P. E. 1986, ApJ, 308, 815

Neugebauer, G., Oke, J. B., Becklin, E. E., & Mathews, K. 1979, ApJ, 230, 79
Ohashi, T., et al. 1992, ApJ, 398, 87
Oke, J., & Gunn, J. 1983, ApJ, 266, 713
Orr, M. J. L., & Browne, I. W. A. 1982, MNRAS, 200, 1067
Owen, F., Porcas, R. W., Mufson, S. L., & Moffett, T. J. 1978a, AJ, 83, 685
Owen, F., Porcas, R. W., & Neff, S. G. 1978b, AJ, 83, 1009
Owen, F., & Puschell, J. 1982, AJ, 87, 595
Padovani, P., & Rafanelli, P. 1988, A&A, 205, 53
Perley, R. A. 1982, AJ, 87, 859
Pooley, G. G., & Henbest, S. N. 1974, MNRAS, 169, 477
Preston, R. A., et al. 1985, AJ, 90, 1599
Price, R. M., & Milne, D. K. 1965, Australian J. Phys., 18, 329
Rieke, G. H. 1978, ApJ, 226, 550
Rieke, G. H., & Lebofsky, M. J. 1985, ApJ, 288, 618
Robson, E. I., Gear, W. K., Smith, M. G., Ade, P. A. R., & Nolt, I. G. 1985, MNRAS, 213, 355
Rudnick, L., Sitko, M. L., & Stein, W. A. 1984, AJ, 89, 753
Rudy, R. J., LeVan, P. D., & Rodriguez-Espinoza, J. M. 1982, AJ, 87, 598
Sandage, A. 1965, ApJ, 141, 1560
Sanders, D. B., et al. 1989, ApJ, 347, 29
Savage, B. D., & Mathis, J. S. 1979, ARA&A, 17, 73
Saxton, R. D., et al. 1993, MNRAS, 262, 63
Schmidt, M., & Green, R. F. 1983, ApJ, 269, 352
Shields, G. A. 1978, Nature, 272, 706
Shimmins, A. J., & Bolton, J. G. 1972a, Australian J. Phys. Ap. Suppl., 23, 1
———. 1972b, Australian J. Phys. Ap. Suppl., 26, 1
———. 1981, Australian J. Phys., 34, 471
Shimmins, A. J., Day, G. A., Ekers, R. D., & Cole, D. J. 1966, Australian J. Phys., 19, 837
Siemiginowska, A., Kuhn, O., Elvis, M., McDowell, J. C., & Wilkes, B. J. 1994, in preparation
Sitko, M. L., Stein, W. A., Zhang, Y-X, & Wisniewski, W. Z. 1982, ApJ, 259, 486
Smith, E., Heckman, T. M., Bothun, G. D., Romanishin, W., & Balick, B. 1986, ApJ, 306, 64
Spencer, R. E., McDowell, J. C., Charlesworth, M., Fanti, C., Parma, P., & Peacock, J. A. 1989, MNRAS, 240, 657
Stark, A. A., Gammie, C. F., Wilson, R. W., Bally, J., Linke, R. A., Heiles, C., & Hurwitz, M. 1992, ApJS, 79, 77
Stark, A. A., Heiles, C., Bally, J., & Linke, R. 1984, privately distributed magnetic tape
Steppe, H., Salter, C. J., Chini, R., Kreysa, E., Brunswig, W., & Lobato Perez, J. 1988, A&AS, 75, 317
Sun, W.-H., & Malkan, M. 1989, ApJ, 346, 68
Swarup, G., Sinha, R. P., & Hilldrup, K. 1984, MNRAS, 208, 813
Tananbaum, H., Avni, Y., Green, R. F., Schmidt, M., & Zamorani, G. 1986, ApJ, 305, 57
Thronson, H. A., Jr., Hunter, D. A., Casey, S., Engargiola, G., & Harper, D. A. 1990, in 2nd Wyoming Conference: The Interstellar Medium in External Galaxies, ed. D. J. Hollenbach, & H. A. Thronson, Jr. (NASA CP-3084) 116
Tokunaga, A. 1984, AJ, 89, 172
———. 1986, IRTF Photometry Manual
Treves, A., Bouchet, P., Chiapetti, L., Ciapi, A., Falomo, R., Maraschi, L., & Tanzi, E. G. 1988, ApJ, 330, 178
Turner, T. J., & Pounds, K. A. 1988, MNRAS, 232, 463
———. 1989, MNRAS, 240, 833
Unger, S. W., Lawrence, A., Wilson, A. S., Elvis, M., & Wright, A. E. 1987, MNRAS, 228, 521
Urry, C. M., & Reichert, G. 1988, NASA IUE Newsletter, 34, 95
Van Breugel, W., Miley, G., & Heckman, T. 1984, AJ, 89, 5
Véron-Cetty, M. P., & Véron, P. 1987, ESO Sci. Rept., 5
Ward, M., Elvis, M., Fabbiano, G., Carleton, N. P., Willner, S. P., & Lawrence, A. 1987, ApJ, 315, 74
White, R. L., & Becker, R. H. 1992, ApJS, 79, 331
Wilkes, B. J., & Elvis, M. 1987, ApJ, 323, 243 (WE87)
Williams, O. R., et al. 1992, ApJ, 389, 157
Willner, S. P., Elvis, M., Fabbiano, G., Lawrence, A., & Ward, M. J. 1985, ApJ, 299, 443
Wills, B. J. 1975, Australian J. Phys. Ap. Suppl., 38, 1
Wills, B. J., Netzer, H., & Wills, D. 1985, ApJ, 288, 94
Wills, D. 1979, ApJS, 39, 291
Wright, A. E., Wark, R. M., Troup, E., Otrupcek, R., Jennings, D., Hunt, A., & Cooke, D. J. 1991, MNRAS, 251, 330
Yee, H. K. C., & Green, R. F. 1987, AJ, 94, 618
Zamorani, G., et al. 1981, ApJ, 245, 357